Annual Report 1991

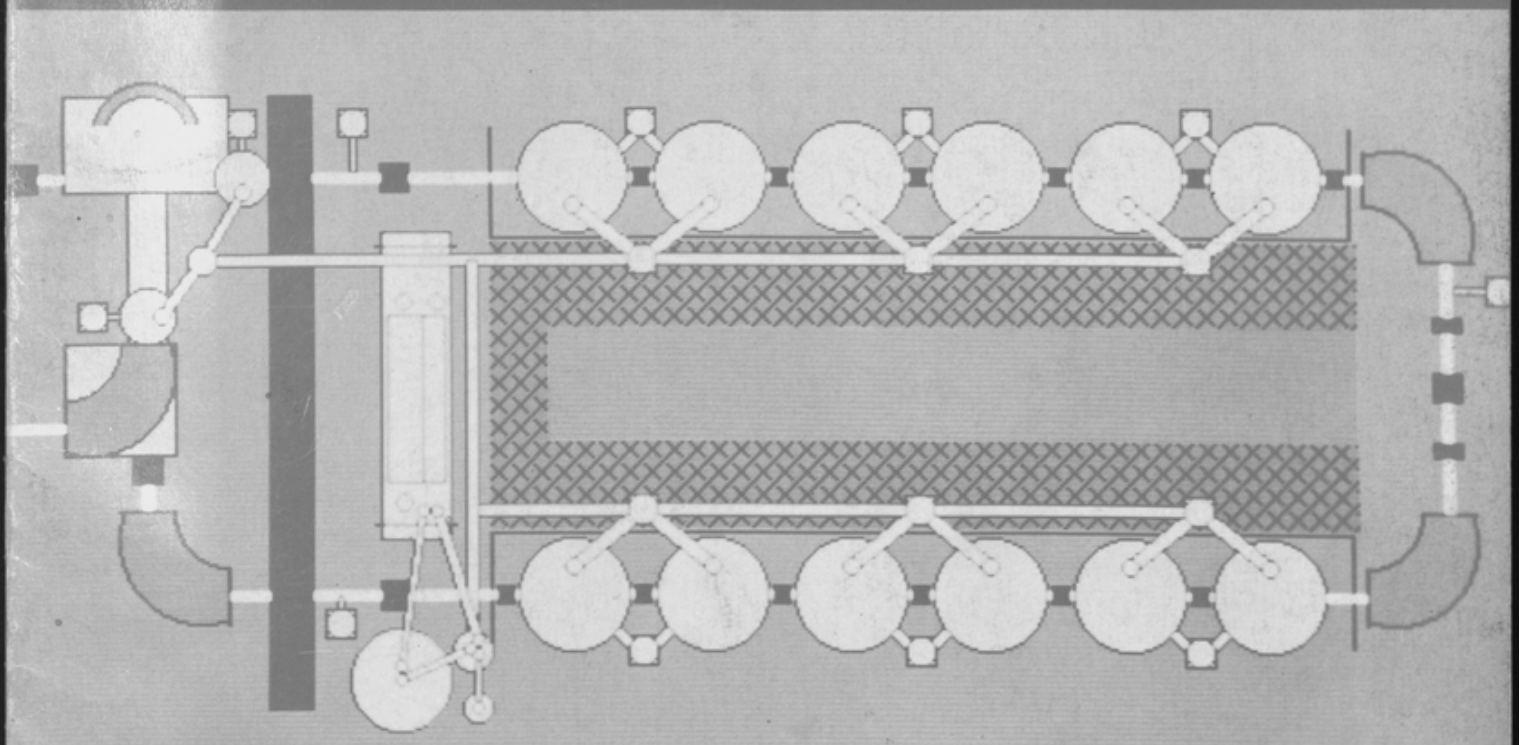

Nuclear Physics Laboratory
University of Washington

ANNUAL REPORT

Nuclear Physics Laboratory
University of Washington
April, 1991

Supported in part by the United States Department of Energy
under grant DE-FG06-90ER40537

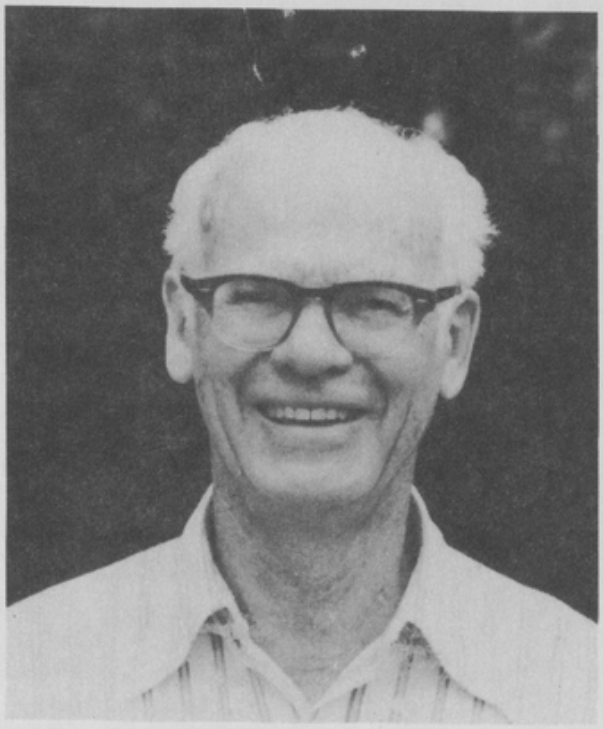

FRED H. SCHMIDT

1915 - 1991

DEDICATION

Fred Schmidt came to the University of Washington as an Assistant Professor in 1946, having spent the war years working on the atomic bomb project, particularly in helping to set up the Calutron isotope separators at Oak Ridge. From this work and his closely related work with E.O. Lawrence's group at the University of California, Fred had become a leading cyclotron expert, and the University of Washington was fortunate to attract him at a time when many universities were eager to get into nuclear physics. It was decided to build a 60" cyclotron to accelerate protons, deuterons, and alpha particles, the latter to the then relatively high energy of 40 MeV.

In parallel with the construction of the accelerator it was necessary to build a group to use it, and Fred played a leading role in adding colleagues and in setting a tone at the Nuclear Physics Laboratory in which research workers gave each other both freedom and help in pursuing their individual physics interests. From its inception, the Laboratory established a reputation for generating a broad spectrum of fruitful investigations, rather than becoming concentrated in the field of the senior investigator.

In those years Fred also established a separate laboratory for studies of beta-ray spectroscopy. When parity breakdown was discovered, his investigations began to focus on the polarization of beta-particles, leading to the work that Fred and his many students did at the cyclotron and the tandem Van de Graaff on studies of the polarization states of nuclei induced in nuclear reactions.

Although Fred and his colleagues decided in the early 1960s to add a tandem Van de Graaff accelerator, the cyclotron remained in operation for many years thereafter, with the emphasis in its use gradually shifting to medical experiments and treatments. Its unusually long life was a tribute to Fred and to his coworkers who helped build it. The tandem accelerator was purchased rather than built locally, but Fred played a central role in getting it to operate properly.

During the early 1970s, Fred developed a strong interest in world energy problems and in particular in the role of nuclear power. His thinking was strongly influenced by the environmental hazards of fossil fuels, including perturbations of the Greenhouse Effect from CO_2 emissions. This led to extensive studies and writings on energy matters, which continued through 1990, and began with "The Energy Controversy: The Fight Over Nuclear Power," co-authored in 1976.

In recent years, Fred joined others in using the Van de Graaff accelerator for ultrasensitive measurements of the radiocarbon content of samples from the natural environment. Among his technical contributions in this field was the development of submilligram graphite pellets to maximize the carbon ion yield. This technique made possible the first study of the time dependence of carbon uptake by trees within a single year, as exhibited by ^{14}C variations within a single growth ring.

We will all miss Fred for his infectious warmth, for the technical advice that he was always willing and often eager to give, and for the humorous comments which enlivened the weekly meetings of the Laboratory research and technical staff. We are all very conscious that this Laboratory, in which he worked with such enthusiasm and pleasure, has derived much of its spirit and its scientific and technical strength from Fred's leadership.

INTRODUCTION

We have a diverse experimental program that exploits our local accelerators, our interest in instrumentation, and the opportunities afforded by user facilities across the country and around the world. Our local studies of nuclear structure include polarization phenomena, β-decay, topics in nuclear astrophysics, fission and fusion phenomena, and the structure of hot rotating nuclei. We also used our facilities to develop and test instruments for experiments at Argonne and CERN. Our interest in pion and electromagnetic induced reactions took us to TRIUMF, Frascati, LAMPF, Saskatchewan, and SLAC. In addition to basic research, we applied nuclear technology to global change research with an active program in accelerator mass spectrometry.

Our completed study of hot rotating ^{90}Zr*–^{92}Mo* nuclei shows clear evidence for a spherical to deformed-oblate shape transition. Both the spectral shapes and the angular distributions are well-described by an adiabatic fluctuation theory which includes both intrinsic-shape and shape-orientation fluctuations. Our compound nuclear isospin mixing studies based on GDR decays in nuclei near A = 28 indicate relatively pure isospin at excitation energies higher than previously studied. A measurement of GDR decays in ^{58}Ni + ^{92}Zr fusion-evaporation shows no evidence for anomalous deformation effects. This is contrary to a previous explanation of particle evaporation anomalies observed in ^{64}Ni + ^{92}Zr at similar energies.

Two new large-volume BaF_2 detectors significantly upgraded our photon detection capabilities during the past year. The combination with our large NaI detector made it practical to measure angular distributions for rare processes such as hard photon emission in proton-nucleus bremsstrahlung. We have also obtained several high-efficiency Ge detectors with BGO Compton suppression. These were used to probe spin distributions in sub-barrier fusion reactions by measuring rotational state populations.

We have measured angular distributions of vector and tensor analyzing powers in ^{2}H$(\vec{d},\gamma)^4$He at E_d = 1 MeV. We see clear evidence for non-E2 radiation amplitudes. Upon completion of cross section and analyzing power measurements, we expect to quantify the extent to which D-state effects in ^{4}He and isospin-forbidden E1 amplitudes contribute to this reaction. We have measured the vector analyzing power in π-d elastic scattering at 50 MeV. We find that in contrast to polarization measurements at higher energy, our results are in agreement with models which include the π-N P_{11} amplitude.

We continue to study nuclear structure questions of interest to astrophysics. We report the discovery of a missing 3^+ state that was expected to greatly increase the ^{17}F(p,γ) rate in explosive nucleosynthesis. We find instead that this 3^+ resonance gives only a small enhancement. We made a new measurement of ^{37}Ca β^+ decay at CERN (ISOLDE) that revealed roughly twice as much Gamow-Teller strength as was seen in previous β-decay work. This result indicates that the accepted efficiency of the ^{37}Cl detector for ^{8}B neutrinos should be increased by $\approx 8\%$, making the solar neutrino problem even more severe.

A major complex of detectors, made possible by a DOE equipment grant, is under construction to completely reconstruct β-decays in ^{8}Li and ^{8}B. This experiment will make independent tests of time reversal invariance, vector current conservation, and set new limits on second class currents.

We have recently shown that existing tests of the equivalence principle and of the $1/r^2$ law

set constraints on gravi-vector interactions that are much more stringent than the limits expected from direct tests of the gravitational acceleration of antiprotons. A new torsion balance apparatus is under construction to search for macroscopic parity- and time-reversal-violating spin-dependent forces mediated by ultra low mass scalar/pseudo-scalar particles.

The accelerator mass spectrometry (AMS) group has found evidence of the El Niño-Southern Oscillation phenomenon in the radiocarbon (^{14}C) profiles of growth bands of corals from the Galápagos Islands. A study of paleoclimate has begun, using radiocarbon dating of pollen extracted from lake sediment cores. Improvements to the UW AMS technology have made possible 0.5 to 1.0% accuracy in measurements from graphitic carbon samples as small as 200 μg.

The interactions between pions and nuclei were pursued in a photoproduction experiment done at the Saskatchewan Accelerator Laboratory, and in the analysis of the data from a LAMPF experiment which compared inclusive inelastic scattering of positive and negative pions. Both of these experiments are surveys of targets from mass 12 to 208. The experiment at Saskatchewan was the first experiment done on the new tagger at the new stretcher ring facility. We also studied photoabsorption below pion threshold at the LADON facility at Frascati. We continue to investigate proton and deuteron structure with high energy electrons. We discuss a proposal for high energy Compton measurements on the proton that would complement elastic form factor experiments.

Work progresses on our contributions to the APEX apparatus at ATLAS. We have completed development and construction of high resolution ion chambers to monitor beam-target interactions. We are presently constructing a nitrogen gas cooling system for the silicon detector arrays. Beam test of these systems should begin in mid-summer.

This year we started a new initiative in ultrarelativistic heavy ion collisions at the CERN SPS and eventually at RHIC. This has resulted in new applications for large-area planar avalanche detectors, under design at the UW. These applications include segmented avalanche detectors to obtain multiplicity distributions for fast (hardware) trigger applications and, by simultaneous detection of $\approx$1000 charged particles from a single event, to obtain timing signals with sub-100 ps resolution for TOF and vertex reconstruction. In addition to detector developments, we have developed the theory of novel mixed-charge multi-pion correlation measurements of the Hanbury-Brown Twiss type.

The Nuclear Physics Laboratory provides charged particle and neutron beams for a variety of research projects outside the conventional boundaries of nuclear physics. This year we report tests of space radiation effects on microelectronics, production rates for radioisotopes of interest to medical imaging, and neutron irradiation of acoustic charge transport (ACT) delay lines.

Our tandem Van de Graaff operated a larger fraction of the year than any year since 1984, when we reduced operations to build the superconducting booster linac. The linac continued to perform well this year. Towards the end of the period we repaired stuck couplers, fixed an open RF cable and replaced poorly performing resonators in a total of four cryostats. We successfully produced thinly plated resonators, discussed in the 1990 annual report, and installed two of these when we opened the cryostats.

As always, we welcome applications from outsiders for the use of our facilities. As a convenient reference for potential users, the table on the following page lists the vital statistics of our accelera-

tors. For further information, please write or telephone Prof. W.G. Weitkamp, Technical Director, Nuclear Physics Laboratory, University of Washington, Seattle, WA 98195; (206) 543-4080.

We close this introduction with a reminder that the articles in this report describe work in progress and are not to be regarded as publications or quoted without permission of the authors. In each article, the names of the investigators have been listed alphabetically, with the primary author underlined.

We thank Ida Tess for help in producing this report.

Charles Hyde-Wright
Editor

María Ramírez
Assistant to the Editor

TANDEM VAN DE GRAAFF ACCELERATOR

A High Voltage Engineering Corp. Model FN purchased in 1966 with NSF funds; operation funded primarily by the U.S. Department of Energy. See W.G. Weitkamp and F.H. Schmidt, "The University of Washington Three Stage Van de Graaff Accelerator," Nucl. Instrum. Meth. **122**, 65 (1974).

Available Energy Analyzed Beams

Ion	*Max. Current* (pμA)	*Max. Practical Energy* MeV
p,d	10	18
polarized p,d	0.3	18
He	2	27
Li	1	36
C	3	63
O	2	72
Si	0.3	90
Ni	0.2	99
I	0.01	108

BOOSTER ACCELERATOR

We give in the following table maximum beam energies and expected intensities for several representative ions.

Available Energy Analyzed Beams

Ion	*Max. Current* (pμA)	*Max. Energy (MeV)*
p	> 1	35
d	> 1	37
He	0.5	65
Li	0.3	94
C	0.6	170
N	0.03	198
O	0.2	205
O	0.1	220
Si	0.1	300
^{35}Cl	0.02	358
Ni	0.001	395

Contents

1 GIANT DIPOLE RESONANCES IN EXCITED NUCLEI

1.1 Giant Dipole Radiation and Isospin Purity in Highly Excited Compound Nuclei

J.A. Behr, Z.M. Drebi, C.A. Gossett, J.H. Gundlach, M.S. Kaplan, K.A. Snover and D.P. Wells

We have continued our studies of isospin violation in highly excited light compound nuclei. We have measured inclusive γ-ray cross-sections for heavy-ion fusion reactions forming isospin T=0 ^{28}Si and ^{26}Al, T=$\frac{1}{2}$ ^{29}Si, and T=1 ^{28}Al, ^{30}Si and ^{26}Mg compound nuclei with initial excitation energies $E^* \approx$ 33, 45 and 65 MeV. We look for γ decay of the Giant Dipole Resonance built on excited states. Since the E1 operator is isovector, T=0 to T=0 transitions are isospin forbidden. So the statistical GDR γ-yield from an N=Z compound nucleus will come from isospin-allowed decays to T=1 final states, from the decay of T=1 initial states populated by isospin mixing, and from daughter nuclei populated by particle decay. We see a suppression of the isovector E1 giant resonance γ-ray yield from the isospin-inhibited decay of the N=Z compound nuclei, compared to the decays of the other compound nuclei which are isospin-allowed, by factors of 2–3.

We extract the degree of isospin mixing from comparison of statistical model calculations with the data. We test the statistical model with the spectra from the reactions populating N$\neq$Z nuclei. Essentially the only physics, other than isospin mixing, that is not tested in this manner is the ratio of the T=1 final state level density to the total level density, $\rho_{T=1}/\rho$, in the N=Z nuclei, which determines the isospin-allowed yield from the initial compound nucleus. Each T=1 level in ^{28}Si must have an isobaric analog in ^{28}Al. So we can calculate the T=1 level density in ^{28}Si from the total level density in ^{28}Al (after a similar correction for T=2 states in ^{28}Al by comparison with ^{28}Mg), shifted in excitation energy. For very low excitation, this shift is the energy of the first T=1 excited state in ^{28}Si, 9 MeV. At high excitation, where shell and pairing effects have dissolved away, the shift is related to the nuclear symmetry energy (3–5 MeV in these nuclei). Results presented earlier[1] were based on analyses with an energy shift which was too large. This smaller energy shift greatly increases $\rho_{T=1}/\rho$, which similarly increases the calculated isospin-allowed γ-ray yield, and thus reduces the amount of isospin mixing necessary to explain the observed yields.

Our results are consistent with little or no isospin mixing. Typical upper limits on the admixture of T=1 initial states in the T=0 compound nuclei are $\alpha^2 \leq 0.10$, which imply upper limits $\Gamma^{\downarrow} \leq$ 150 keV for isospin-violating Coulomb spreading widths of the T=1 states. An exception is the case of ^{26}Al at E^*=63 MeV, where we are less sensitive to mixing by a factor of 2 than we are in ^{28}Si (the compound nuclear widths are larger, and the daughter decays contribute more because particle binding energies are lower) and so can only set an upper limit of $\alpha^2 \leq 0.3$. The results are consistent with the idea that isospin is a good symmetry in these reactions because these short-lived compound nuclei decay before the isospin degree of freedom equilibrates.[2]

[1] Nuclear Physics Laboratory Annual Report, University of Washington (1990) p. 1.
[2] D.H. Wilkinson, Phil. Mag. **1** (1956) 379.

1.2 Isospin Purity of Highly Excited Medium-Mass Nuclei

J.A. Behr, Z.M. Drebi, M.S. Kaplan, K.A. Snover and D.P. Wells

We have extended our studies of isospin purity in highly excited compound nuclei to the A $\approx$ 60 mass region. Inclusive γ-ray cross sections at 90° from the decay of the compound nuclei ^{60}Zn, ^{59}Cu and ^{58}Ni at 46.6, 46.9 and 53.4 MeV excitation energy, respectively, have been measured. These three compound nuclei were formed with the fusion reactions ^{32}S + ^{28}Si, ^{31}P + ^{28}Si, and ^{31}P + ^{27}Al, which have entrance channel isospins T = 0, T = $\frac{1}{2}$ and T = 1, respectively. The quantity of interest is the statistical γ-ray yield from the decay of the giant dipole resonance (GDR) built on excited states, which is sensitive to the isospin purity of the compound nucleus.[1]

The E1 GDR decays must obey the isospin selection rule ΔT = 0, $\pm$1, but no T = 0 to T = 0. Thus, if the entrance channel isospin purity is maintained throughout the equilibration and decay process, one expects the decay of the (T = 0) ^{60}Zn* compound nucleus to yield considerably fewer GDR γ rays than the other two compound nuclei since it can only decay to a T = 1 level whereas the non-(T = 0) compound nuclei can decay to all levels consistent with ΔT = 0, $\pm$1. This effect is somewhat diminished by GDR γ rays emitted from daughter nuclei of each of these compound nuclei. Thus proper interpretation of these data must include all such daughters that significantly contribute.

Preliminary analysis of the ratios of the ^{60}Zn to ^{59}Cu and ^{60}Zn to ^{58}Ni cross sections using a statistical CASCADE calculation that includes the effects of isospin suggests that there is nonzero isospin mixing in these compound nuclear reactions. One expects the ratios of these cross sections to largely cancel experimental systematic errors. Moreover, by comparing the experimental cross section ratios to the ratios of CASCADE calculations we avoid a strong dependence of our conclusions on the level densities and we need to know only the ratios of the fusion cross sections. Our preliminary results imply isospin-mixing Coulomb spreading widths of $\Gamma^{\downarrow}$ = 20 – 40keV for the T=1 states, which in ^{60}Zn corresponds to a T = 1 admixture in the compound nucleus of $0.07 \leq \alpha^2 \leq 0.12$. We are currently investigating the systematic errors in our estimated isospin mixing.

[1] M.N. Harakeh, G. Feldman, E.F. Garman, R. Loveman, J.L. Osborne, and K.A. Snover, Phys. Lett. B 176, 297 (1986).

1.3 Giant Dipole Resonance Decays of $^{32}S + ^{27}Al$ Reaction at High Spins and Temperatures

J.A.Behr, A.W.Charlop, Z.M.Drebi, M.S.Kaplan, K.A. Snover and D.P. Wells

We measured spectral shapes and angular distributions of high energy γ rays emitted from the fusion reaction $^{32}S + ^{27}Al$ at bombarding energies of 90.2 MeV, and 215.0 MeV in the center of the target. The motivation was to study nuclear shapes and shape changes as a function of spin and nuclear temperature. The compound nucleus is produced at average spins $\overline{I}$=15$\hbar$, 28$\hbar$, and at average temperatures $\overline{T}$ = 1.7 MeV, 2.6 MeV for the two bombarding energies, respectively. We used the gain stabilized 10"×15" NaI detector. Cosmic rays were rejected by an anticoincidence plastic shield. Prompt γ rays were separated from fast neutrons by time of flight technique. The angular distributions were measured at five lab angles θ_{lab} =40, 55, 90, 125, and 140 degrees. The measured γ-ray yield was corrected for random background and pileup, and then transformed to the compound nucleus center of mass frame. The statistical model code CASCADE was used to fit the 90 degree cross-sections. The angular distributions were fitted with a second order Legendre polynomial expansion.

For the lower spin case, the shape of the spectrum is well described by a single Lorentzian fit, as shown in the first and second row of Fig. 1.3-1. The region of the fit is from E_γ =11.5 MeV to 22.0 MeV. The GDR fit parameters are E_D =17.5 MeV, Γ_D =10.0 MeV, and S_1 = .42. Since the initial compound state is an isospin $T = 1/2$ state, E1 gammas are partially inhibited. Calculations using a CASCADE version which takes isospin into consideration shows that high energy gamma yield is about a factor of two less than the normal CASCADE code prediction, which partially explains the low strength factor S_1 obtained from the fit.

The $a_1(E_\gamma)$ coefficients are consistent with zero, within the statistical errors, as shown in the fourth row of Fig. 1.3-1, for $E_\gamma > 12$ MeV, consistent with the assumption of statistical decay. However, a small negative a_1 around E_γ = 10 MeV, associated with a small increase in σ_γ for $E_\gamma < 11$ MeV, is observed. This can be attributed to a target-like excitation. The $a_2(E_\gamma)$ is small and negative below the mean GDR energy, which implies that the nucleus has a prolate collective or oblate noncollective shape.

In the higher spin case, a big deviation from statistical γ decay is evident at $E_\gamma < 13$ MeV. This can be seen both in the spectral shape and in the angular distribution as shown in the second column of Fig. 1.3-1. An order of magnitude larger γ-yield than what CASCADE predicted is observed along with a large negative a_1 values. However a_1 is consistent with zero for $E_\gamma > 13.5$ MeV. This encouraged us to try a one Lorentzian fit to the data in E_γ =13.5 MeV to 21.0 MeV range. As can be seen in the figure, this fit is poor in the high energy region, and misses the data entirely at the low energy portion. It is worth pointing out that the observed a_1 values at the low gamma energies are a clear signature of a γ-source moving with a negative velocity in the compound nucleus C.M. frame, in other words a target-like excitation.

Deep inelastic reactions of $^{32}S + ^{27}Al$ system have been studied[1] at E_{proj} = 175 MeV, for which the observed Q-value distributions of the primary D.I. process range down to ~ -30 MeV. So for our case one would expect large fragment excitations $\sim$ 20 MeV which can emit a lot of low energy

[1] Rosner *et al.*, Nuc. Phys. A **385**, 174 (1982).

gamma rays. Another mechanism that can produce fragments at high excitation energies and spins is fusion-fission. Mass symmetric fission of our system can give fragments with $E_f^* = 32$ MeV, and $\overline{I}_f$=12$\hbar$. Although these processes can account for the extra γ yield at low E_γ, the large a_1 observed for E_γ ~9–13 MeV remains puzzling.

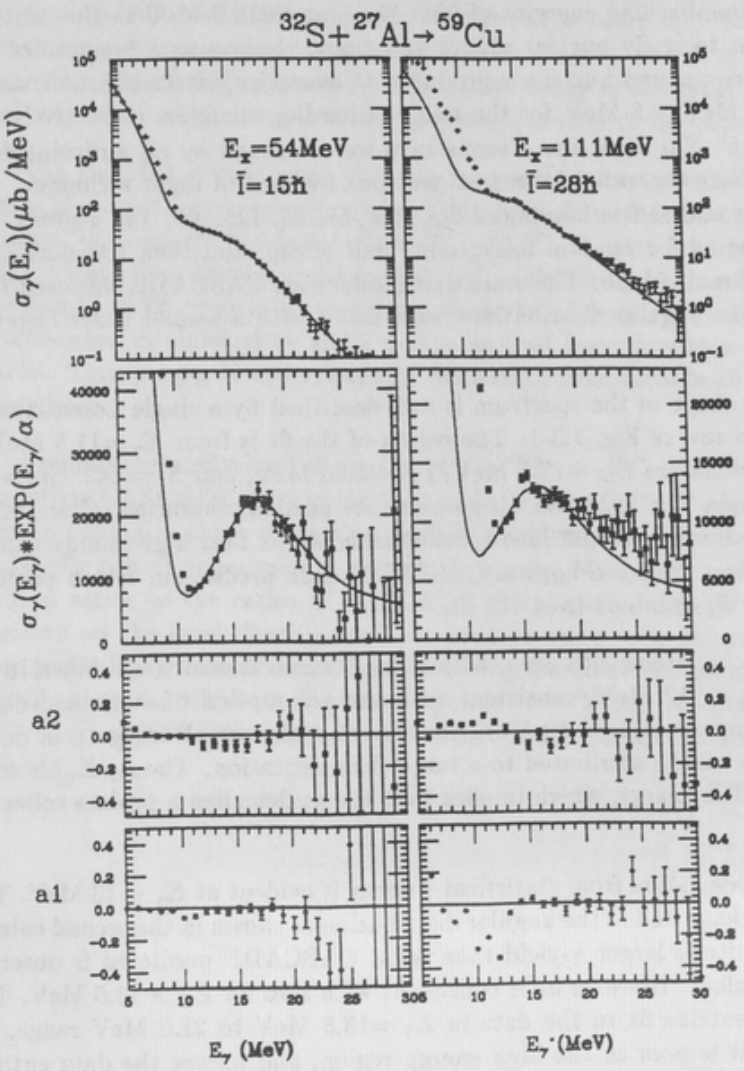

Figure 1.3-1. First row: The measured γ cross section for 90.2 MeV (left column) and 215 MeV (right column) bombarding energies, and the corresponding one Lorentzian CASCADE fits (solid lines). Second row: The γ cross section multiplied by exp(E_γ/α), where α=2.5, and 3.0 for the two cases respectively. Third row: The measured $a_2(E_\gamma)$ Legendre coefficients of the CM γ ray angular distributions. Fourth row: the measured $a_1(E_\gamma)$ coefficients.

1.4 Giant Dipole Resonance Decays of ^{63}Cu Formed at High Spins and Temperatures in the ^{18}O + ^{45}Sc Reaction

A.W. Charlop, Z.M. Drebi, M.S. Kaplan, K.A.Snover and D.P. Wells

We measured spectral shapes and angular distributions of high energy γ rays to probe the shape evolution of the excited ^{63}Cu nucleus as a function of spin and temperature. Beams of ^{18}O at E_{proj} = 52.3 MeV, 70.2 MeV, and 105.5 MeV were bombarded on a ^{45}Sc target. We used a 10"×15" NaI detector, which is gain stabilized, anticoincidence shielded (for cosmic ray suppression), and lead shielded. A Geli detector was used to independently check the normalization. A pulsed beam was used in order to suppress fast neutrons by the TOF technique. The target was self supported natural Scandium of thickness 974μg/cm^2. These reactions produced the ^{63}Cu compound nucleus with average spins $\overline{I}$=15$\hbar$, 21$\hbar$, and 30$\hbar$, and average temperatures $\overline{T}$ = 1.8 MeV, 2.0 MeV, and 2.2 MeV. The angular distributions were measured at the five lab angles: θ_{lab} =40, 55, 90, 125, and 140 degrees. These data were corrected for random background and pileup, and then transformed to the compound nucleus center of mass frame.

The measured spectral shapes were fitted with CASCADE using a one-Lorentzian GDR strength function parametrization, and the Puhlhofer level density approach[1] with $a = A/9$. The region of the fit is from E_γ =11.5 MeV to 22.0 MeV. In all cases a strongly broadened GDR width is observed (Γ_D =10.2 MeV, 11.6 MeV, and 11.4 MeV respectively) as compared to the ground state GDR width $\Gamma_D^{g.s.}$ of 5.0 MeV.[2] However, the fitted spectrum of E_{proj} = 105.5 MeV at low γ ray energy underestimates the measured cross section at high γ-ray energy, indicating that other reaction mechanisms are present. The fitted and divided spectra for all cases are shown in the first and second rows of Fig. 1.4-1.

The angular distributions in the C.M. frame of the compound nucleus were fitted with a second order Legendre polynomial expansion. As shown in the fourth row of Fig. 1.4-1, the $a_1(E_\gamma)$ coefficients were found to be consistent with zero, within the statistical errors, for $E_\gamma > 12$ MeV, confirming the statistical nature of the decay. However, nonzero a_1 values are evident at lower E_γ especially for the higher energy cases, which indicate that nonstatistical processes are contributing to the γ ray cross section in this region.

On the other hand the inferred $a_2(E_\gamma)$ coefficients are clearly negative in the low-energy side of the GDR, $E_\gamma \sim 11 - 17$MeV. This a_2 anisotropy in the angular distribution is characteristic of either oblate noncollective or prolate collective rotations. A more negative a_2 in this region is suggested as $\overline{I}$ increases from 15 $\hbar$ to 30 $\hbar$. In order to understand the magnitude of the deformation implied by the observed a_2 values, it is necessary to perform a full fluctuation calculation. Such calculations are in progress. We plan to extend these measurements to higher bombarding energies in order to search for large deformations.

[1] F. Puhlhofer, Nucl. Phys. A **280**, 267 (1977).
[2] R.E. Sund *et al.*, Phys Rev. **176**, 1366 (1968).

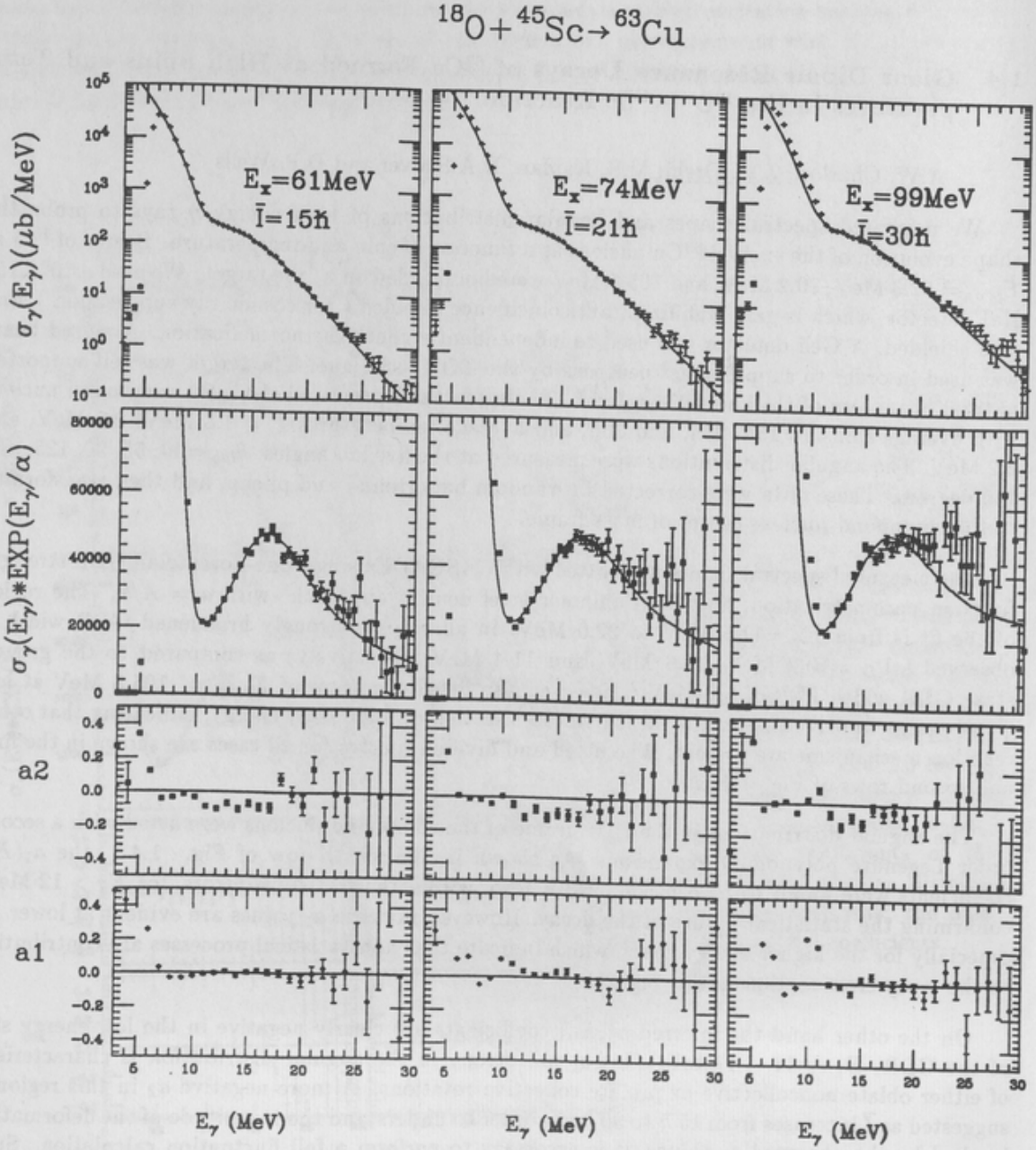

Figure 1.4-1. First row: The measured γ cross section for 52.3 MeV (left column), 70.2 MeV (middle column), and 215 MeV (right column) bombarding energies, and the corresponding one Lorentzian CASCADE fits (solid lines). Second row: The γ cross section multiplied by exp(Eγ/α), where α=2.5, 2.6, and 2.75 for the three cases respectively. Third row: The measured $a_2(E_\gamma)$ Legendre coefficients of the CM γ ray angular distributions. Fourth row: the measured $a_1(E_\gamma)$ coefficients.

1.5 Giant Dipole Resonance Decay Width of ^{108,112}Sn Isotopes Formed at Moderate Temperatures in the ^{16}O + ^{92,96}Mo Reactions

A.W. Charlop, Z.M. Drebi, M.S. Kaplan and K.A. Snover

It was recently suggested that, in analogy with nuclear magnetic resonance in condensed-matter systems, the GDR could display a phenomenon known as "motional narrowing". The basic idea is that the nuclear shape fluctuations are not adiabatic, the nucleus is hopping so fast between its various shapes so that the dipole vibration does not have enough time to probe separately each nuclear shape, which results in a smaller broadening of the GDR. Extensive work has been done to develop time dependent thermal quadrupole shape fluctuation theories.[1] Although the majority of experimental measurements are described well by the adiabatic theory, there exist measurements of the GDR strength functions in some Sn isotopes at temperatures of 1–2 MeV which suggest a significant reduction in the GDR width, compared to the adiabatic limit calculations. A GDR width Γ_D of 6.0±0.7 MeV at E_x=51.8 MeV of ^{108}Sn in the reaction ^{16}O + ^{92}Mo,[2] and Γ_D=6.7±0.4 MeV at E_x=62.2 MeV of ^{112}Sn in the reaction ^{19}F + ^{93}Nb,[3] have been reported. A considerable amount of nonadiabaticity was needed in the theoretical calculations to reproduce these measured strength functions.

In this project, we plan to investigate further the question of motional narrowing. We started by measuring the spectral shapes of ^{16}O + ^{92}Mo, and ^{16}O + ^{96}Mo at $\overline{E}_{proj}$ = 70.8 MeV, and at θ_γ=90. These reactions produced ^{108}Sn* and ^{112}Sn* at excitation energies E_x=50.8 MeV, 55.8 MeV, and average temperatures=1.35 MeV, 1.41 MeV respectively. We used a 10"×15" NaI detector, which is gain stabilized, anticoincidence shielded (for cosmic ray suppression), and lead shielded. Pulsed beam was used to suppress fast neutrons by TOF. The data was corrected for random background and pileup.

The measured spectral shapes were fitted with CASCADE using one and two Lorentzian GDR strength functions, and with different level density parameter values. We found that, for both cases, a two Lorentzian GDR strength function fits the data better than one Lorentzian ones. The sensitivity to the level density parameter a is small. The GDR width extracted from the best fit is 7.5±0.2 MeV for ^{16}O + ^{92}Mo, and is 8.5±0.2 MeV[4] for ^{16}O + ^{96}Mo system. The measured spectral shape divided by exp(-Eγ/α) for the ^{16}O + ^{92}Mo reaction is shown in Fig. 1.5-1, along with the CASCADE fits, the solid line is the best 2-Lorentzian fit, and the dashed line is the best 1-Lorentzian fit. From these measurements and CASCADE fits it's clear that no non-adiabatic effects are evident.

The width observed in the ^{16}O + ^{96}Mo reaction is however, surprisingly wide, since all Sn* isotopes would be expected to exhibit similar widths. Further experiments are planned to verify this preliminary result, as well as further calculations to investigate systematic errors.

---

[1] Alhassid, and Bush, Nuc. Phys. A **514**, 434 (1990); Ormand *et al.*, Nuc. Phys. A **519**, 61c (1990).

[2] Gaardhoje *et al.*, Phys. Rev. Lett. **53**, 148 (1984).

[3] Chakrabarty *et al.*, Phys. Rev. C **36**, 1886 (1987).

[4] The assigned errors are predominately systematics, the statistical errors in these measurements are negligible.

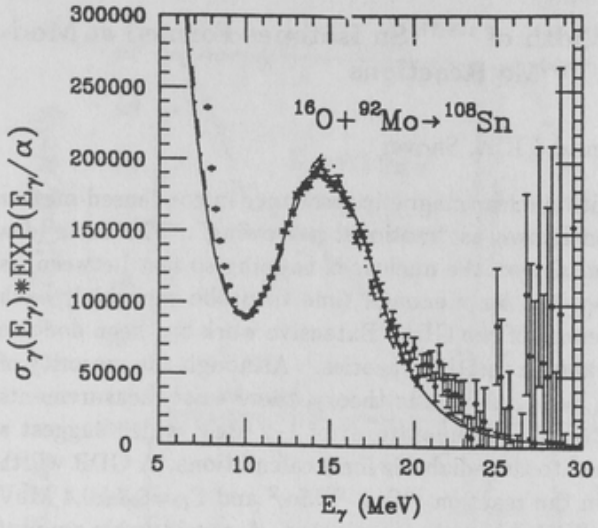

Figure 1.5-1. The measured γ cross section for ^{16}O + ^{92}Mo multiplied by exp(Eγ/α),where α=2.0 . The solid line is the best 2-Lorentzian, and dotted line is the best 1-Lorentzian CASCADE fit.

1.6 High Energy Gamma-Ray Emission Following Fusion of ^{58}Ni and ^{92}Zr

Z.M. Drebi, M.S. Kaplan, K.A. Snover and D.P. Wells

We have measured inclusive high energy γ-ray spectra from the decay of ^{150}Er with initial excitation energy $E^* = 57$ MeV, formed in the nearly mass symmetric reaction ^{58}Ni + ^{92}Zr at E_{lab} = 241 MeV. Previous studies[1,2] of particle and low energy γ-ray emission in ^{64}Ni + ^{92}Zr $\rightarrow$ ^{156}Er* indicate anomalous behavior, including the suppression of neutron emission compared to statistical model calculations, whereas ^{12}C + ^{144}Sm induced reactions appear normal. It was suggested that the anomalous behavior may result from the persistence of large deformation associated with the mass symmetric entrance channel for times comparable to the lifetime of the compound nucleus. Gamma-emission from the Giant Dipole Resonance (GDR) should provide a good test of this hypothesis, since it occurs in the early stages of the compound nucleus decay and is sensitive to deformation.

Measurements were made at 90° with the 10" x 15" NaI detector and with two 5.7" x 6.7" BaF_2 detectors at 41° and 139°, respectively. In the energy region of the giant dipole resonance ($E_\gamma \geq 11$ MeV), the NaI spectrum for ^{58}Ni + ^{92}Zr, shown in Fig. 1.6-1, is in good agreement with CASCADE statistical model calculations using level densities ($a = A/8$) and GDR parameters ($\langle E_{GDR} \rangle$ = 14 MeV, Γ_{GDR} = 7.5 MeV) taken from systematics of nearby nuclei, together with a GDR strength, S = 1.4, adjusted to fit the observed cross section. Although this value for S is somewhat high, it is also uncertain since it depends on our estimate for the ^{58}Ni + ^{92}Zr fusion cross section derived from ^{64}Ni + ^{92}Zr measurements.[3] Thus we find no evidence for anomalous behavior, and in particular, no evidence for large deformation in this system. The excess yield observed at low gamma-ray energies is probably due primarily to deep inelastic collisions. A front-back asymmetry between the yields measured by the two BaF_2 detectors would be a clear indication of such non-statistical emission. The analysis of these data is in progress.

A similar study of ^{64}Ni + ^{92}Zr is planned. In addition, the possibility of collecting evaporation residue - high energy gamma-ray coincidence data is being considered.

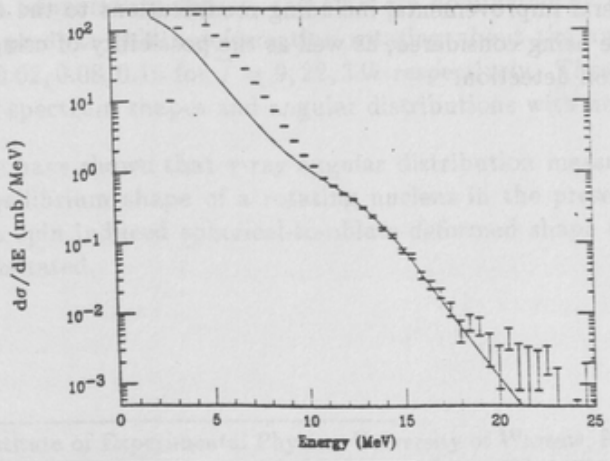

Figure 1.6-1. ^{58}Ni + ^{92}Zr γ-yield at 90° compared to results of CASCADE calculation.

[1] Kuhn *et al.*, Phys. Rev. Lett. **51** (1983), 1858.

[2] Ruckelshausen *et al.*, Phys. Rev. Lett. **56** (1986), 2356.

[3] A.M. Stefanini, Invited paper at the Workshop on Heavy Ion Collisions at Energies Near the Coulomb Barrier, Daresbury, England, 5–7 July 1990.

1.7 Feasibility of High Energy Gamma-ray, Evaporation Residue Coincidence Studies

Z.M. Drebi, M.S. Kaplan, K.A. Snover and D.P. Wells

The application of coincidence techniques to the study of high energy gamma-ray decay from excited compound nuclei has great potential. For example, the extension of gamma decay studies of the giant dipole resonance built on states of very high excitation energy requires the use of higher bombarding energies, where deep inelastic collisions (DIC) as well as other reaction mechanisms besides complete fusion contribute a significant background. Also, for heavy nuclei such as Ni + Zr, DIC are known to account for a large fraction of the total reaction cross section even at bombarding energies near the Coulomb barrier. Detection of high energy gamma-rays in coincidence with evaporation residues would allow for exclusive complete fusion measurements.

Recently, we performed a preliminary test of this technique using the electrostatic deflector[1] and one of the BaF_2 detectors. The reaction studied was $^{28}Si + ^{nat}Ni$, using a bunched beam of 99 MeV. Both elastic and inelastic scattered beam particles and evaporation residues were separated by their energy and time of flight measured with a a 4.6 cm x 6.2 cm silicon detector consisting of 7 independent strips and placed 92 cm from the target. The segmentation of the detector provided some position sensitivity, which proved useful for diagnostic purposes. To normalize the results, a silicon monitor detector was placed at an angle of 40°, 5 cm from the target. The yield of elastically scattered beam particles thus detected was then normalized to the integrated beam current with the deflector plates grounded.

An on-line comparison of the inclusive prompt gamma-ray yield to the yield coincident with detected evaporation residues provided an estimate of 4% for the overall deflector detection efficiency. This value is consistent with estimates based on the detector geometry and calculations of the angular distribution of the residues following light particle evaporation and multiple scattering in the target foil. Because of the small branching ratio for statistical gamma decay of an excited nucleus, we conclude that the efficiency must be improved for this technique to be feasible in a high energy gamma decay study. Several improvements, including modifications to the deflector geometry and recoil detector design are being considered, as well as the possibility of using a bare parallel plate avalanche counter for recoil detection.

[1] Nuclear Physics Laboratory Annual Report, University of Washington (1988), p. 73.

1.8 Observation of Oblate Deformed Shapes in Hot Rotating A= 90, 92 Nuclei

J.A.Behr, C.A. Gossett, J.H. Gundlach, M. Kicinska-Habior,* K.T. Lesko† and K.A. Snover

We have studied excited ^{90}Zr and ^{92}Mo compound nuclei with average spins $\overline{I} \approx 9\hbar, 22\hbar$ and $33\hbar$ and temperatures $\overline{T}$ ≈1.6 MeV,1.7 MeV and 2.0 MeV,[1,2] respectively, formed in heavy ion fusion reactions. Our purpose is to examine the evolution of the nuclear shape with rotation and temperature.

High energy (GDR) γ-ray spectra and angular distributions were measured and analyzed. The 90° energy spectra were fit with statistical model calculations in order to extract the E1 strength function. We found the E1 sum rule and mean resonance energy in agreement with ground state systematics. The strength function is not resolved into two components as is seen in some ground state GDR studies, although a significant increase of the total width was found. It is more than doubled as compared to the ground state, even for the lowest spin case. We showed that this width increase can be understood when temperature-driven shape fluctuations are considered. These fluctuations made it impossible to extract the equilibrium deformation of the hot rotating nuclei from the measured spectral shapes.

The angular distribution measurements provide statistical model-independent information and proved to be very sensitive to the deformation despite the thermal shape fluctuations. We extracted the a_2 coefficient in the center of mass. Directly from the observed increase of the anisotropy with increasing spin, the shape evolution from spherical to deformed could be demonstrated. However, for a quantitative interpretation fluctuations must be considered. Here it is important not only to include the β and γ shape degrees of freedom but also fluctuations in the orientation degrees of freedom of the nucleus around the spin axis described by the Euler angles ϕ and θ. We found remarkable agreement in the GDR region ($E_\gamma = 11 - 20$ MeV) with a theory[3] based on calculated potential energy surfaces (PES) F, together with the probability factor $e^{-\frac{F}{T}\beta^4} \mid \sin 3\gamma \mid d\beta d\gamma \sin\theta d\theta d\phi$.[4] In this temperature regime, the PES are dominated by the properties of a rotating liquid drop, which predicts oblate deformation rotating about the nuclear symmetry axis, with a magnitude $\beta_0 = 0.02, 0.08, 0.16$ for $\overline{I} = 9, 22, 33\hbar$ respectively. These calculations correctly describe the observed spectrum shapes and angular distributions with no free parameters.

We have shown that γ-ray angular distribution measurements can be used to reliably extract the equilibrium shape of a rotating nucleus in the presence of shape fluctuations. For the first time a spin induced spherical-to-oblate-deformed shape transition in a hot rotating nucleus was demonstrated.

*Institute of Experimental Physics, University of Warsaw, Poland.
†Lawrence Berkeley Laboratory (LBL), Berkeley, CA 94720.

[1]Nuclear Physics Laboratory Annual Report, University of Washington (1990) p. 5.
[2]J.H. Gundlach *et al.*, Phys. Rev. Lett. **65**, 2523 (1990).
[3]Y. Alhassid and B. Bush, Phys. Rev. Lett. **65** 2527 (1990).
[4]N. Bohr and B.R. Mottelson, Nuclear Structure Vol. 2. (Benjamin, New York, 1975).

2 NUCLEUS-NUCLEUS REACTIONS

2.1 Search for High Energy γ-rays from the Spontaneous Fission of ^{252}Cf

C. A. Gossett, S. J. Luke and R. Vandenbosch

Last year[1] we reported on an experimental program to search for the emission of very high energy γ rays from the spontaneous fission of ^{252}Cf. This search was undertaken in two ways: the measurement of high energy γ rays in coincidence with fission fragments and high energy γ rays coincident with other γ rays assumed to be arising from the fission fragments.

Last year we reported the upper level established by the fission fragment/γ-ray coincidence measurement. The data from the γ-γ measurements have been analyzed and the upper limit established in this mode is about an order of magnitude higher than the upper limit in the fission fragment/γ-ray measurement. These upper limits along with the reported level of Kasagi *et al.*[2] are shown in Figure 2.1-1.

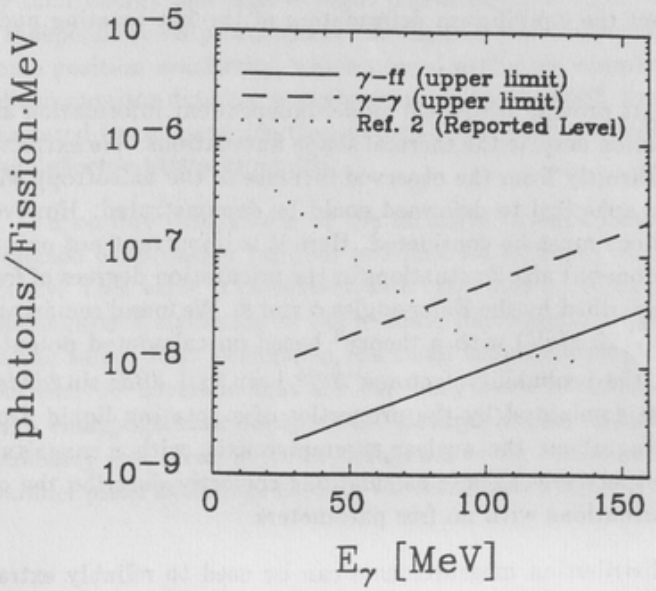

Figure 2.1-1: Upper limits set by present measurements. The dashed line corresponds to the upper limit set by the γ-γ coincidence measurement. The solid line is the upper limit established by the fission fragment/γ-ray coincidence measurement. The dotted line is the reported level of photon production reported by Kasagi *et al.*[2]

In addition we have finished three model calculations for the expected emission of high energy γ rays from the spontaneous fission of ^{252}Cf via a bremsstrahlung mechanism.[3] This bremsstrahlung arises from the acceleration of the fission fragments after the scission process. The three calculations represent three different scenarios. The first calculation involves a sudden approximation, and can only be regarded as an upper limit. It assumes that the fission fragments obtain their asymptotic

[1] Nuclear Physics Laboratory Annual Report, University of Washington (1990) pp. 7–8.

[2] J. Kasagi *et al.*, *Proc. Fifth Int. Conf. Clustering Aspects in Nucl. and Subnucl. Systems*, Kyoto, 1988, J. Phys. Soc. Jpn. 58(1989) Suppl. pp. 620–625.

[3] S.J. Luke, C.A. Gossett and R. Vandenbosch, submitted to Phys. Rev. C.

velocity instantaneously. The results of the sudden calculation are shown as a dotted line in Figure 2.1-2. The second calculation assumes Coulomb acceleration of the fission fragments, but does not take into account the perturbation to the fissioning system caused by the emission of a very high energy γ ray. The results of this calculation are shown in Figure 2.1-2 as a long dashed line. Finally, the third calculation assumes Coulomb acceleration of the fission fragments and also takes into account the "sub-barrier" nature of the production of the higher energy γ rays by reducing the bremsstrahlung probability by a barrier penetration requirement. The results of this calculation are shown as a solid line in Figure 2.1-2.

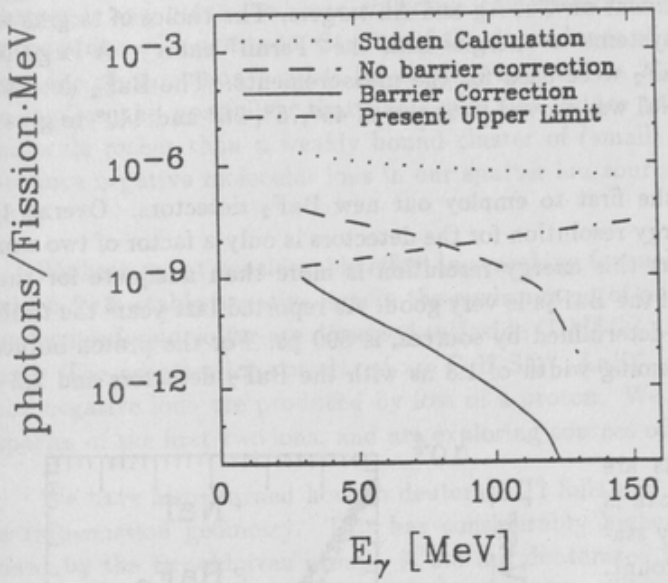

Figure 2.1-2: Various scenarios of high energy photon production arising from the spontaneous fission of ^{252}Cf. The dotted line is the result of sudden acceleration scenario. The dashed line is the result of hard photon production arising from Coulomb acceleration without any barrier correction. The solid line is the result of the Coulomb acceleration scenario with the inclusion of a barrier correction. The dash-dotted line is the upper limit established by our present experiment in the fission fragment/γ-ray coincidence mode.

Our data clearly excludes the sudden calculation as a possible production scenario. The production of high energy γ rays by a Coulomb acceleration mechanism is excluded below 80 MeV. Our data does not not answer any questions relating to the Coulomb acceleration scenario including barrier penetration. Several orders of magnitude more fission events would be needed to answer this question.

2.2 High Energy γ rays from X(p,γ) at 33.5 MeV

C. A. Gossett, M. S. Kaplan, S. J. Luke, B. T. McLain, R. Vandenbosch and D.P. Wells

In our continued effort to understand the production of high energy γ rays in nuclear collisions we have measured the hard photon production in proton induced reactions. Proton-induced hard photon production should be the lowest order test of any γ-ray production model. We therefore are using these data as a test and as a tool for optimization of the hard photon production model of Randrup and Vandenbosch.[1]

We have made measurements of the energy spectra and angular distribution of high energy γ rays produced by 33.5 MeV protons incident on Cu, Ag and Au targets. The choice of targets was to extend the data set[2] for the same systems to energies near the "Fermi" energy. A large NaI spectrometer and two large volume BaF_2 were used for the measurements. The BaF_2 detectors were placed at 30° and 90°, while the NaI was moved to angles of 45°,75°, 90° and 140° to give us an angular distribution.

These measurements were one of the first to employ our new BaF_2 detectors. Overall the detectors performed very well. The energy resolution for the detectors is only a factor of two worse than that of the NaI at 22.6 MeV, but this energy resolution is more than adequate for these measurements. The timing resolution of the BaF_2s is very good. As reported last year[3] the timing resolution of the Barium Fluorides, as determined by sources, is 600 ps. For the proton-induced measurements we obtained an overall timing width of 1.5 ns with the BaF_2 detectors and 2.2 ns with the NaI.

The data from these measurements are nearly analyzed. An example of the data is shown in Figure 2.2-1. In this figure only statistical errors have been taken into account. When the data analysis is complete we will use this data along with the higher energy (p,γ) data to understand more fully the production of high energy photons in heavy ion induced reactions.

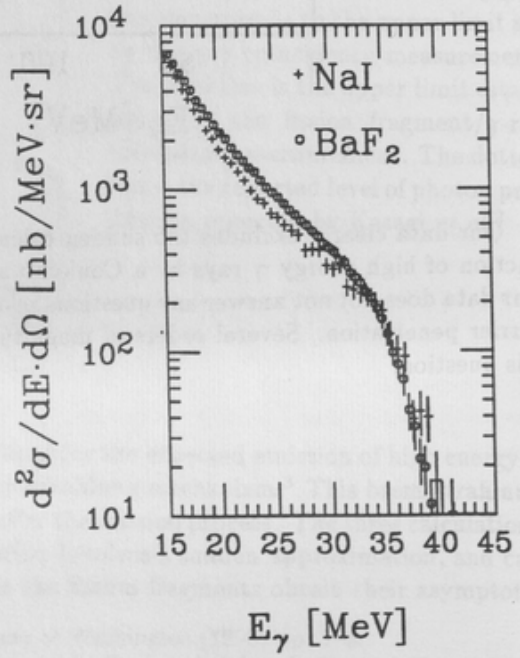

Figure 2.2-1: The measured energy spectra for both the BaF_2 and NaI detectors at 90° for 33.5 MeV protons incident on a Ag target.

[1] Nucl. Phys. A 490, 418(1988).
[2] H. Nifenecker *et al.*, Phys. Lett. B 207, 269(1988).
[3] Nuclear Physics Laboratory Annual Report, University of Washington (1990) p. 65.

2.3 Molecular-Impact Nuclear Fusion

J. Neubauer, T.A. Trainor, R. Vandenbosch and D.I. Will

A group at Brookhaven has reported observing protons from the reaction D+D=H+T when deuterated water clusters are accelerated and then bombard a deuterated Ti foil.[1,2] In a typical experiment a cluster of about 100 water molecules is accelerated to 300 keV, leading to clusters with velocities corresponding to 0.15 keV/A deuterons. This energy is more than an order of magnitude below the lowest energy at which free D+D nuclear fusion has been experimentally observed, and points to some collective compressional effect which enhances the fusion rate by many orders of magnitude. Studies of the dependence of the fusion yield on cluster size has shown that the phenomenon persists for clusters as small as 20 water molecules. This has motivated us to explore the possibility that one could also induce this collective process using a large single molecule rather than a weakly bound cluster of (small) water molecules. Specifically, we would produce negative molecular ions in our sputter ion source and accelerate them to several hundred keV.

We have spent considerable effort in searching for molecular species that contain hydrogen and which form stable negative ions in the environment of our sputter ion source. The most promising molecules found so far are dimethyl sulfoxide (DMSO), lanthanum hydride, and p-toluene sulfonic acid. The negative ions produced are $C_2H_4SO^-$, LaH_4^-, and $C_7H_7SO_3^-$. For the organic molecules the negative ions are produced by loss of a proton. We have produced beams of fully deuterated species of the first two ions, and are exploring sources of the latter species.

We have also learned how to deuterate Ti foils and have assembled a detection system using a transmission geometry. This has considerably higher geometric efficiency than the geometry used by the Brookhaven group. A 0.5 mil deuterated foil is followed by a thin Al absorber foil and a large-area silicon surface barrier detector. This system has been tested with a deuteron beam from our injector deck, and the excitation function for the D+D reaction has been measured between 100 and 250 keV. We have also demonstrated the capability of magnetically suppressing deuterons which might be produced by molecular breakup in or prior to the acceleration column when molecular ion beams are used. Such deuterons could cause spurious events.

A major limitation to our work so far has been the electrostatic potential through which we accelerate the ions. Our injector deck was designed to be elevated to 300 keV, and was successfully tested at that voltage. The isolation transformers have proved unreliable, and one of the transformers sparked down at 230 kV during one of our experiments. Although no permanent damage was done to the transformer, a junction box and cabling was destroyed. A new isolation transformer is under construction. Until this spare transformer is successfully tested we are limited to operation at 200 kV, and most of our efforts at present are directed towards source and detector improvements.

---

[1] R.J. Beuhler, G. Friedlander, and L. Friedman, Phys. Rev. Lett. 63, 1292 (1989).

[2] R.J. Beuhler, Y.Y. Chu, G. Friedlander, L. Friedman, and W. Kunnmann, J. Phys. Chem. 94, 7665 (1990).

2.4 Elastic and Inelastic Scattering of ^{6,7}Li on ^{12}C at 10–15 Mev/Nucleon

W.J. Braithwaite,* J.G. Cramer, S.J. Luke, B.T. McLain, D.J. Prindle and D.P. Rosenzweig

We have continued our study of the scattering of loosely bound projectiles at 10–15 MeV/nucleon, looking for unique optical model potentials, nuclear rainbow scattering, and the effects of breakup on the elastic and inelastic channels. We have taken data for 87 MeV ^{6}Li + ^{12}C from 4° to 100° in the center of mass and for 87 MeV ^{7}Li + ^{12}C from 4° to 56°. We also have ^{7}Li cross sections out to 72 ° but the first excited state of ^{7}Li was not resolved in that data.[1] Very recently we took more ^{7}Li date extending to 85°, which we have just begun to analyze.

Unique potential well depths can be found in optical model analyses of elastic cross sections if the data is sensitive to the potential inside the surface region. This requires data out to very large angles at projectile energies high enough to probe the area where nuclear refraction is dominant. Our ^{6}Li data in Fig. 2.4-1 show evidence that we have achieved this. Diffractive oscillations due to interference between the roughly equal nearside and farside scattering amplitudes die out at around 60° and the farside amplitude dominates beyond this angle. The presence of a slight bump in the large angle data is indicative of a nuclear rainbow due to incomplete absorption inside the surface region, which should make the data sensitive to the potential at smaller radii. Data from another group at 210 MeV out to 61° is similar to ours except that the higher energy makes it compressed in angle so that the diffractive oscillations die out at about 25°.[2] Their analysis showed that the data beyond 30° selected a unique potential from several that fit the data out to 29° equally well. We believe our data from 60° to 100° will select a unique potential at 87 MeV and we will investigate this and the radial range over which our data is sensitive to the potential.

We also have inelastic data for the first few excited states of the ^{12}C target and the ^{6}Li and ^{7}Li projectiles. Analysis of higher energy data seemed to show that breakup played a large role in the elastic and inelastic scattering and by taking it into account in coupled channel calculations the various cross sections could be fit reasonably well with just one adjustable parameter.[3] Our data should provide a further test of these results. The data we took this past year reflected significant improvements in beam tuning with the booster. We had peak currents of 600 to 700 nA lasting a few hours and steady currents of 300 nA for many hours. The beam stability kept the angular resolution due to beam angle and beam spot position under 0.03°. Using the rebuncher for the first time, we obtained a total energy resolution, with a nickel target, of 125 KeV in our silicon telescope detector. This allowed excellent separation of the first excited state of ^{7}Li as shown in Fig. 2.4-2. We are very pleased with these improvements and plan to extend our ^{7}Li data to large angles and to use other projectile-target combinations as soon as possible.

---

*Department of Physics and Astronomy, University of Arkansas at Little Rock, Little Rock, AK 72204.

[1] Nuclear Physics Laboratory Annual Report, University of Washington (1989) p. 16.

[2] A. Næsen *et al.*, Phys. Rev. C **37**, 132 (1988).

[3] K. Katori *et al.*, Nucl. Phys. A **480**, 323(1988).

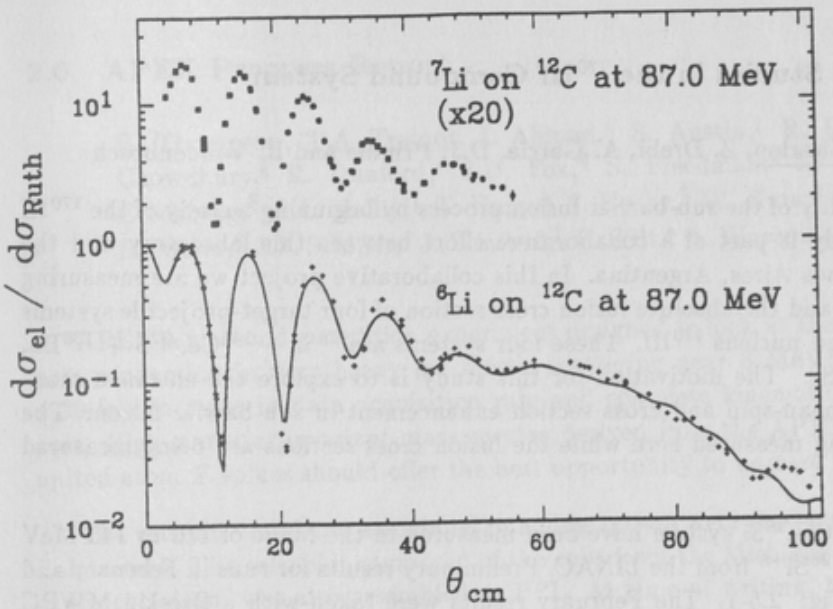

Figure 2.4-1. Elastic scattering angular distributions for 87.0 MeV ^{7}Li + ^{12}C and for 87.0 MeV ^{6}Li + ^{12}C with a preliminary optical model fit.

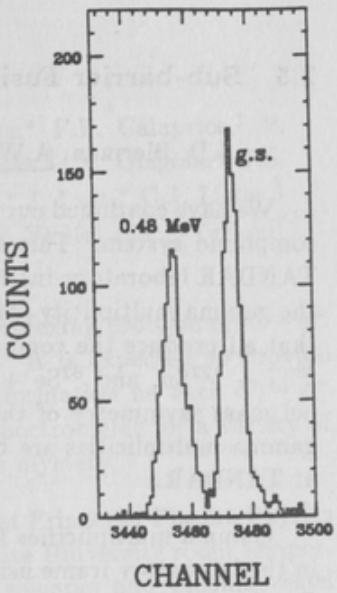

Figure 2.4-2. Energy spectra for 87.0 MeV ^{7}Li + ^{12}C at 12.5° in the lab.

2.5 Sub-barrier Fusion Studies in the ^{170}Hf Compound System

J.D. Bierman, A.W. Charlop, Z. Drebi, A. García, D.J. Prindle and R. Vandenbosch

We have continued our study of the sub-barrier fusion process by beginning a study of the ^{170}Hf compound system. This study is part of a collaborative effort between this laboratory and the TANDAR laboratory in Buenos Aires, Argentina. In this collaborative project we are measuring the gamma multiplicity (M_γ) and the absolute fusion cross section of four target-projectile systems that all produce the compound nucleus ^{170}Hf. These four systems are ^{28}Si + ^{142}Ce, ^{32}S + ^{138}Ba, ^{48}Ti + ^{122}Sn, and ^{82}Se + ^{88}Sr. The motivation for this study is to explore the entrance channel mass asymmetry of the mean-spin and cross section enhancement in sub-barrier fusion. The gamma multiplicities are being measured here while the fusion cross sections are being measured at TANDAR.

Gamma multiplicities for the ^{28}Si system have been measured in the range of 110 to 145 MeV in the laboratory frame using ^{28}Si^{+8} from the LINAC. Preliminary results for runs in February and October 1990 are shown in Fig. 2.5-1. The February results were taken with a Breskin MWPC gas evaporation residue detector, while the October results were taken with a solid state silicon evaporation residue detector. The inconsistencies between the two sets of data are now being investigated. Also a first measurement of M_γ for the ^{48}Ti system in the range of 170 to 215 MeV in the laboratory frame has been done, but statistics are poor due to source problems. We also participated in the fusion cross section measurements preformed at TANDAR in August 1990. The fusion excitation functions of the ^{28}Si and ^{48}Ti systems were measured over the same energy ranges as our M_γ measurements. They also measured the fusion excitation function for the ^{32}S system from 115 to 160 MeV in the laboratory frame. These cross section data are currently under analysis at TANDAR.

We currently plan to do M_γ and fusion cross section measurements for the ^{82}Se system in early 1991. We also plan to make more measurements of the ^{48}Ti system and begin work on the ^{32}S system in 1991.

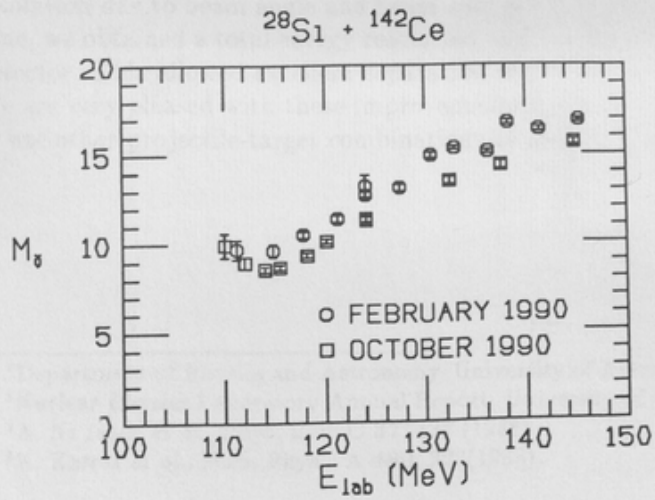

Figure 2.5-1. Gamma multiplicities as a function of laboratory energy for ^{28}Si + ^{142}Ce.

2.6 APEX Progress Report

B. Thompson, T.A. Trainor, I. Ahmad,* S. Austin,† R. Betts,* F.P. Calaprice,‡ P. Chowdhury,§ R. Dunford,* J.D. Fox,¶ S. Freedman,* S. Gazes,‖ B. Glagola,* J.S. Greenberg,§ A.L. Hallin,‡ T. Happ,* E. Kashy,† W. Kutschera,* J. Last,* C.J. Lister,§ M. Maier,† J.P. Schiffer,* J. Winfield,† P. Wilt,* A. Wuosmaa,* F. Wolfs‖ and J. Yurkon†

APEX is a second generation experiment designed to look at the perplexing problem of $e^+ - e^-$ pair production in very heavy ion elastic scattering near 6 MeV/u.[1] It is expected to provide a 20-fold increase in data acquisition rate and complete kinematic information on each $e^+ - e^-$ pair. High-statistics invariant mass spectra derived from the APEX spectrometer for a variety of united-atom Z values should offer the best opportunity to unravel this mystery.

The vacuum vessel and associated pumping system were produced at Princeton Plasma Physics Laboratory. The solenoid, composed of the coils from the Michigan State University room temperature cyclotron, was also assembled at PPL. At time of writing, the solenoid and vacuum vessel had just arrived (March 12) at Argonne and were being installed (see Fig. 2.6-1).

Prototype bars for the NaI detector arrays to be assembled at Yale have been accepted and a production run is in progress to complete the arrays. Each of the bars is a position sensitive γ detector used in an array to determine hit positions of positrons on the silicon detector array from the annihilation photons. The prototype performance is slightly worse than specified but Monte Carlo studies indicate that this will have negligible impact on spectrometer performance.

A prototype position sensitive heavy ion PPAC detector fabricated at MSU has met specifications and production of the balance of eight total large-area detectors is proceeding. This array will detect scattered heavy ions in the angular region 20–70° in the lab, and at nearly all azinuthal angles.

The data acquisition system, based on LeCroy 4300B FERAs, will read out 216 silicon array channels and 48 NaI array channels in addition to the heavy ion detector system. The acquisition software is based on the DAPHNE system developed at Argonne. The APEX acquisition system integration is being performed at Rochester.

The rotating target and vacuum lock system were produced at Florida State University and have recently arrived at Argonne. The target holder consists of a thin G-10 wheel divided into four quadrants and connected by drive belt to a motor external to the APEX vacuum vessel. The wheel position is synchronized by LED sensor to the chopped heavy ion beam.

The two silicon detector arrays consist of 72 detectors each in 12 rings of six detectors. A

*Argonne National Laboratory, Argonne, IL 60439.
†Michigan State University, East Lansing, MI 48824.
‡Princeton University, Princeton, NJ 08543.
§Yale University, New Haven, CT 06520.
¶Florida State University, Tallahassee, FL 32306.
‖University of Rochester, Rochester, NY 14627.

[1] Nuclear Physics Laboratory Annual Report, University of Washington (1990), p. 41.

detector element is 3 cm long and approximately 1 cm wide with a slight keystone shape. Each detector is divided into three segments for a total of 216 segments on each array. Readout is by copper-coated kapton strip lines. The detector depletion depths are ~1 mm.

Prototype silicon detectors are still being evaluated. The desired properties are certainly attainable within the present detector technology. The Norwegian firm SI has, in some cases greatly exceeded the minimum specifications, but consistency in detector fabrication seems to be a problem. The British firm Micron has consistently met specifications. A partial order has gone out to Micron. Argonne has developed the detector specifications and quality assurance program and has designed the detector mounting system. The alignment and cooling aspects of the silicon array support system were developed in a joint Argonne-University of Washington effort.

The silicon array is to be cooled with nitrogen gas at ~100K. Such cooling improves silicon detector time and energy resolution to required levels. The gas is contained around the silicon array by a kapton shroud.[2] The shroud is 39 cm long and 5 cm diameter. The aluminized kapton is 8μm thick. The kapton tube is terminated by acrylic flanges on each end. Armstrong A-12 epoxy in a cryogenic ratio is used to form the tube seam and the flange connections. The aluminized shroud is connected to APEX ground to serve as an EM shield for the silicon array. The shroud design was developed at Washington. Various prototypes have been successfully pressure tested, and the final models are in production.

Silicon array cooling is provided by a liquid nitrogen boil-off system developed here (see Sec. 10.4) Gas at ~100K is delivered to each array at flows up to 1 atm-l/s. The return gas is heated to room temperature and pumped through a throttle valve by a high-speed mechanical pump. Shroud pressure will be ~150 Torr.

In addition to the primary detector systems the APEX spectrometer requires various monitor systems. Beam energy, timing properties, and target condition are monitored by a pair of high resolution ion chambers (see Sec. 10.3) and a PPAC. These detectors were developed at Washington. The ion chambers should have resolution for 1.4 GEV uranium well under 0.5% based on studies here with a variety of heavy ion beams and improved detector designs. The contribution to resolution from the detectors is then comparable to or less than that from the target. Additionally the beam position on target is monitored by four scintillator/PIN diode combinations at 11° and 17°. Especially in the vertical plane such information is essential because of beam bending in the spectrometer magnetic field.

At the present rate of progress, beam should be available in late April, and operation with a subset of silicon detectors should be possible in late June. At that point calibration procedures for the spectrometer can begin.

[2]Nuclear Physics Laboratory Annual Report, University of Washington (1990), p. 24.

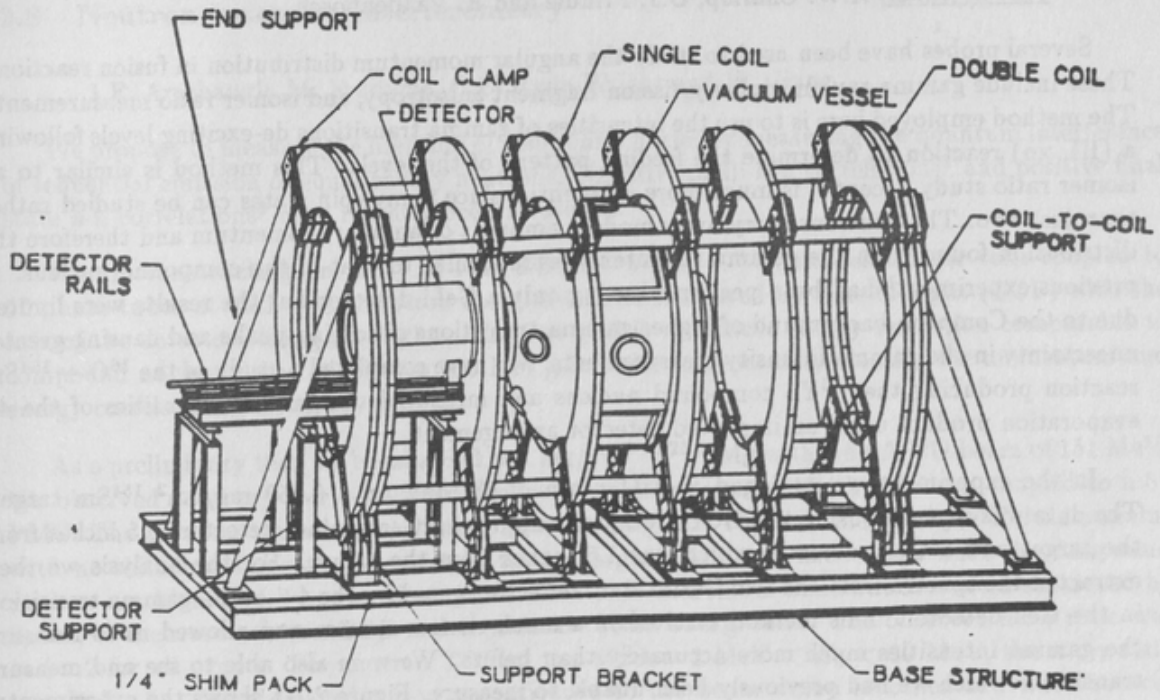

Fig. 2.6-1. APEX spectrometer assembly.

2.7 Rotational State Populations in Near-Barrier Fusion

J.D. Bierman, A.W. Charlop, D.J. Prindle and R. Vandenbosch

Several probes have been used to study the angular momentum distribution in fusion reactions. These include gamma ray multiplicity, fission fragment anisotropy, and isomer ratio measurements. The method employed here is to use the intensities of gamma transitions de-exciting levels following a (HI, xn) reaction to determine the feeding pattern of the levels. This method is similar to an isomer ratio study except it is much more differential since many spin states can be studied rather than just two. The neutrons carry away modest amounts of angular momentum and therefore the distribution found from the gamma ray intensities is similar to that of the compound nucleus. A previous experiment[1] had been performed using only a GeLi detector but the results were limited due to the Compton background of higher gamma transitions obscuring peaks and causing greater uncertainty in the gamma intensity measurements. We have completed a study of the $^{16}O + ^{154}Sm$ reaction producing the ^{170}Yb compound nucleus and measured the gamma intensities of the 4n evaporation product using an improved detector arrangement.

In the experiment we impinged an ^{16}O beam of 68 MeV on a 0.450 mg/cm^2 ^{154}Sm target. The data was recorded using two BGO Compton-suppressed Germanium detectors 5.5 inches from the target and a GeLi detector which was 1.5 inches from the target. For the analysis we then extracted the spectra from the two Germanium detectors gated by the $4+ \rightarrow 2+$ gamma transition in the Geli detector. This method resulted in a much cleaner spectra and allowed us to measure the gamma intensities much more accurately than before. We were also able to see and measure transitions which we had previously been unable to measure. Figure 2.7-1 shows the experimental gamma intensities plotted against the initial angular momentum values. We are currently planning a calibration experiment using $^{4}He + ^{166}Er$ to produce the same compound nucleus. This will be used to confirm the statistical model calculations relating the initial compound nuclear spin distribution to observed rotational state populations.

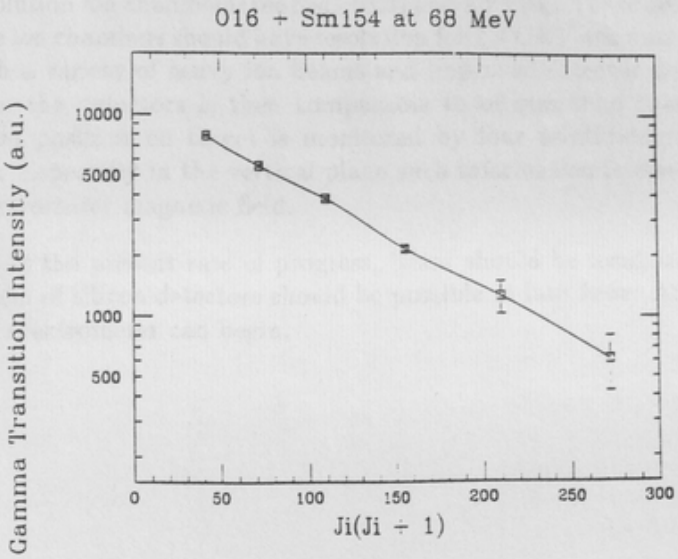

Figure 2.7-1. Gamma transition intensity corrected for detector efficiency and internal conversion versus initial angular momentum.

[1] R. Vandenbosch, B.B. Back, S. Gil, A. Lazzarini, A. Ray, Phys. Rev. C **28**, 1161 (1983).

2.8 Neutron Intensity Interferometry

J.F. Amsbaugh, M. Frodyma, C.E. Hyde-Wright and W. Jiang

We propose to measure the lifetimes of compound nuclei by measuring the quantum interference of sequential emission of equal energy neutrons. Negative pauli n-n correlations[1] and positive final state p-n correlations[2] have recently been measured.

We are constructing an array of four BC501A 5"ϕ × 10" liquid scintillator cells coupled to 5" photo-tubes at each end. Neutron energies will be measured by time-of-flight (TOF) with the axis of the detectors along the flight path. Our goal is to achieve energy resolution comparable to compound nuclear decay widths ($\approx$ 100 KeV), in order to separately identify the momentum and energy correlations[3] for the first time.

As a preliminary test, we bombarded $\approx$ 1 mg/cm^2 ^{24,25,26}Mg with a 6 nA ^{18}O beam of 151 MeV. We observed neutrons and γ-rays in a liquid scintillator detector 5"ϕ by 2" deep coupled to a 5" PMT. The detector was situated 220 cm from the target at 75° and shielded by a 2" lead annulus with no shielding along the line-of-light to the target. Neutrons and γ-rays from the compound nucleus are identified by pulse shape discrimination. Individual linac bunches were separated by 2μsec, to measure neutron TOF and to measure room background. The observed $n:\gamma$ ratio was $\approx 1:2$ for all events. For neutron TOF in the window 2 MeV $< E_n <$ 30 MeV, the $n:\gamma$ ratio was $\approx 5:1$. These delayed γ-rays we attribute to the beam dump or other activation sources in the room. We placed a software cut on pulse height corresponding to a 0.5 MeV electron. This effectively precludes detection of neutrons below 2 MeV. For flight times longer than that corresponding to E_n = 2 MeV, the neutron and γ-ray time spectra were flat, corresponding to a room activation background dependent only on the average current. This background, projected back into the timing window 2MeV $< E_n <$ 30 MeV yields a neutron background of less than 1% in our spectra.

We have normalized our measured rates to expected rates with our larger detectors. With 100 nA ^{18}O on 1 mg/cm^2 ^{26}Mg, we expect a rate of 200/sec/detector for 2 MeV $< E_n <$ 30 MeV and a coincidence rate of 1 Hz. If the neutron cascade is completely incoherent then we expect a coincidence rate in a bin of $\Delta E < 100 KeV$ of 2.0/Hr.

In order to achieve our desired energy resolution, we must define the neutron scattering vertex in the detector by a combination of timing from the two ends and the amplitude ratio from the two ends. For the 1.06 MeV compton edge of the 1.3 MeV γ-rays from a ^{22}Na source, by smearing the ideal compton edge with gaussian resolution to fit the spectrum we observed, we deduce the energy resolution is better than 5.9%. This implies at least 290 photo-electrons are collected. Based on a monte-carlo simulation of light collection in a diffuse reflecting cylinder, we expect that if a neutron converts at one end of the scintillator the ratio of the photons collected in the two ends will be 4:1. However the total light collected will be nearly independent of position of neutron conversion. With photo electron statistics of better than 5.9% we expect to localize the neutron longitudinally to 3 cm FWHM.

---

[1] W. Dünnweber, *et al.*, Phys Rev Lett, **65** (1990) 297.

[2] R.A. Kryger, *et al.*, Phys Rev Lett, **65** (1990) 2118.

[3] S.E. Koonin, W. Bauer, A. Schäfer, Phys. Rev. Lett. **62**, 1247 (1989).

3 ASTROPHYSICS

3.1 'Missing' levels in ^{18}Ne and Breakout from the Hot CNO Cycle

E.G. Adelberger, N. Bateman,* A. García, K.I. Hahn,* P.V. Magnus, D.M. Markoff, P.D. Parker,* M.S. Smith† and K.B. Swartz

Wiescher, Görres and Thielemann[1] suggested that a 'missing' $J^\pi = 3^+$ level in ^{18}Ne should occur at $E_x \approx 4.33$ MeV, only ≈410 keV above the ^{17}F+p threshold. They noted that this level would provide an s-wave resonance in the ^{17}F(p,γ) reaction, greatly increasing its thermonuclear reaction rate. This, in turn, would have a pronounced effect on the production of ^{17}O and ^{18}O in explosive stellar environments.

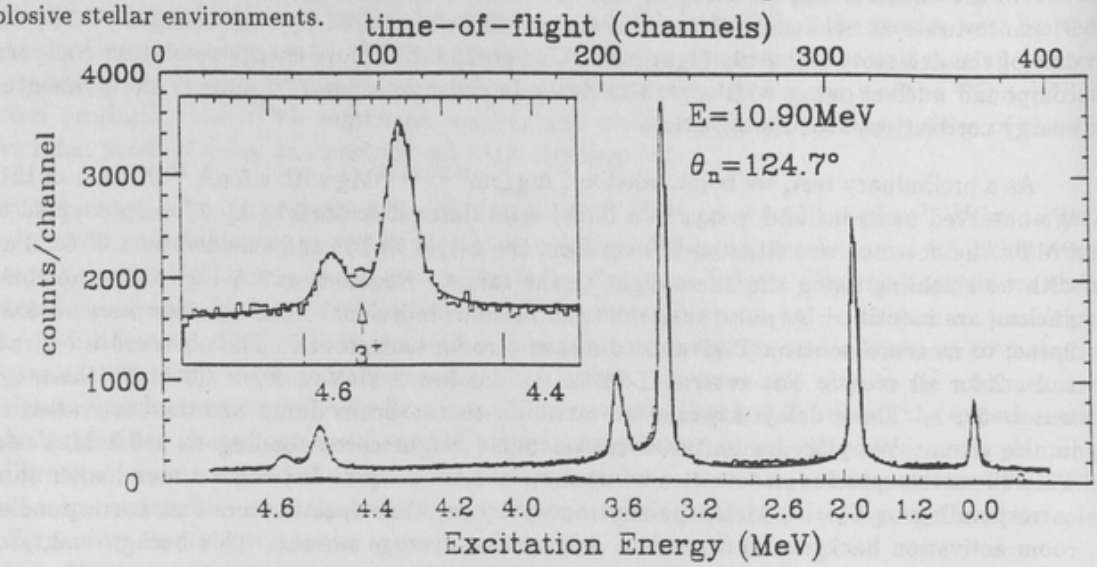

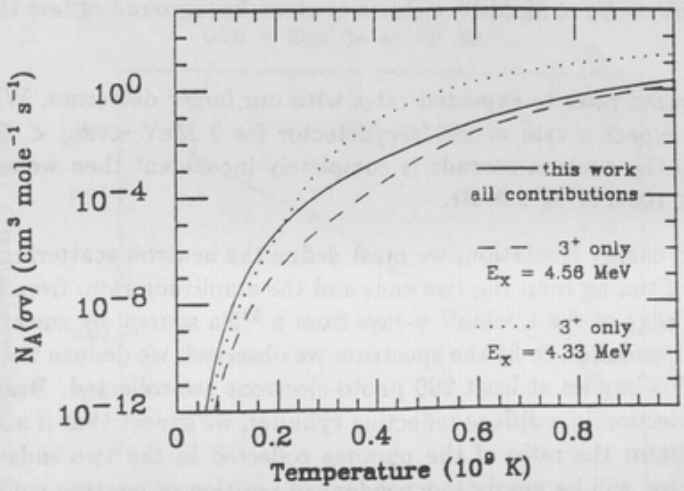

We have successfully concluded our search for the 3^+ level in ^{18}Ne using the ^{16}O(^{3}He, n) reaction.[2] As we show in our time of flight spectrum in the figure on the top, the 3^+ level occurs at $E_x = 4.561 \pm 0.009$ MeV, ≈230 keV higher than suggested. The figure on the bottom shows the effect of our finding on the rate of the ^{17}F(p,γ) reaction and makes a comparison with previous estimations.

*Yale University, A.W. Wright Nuclear Structure Laboratory, New Haven, CT 06511.
†California Institute of Technology, W.K. Kellogg Radiation Laboratory, Pasadena, CA 91125.

[1] M. Wiescher *et al.*, Astrophys. J. **326**, 384 (1988).
[2] A. García *et al.*, Phys. Rev. **C43**, 2012 (1991).

3.2 ^{37}Ca β-decay: Implications for the Efficiency of the ^{37}Cl ν-detector and the Quenching of the Gamow-Teller Strength

E.G. Adelberger, A. García, P.V. Magnus, D.M. Moltz,* H.E. Swanson, O. Tengblad† and D.P. Wells

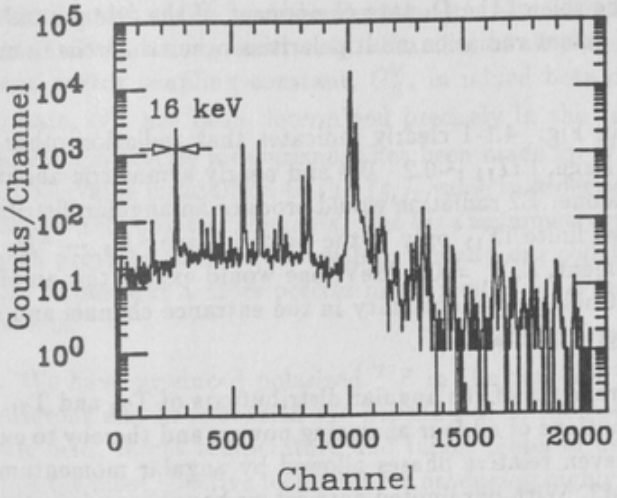

We have recently measured the distribution of the axial vector strength ($B(GT)$) in the decay of ^{37}Ca. A clean measurement of the GT strength distribution provides[1] a way for calibrating the efficiency of the ^{37}Cl ν-detector and, due to the particularly high Q value, an excellent probe for testing the quenching of the GT strength. Production of this nucleus without contaminants proved to be very difficult and earlier trials[2] showed that the only way to make a reliable measurement would be to use a pure radioactive ^{37}Ca beam. Using the Isolde III on-line isotope separator at CERN we were able to obtain a 60 keV beam of ^{37}Ca with an intensity of $\sim$ 65! We developed an apparatus that detected β-delayed protons in coincidence with γ-rays to identify decays that left the recoiling nucleus in an excited state.

Our detection system consisted of: a) A particle telescope (using an ultrathin gas counter[3]) that allowed us to discriminate β's from protons and attain an energy resolution of $\approx$ 16 keV for protons in the range from 0.5 MeV to 6.0 MeV and b) Two NaI detectors covering 65% of 4π. The figure on the top shows our β-delayed proton spectrum and the one on the bottom the integrated $B(GT)$. Our results provide a secure basis for calculating the efficiency of the ν-detector but they also show a strong disagreement with shell-model predictions and do not support the claimed 'quenching' of GT strength. Analysis of the results is continuing.

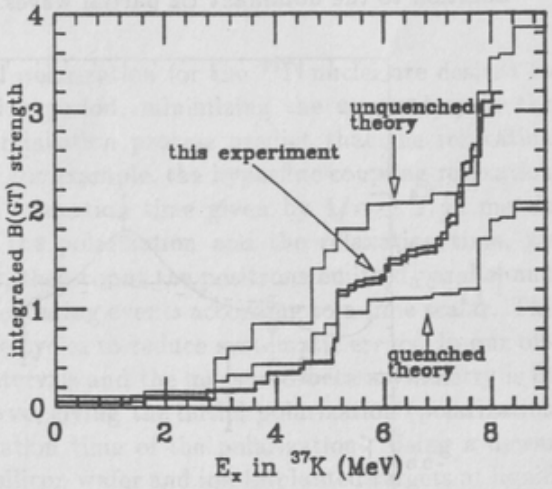

*Lawrence Berkeley Laboratory, 1 Cyclotron Road, Berkeley, Ca 94720.
†PPE Division, CERN, CH-1211, Geneva 23, Switzerland.

[1]E.G. Adelberger and W.C. Haxton, Phys. Rev. **36**, 879 (1987).
[2]A. García *et al.*, Phys. Rev. **C42**, 775 (1990).
[3]This report, Section 10.1.

4 POLARIZATION

4.1 Polarized Radiative Capture in ^{2}H($\vec{d},\gamma$)^{4}He at Low Energies

C.A. Gossett, M.S. Kaplan, S.J. Luke, P.V. Magnus, S.P. Van Verst and D.P. Wells

We have continued our angular distribution measurements of the cross section and analyzing powers for ^{2}H($\vec{d},\gamma$)^{4}He at E_d = 1 MeV, discussed previously in last year's annual report.[1] The motivation for our work is to examine the role of the D-state component of the ^{4}He ground state in this reaction and to quantify to what extent radiation multipolarities other than the dominant E2 contribute to the reaction.

The vector analyzing power shown in Fig. 4.1-1 clearly indicates that radiation other than E2 is present. The measured values are large, $|\, iT_{11}\,| \sim 0.2$ - 0.4 and nearly symmetric about 90°. These data cannot be reproduced by E2 alone. E2 radiation would produce an angular distribution *antisymmetric* about 90° and would give finite iT_{11} only if the partial wave $^5D_2 \rightarrow {}^5D_0$ were present. At the low energy of our experiment, $E_{c.m.}$ = 0.5 MeV, one would expect this amplitude to be small for two reasons; suppressed Coulomb penetrability in the entrance channel and small expected D-state component in the ^{4}He ground state.

We have also obtained partial measurements of the angular distributions of T_{20} and T_{21}. Our plan is to obtain complete angular distributions of all four analyzing powers and thereby to extract the eight partial wave amplitudes and seven relative phases allowed by angular momentum and parity conservation for E1, M1, E2, and M2. With our limited data set we have begun investigation of the matrix elements assuming f- and g-wave capture to be negligible at low energy and d-wave capture to the D-state component of the ^{4}He ground state to be small. The current data set is well reproduced when $\sim$ 10% of the cross section in the form of E1, p-wave capture is included in addition to the dominant E2 partial waves.

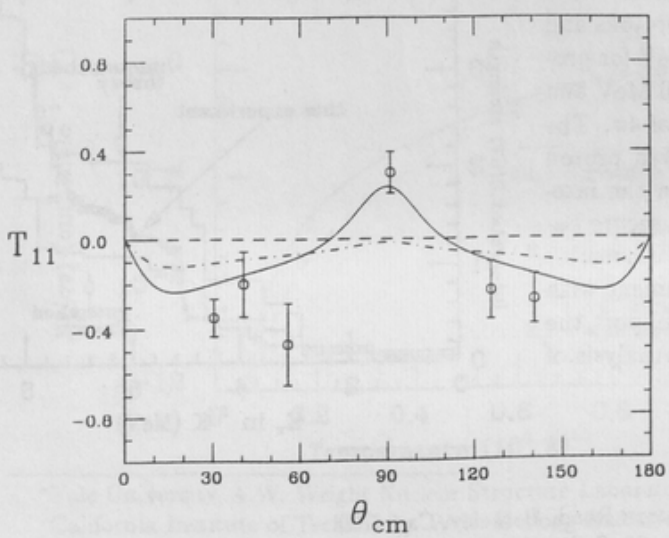

Fig. 4.1-1. Vector analyzing power measurements in ^{2}H($\vec{d},\gamma$)^{4}He at E_d = 1 MeV. The curves are fits to the present data set including measurements of the cross section, iT_{11}, T_{20}, and T_{21}. The dashed curve is for E2 capture only, with the $^1D_2 \rightarrow {}^1S_0$ and $^5S_2 \rightarrow {}^5D_0$ partial waves contributing, and indicates that the vector analyzing power is identically zero for this case. The solid curve is the best fit to the data set when the E1 partial wave, $^3P_1 \rightarrow {}^1S_0, {}^5D_0$ is included in addition to the two E2 amplitudes above. The dot-dashed curve is a fit when instead of E1, the M2 partial wave, $^3P_2 \rightarrow {}^1S_0, {}^5D_0$ is included in addition to E2.

[1] Nuclear Physics Laboratory Annual Report, University of Washington (1990) p. 24.

4.2 Production of Polarized ^{29}P

J.K. Eisenberg, C.A. Gossett, M.S. Kaplan and D.M. Markoff

The β-decay vector coupling constant, G_β^V, has been determined for a number of $0^+ \rightarrow 0^+$ allowed transitions. In these decays, the Gamow-Teller matrix element vanishes, allowing the determination of G_β^V from the Fermi matrix element and measurement of the $ft_{1/2}$ value. However, these transitions represent only a fraction of all β decays. There is interest in measuring the β-decay vector coupling constant, G_β^V, in mixed beta decay transitions in $T = 1/2$ mirror nuclei. To date, G_β^V has been determined precisely in the cases n $\rightarrow$ p, ^{19}Ne $\rightarrow ^{19}$ F, and ^{35}Ar $\rightarrow ^{35}$ Cl while a less precise measurement has been made for ^{29}P $\rightarrow ^{29}$ Si. For mixed beta decays, one needs an observable in addition to the $ft_{1/2}$ value in order to separate the contributions from Fermi and Gamow-Teller matrix elements. The beta asymmetry parameter A, measured in decays of polarized nuclei provides such an observable. We and our collaborators from Argonne National Laboratory plan to perform a more precise measurement of A for the decay ^{29}P $\rightarrow ^{29}$ Si as well as for other systems.

We have produced polarized ^{29}P in the reaction ^{28}Si$(\vec{\mathrm{d}}, \mathrm{n})^{29}$P, using 3 MeV vector-polarized deuterons and have studied the dependence of the polarization on the beam energy, holding magnetic field, target temperature and target material using silicon wafer and ion-implanted targets. Once the most effective technique for producing highly polarized ^{29}P has been determined, the beta asymmetry will be measured in an apparatus constructed by collaborators at Argonne, as described in our previous report.[1] The target polarization, P, will be determined by measuring the product PA for the pure Gamow-Teller decay to the first excited state of ^{29}Si, for which A can be calculated exactly. This decay will be identified by detecting positrons in coincidence with gammas emitted in the decay to the ^{29}Si ground state.

A long spin relaxation time, τ, and large initial polarization for the ^{29}P nuclei are desired to maximize the average polarization over the counting period, minimizing the uncertainty in the measured value of A. Simple models of the spin-relaxation process predict that the relaxation time should lengthen with decreased temperature.[2] For example, the hyperfine coupling relaxation mechanism has a temperature dependence for the relaxation time given by $1/\tau \sim T$ in metals and $1/\tau \sim T^{1/2}$ in semiconductors. To measure the polarization and the relaxation time, we irradiate our target for 4 seconds, wait for 100 msec, then count the positrons emitted parallel and antiparallel to the beam spin direction for 8 seconds, routing events according to a time scalar. The incident deuteron polarization is flipped in alternate cycles to reduce systematic errors. In our off-line analysis, the counts are binned into 1 second intervals and the measured beta asymmetry is fit as a function of time with an exponential decay curve, giving the initial polarization (polarization at the start of the counting period) and the relaxation time of the polarization. Using a dewar with a vacuum feed-through, we have studied both silicon wafer and ion-implanted targets at liquid nitrogen, room, and slightly elevated ($\approx$ 355K) temperatures.

For the silicon wafer targets at room temperature we found an initial value of PA of $(2.01 \pm 0.08)\%$ and a relaxation time of (14.0 ± 3.2) seconds. Surprisingly, at liquid nitrogen temperature ($\approx$ 77K) we observed an initial PA of $(0.96 \pm 0.15)\%$ and a relaxation time of (4.8 ± 1.8) seconds,

[1] Nuclear Physics Laboratory Annual Report, University of Washington (1990), p. 26.

[2] A. Abragam, *The Principles of Nuclear Magnetism*, Oxford, Clarendon Press, 1961.

contrary to expectation. Because of this result, we heated our target to ≈ 355K and measured an initial PA of $(2.31 \pm 0.15)\%$ and a relaxation time of (12.1 ± 4.0) seconds. Thus we found a higher average polarization for the heated target than for the room-temperature target.

Ion-implanted targets were made using 200 keV ^{28}Si momentum-analyzed ions accelerated by the elevation potential of the ion source platform. The ions were stopped in platinum foils 0.1 mm thick mounted ~ 2 m downstream of the source platform. A collimator was inserted in front of the targets and a liquid nitrogen cold trap was placed upstream. The beam was swept simultaneously horizontally and vertically using electrostatic steerers in order to produce a target of uniform thickness.

By making targets of ^{28}Si implanted in platinum, we expect several benefits. First, isotopic purity will eliminate backgrounds from the other silicon isotope reaction products. Also, if the hyperfine coupling mechanism predominates for ^{29}P in platinum, we expect to see the relaxation time lengthen with reduced temperature. Unfortunately in our initial tests the ^{29}P produced in the implanted targets exhibited no asymmetry at either room- or liquid nitrogen-temperature. We have some evidence for contributions in these targets from contaminant beta emitters. By subtracting a spectrum from a silicon wafer target, normalized to the tail area of the ion-implanted target spectrum, we observe a spectrum with a lower endpoint energy than for ^{29}P decay. We plan to examine the targets to look for possible sources of the background and modify the scheme for making ion-implanted targets to further reduce contaminants.

4.3 Polarized Protons from the ^{59}Co(^{3}He,$\vec{p}$) Reaction

M.D. Clarke,* M. Frodyma, W.G. Weitkamp and D.I. Will

In last year's Annual Report[1] we described a study of the polarization $P_{y'}$ of protons from the ^{59}Co(^{3}He,$\vec{p}$) reaction initiated by 27 MeV ^{3}He ions. During the past year, we have added new measurements to our polarization and cross section data set and have worked out a simple explanation for the observed polarization and cross section values. Examples of cross section and polarization data at a reaction angle of 18° are shown in Fig. 4.3-1. Similar data are available at angles from 12° to 42° for polarization and from 9° to 120° for cross sections.

We assume that the protons coming from this reaction can be divided into three groups: protons from compound nucleus evaporation, protons from the breakup of ^{3}He and protons from other processes. The properties of these three groups can be used to make a crude prediction of the proton polarization.

Evaporation: the large cross section at low proton energies, predominant at back angles, is attributed to proton evaporation, which has an exponential form dependent on the nuclear temperature parameter. The shape of the evaporation curve is obtained from cross section data at an angle of 120°, where the cross section results almost entirely from proton evaporation. The spectrum of protons from evaporation at 18° is shown as a dotted curve in Fig. 4.3-1. Evaporated protons are assumed to be completely unpolarized.

Breakup: the breakup of ^{3}He causes a broad proton peak centered at roughly 1/3 of the beam energy. The cross section for breakup can be approximated with a Gaussian, parameters for which come from fitting cross section data near the peak. The resulting curve is the dashed curve in Fig. 4.3-1. An important component of the breakup peak is the ^{59}Co(^{3}He, pp) reaction,[2] which, naively, should produce protons with zero polarization, since the two protons in ^{3}He have antiparallel spins. We assume that the all the protons from ^{3}He breakup are unpolarized.

Other processes: the cross section for the remaining protons, produced by other processes such as direct deuteron stripping and preequilibrium proton emission, is obtained by subtracting the calculated evaporation and breakup cross sections from the measured proton cross section and smoothing the result. The cross section for these protons is not strongly dependent on angle. In this simple model, it is assumed that these protons give rise to all of the polarization observed.

To obtain the polarization prediction we multiply the fraction of protons due to other processes by a constant 0.32, adjusted to fit the measurements of $P_{y'}$ at all reaction angles. The curve in the polarization plot of Fig. 4.3-1 shows the results at 18°.

This simple model accounts for the general trend of the $P_{y'}$ data, although at a proton energy of 10.5 MeV the data seem to be closer to 0.1 than to zero at all angles measured. It is possible that breakup protons have a small polarization or that some other process is contributing.

The fact that the cross section due to "other processes" is not strongly dependent on angle

*The Boeing Company, Seattle, WA.

[1] Nuclear Physics Laboratory Annual Report, University of Washington (1989) p. 27.

[2] E.H.L. Aarts, R.A.R.L. Malfliet, R.J. De Meijer and S.Y. Van Der Werf, Nucl. Phys. **A425**, 23 (1984).

suggests that the polarization above E_p = 20 MeV is due to preequilibrium proton emission. An alternative process, direct stripping of a deuteron from ^{3}He, should result in a strongly forward peaked cross section.

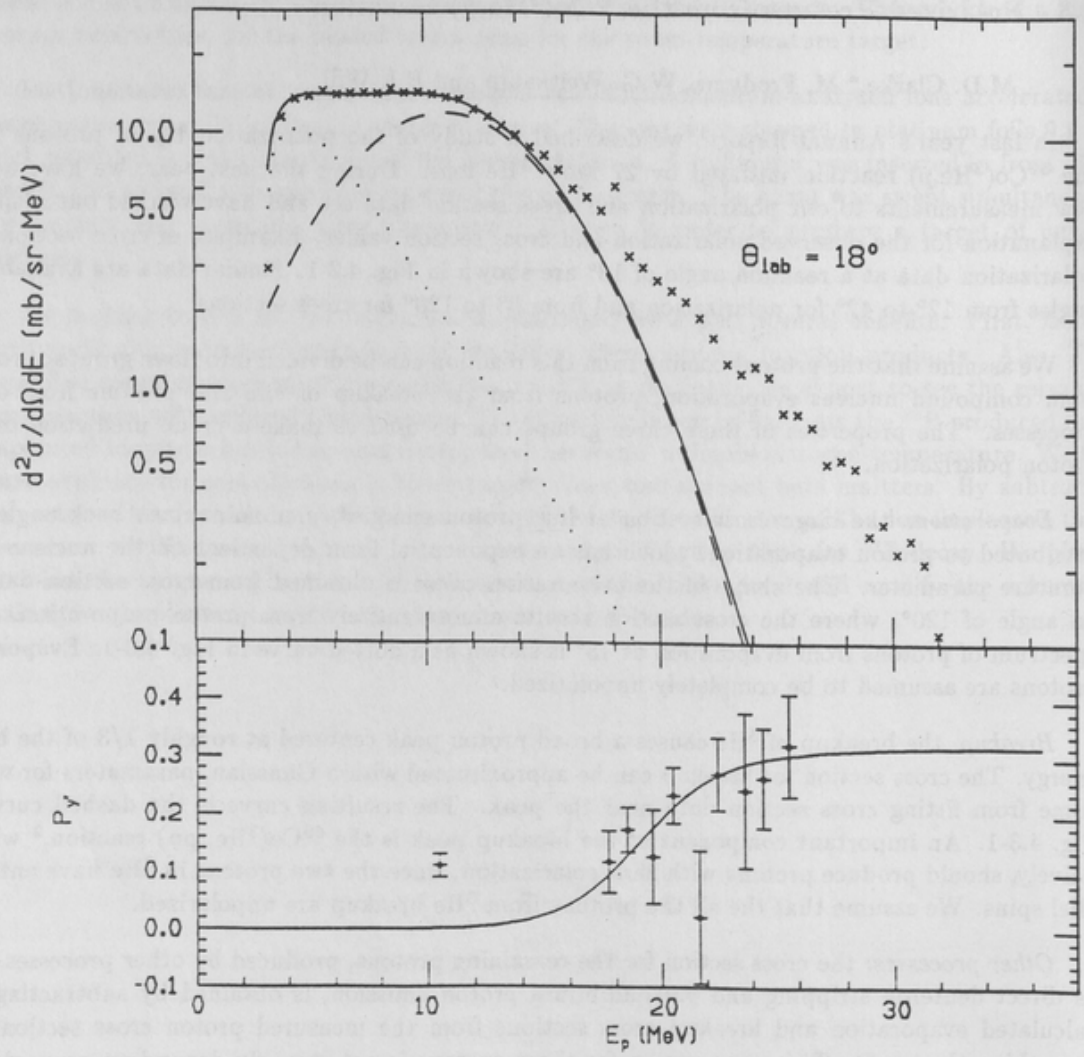

Fig. 4.3-1. Cross section and outgoing proton polarization $P_{y'}$ as a function of proton energy for the ^{59}Co(^{3}He,pX) reaction initiated by 27-MeV ^{3}He ions at a reaction angle of 18°. In the cross section plot the dotted curve shows evaporation, the dashed curve shows breakup and solid curve shows the total of evaporation and breakup. The solid curve in the $P_{y'}$ plot is described in the text.

5 FUNDAMENTAL SYMMETRIES AND INTERACTIONS

5.1 High-Precision Test of the CVC, First-Class Current, and Time-Reversal Symmetries in A=8 $\beta^{\pm}$ Decays

E.G. Adelberger, L. De Braeckeleer, K. Snover and K.B. Swartz

We are developing an experiment to make a precision test of fundamental symmetries via the A=8 system: conserved vector current, second class currents and time reversal invariance. A description of the experiment is given in the last annual report.[1] In short the experiment requires the complete kinematic reconstruction of ^{8}Li and ^{8}B beta decays from measurement of the β and two α momenta. In the last year rapid progress has been made on the experiment. A proposal to the DOE was approved and funding for the project has been received. In the last year work has centered on overcoming the technically difficult parts of the experiment. These are the four α detectors, five β detectors and radioactive isotope production. Progress as briefly described below has been made on all three.

The alpha detector is a low gas pressure wire counter of the Breskin type.[2] The criteria for choosing this type of detector is the need for a fast, position sensitive detector for low energy α particles. A prototype of the gas detector with an active area of 2cm x 2cm has been built. In tests with a ^{241}Am α source the required position resolution of 1mm and timing resolution of 1 nanosecond of the detector were achieved. The first full scale detector with an active area of 20cm x 20cm is currently under construction. The detector should be completed and tested by Summer 91. If it performs as required the subsequent completion of the other three detectors should then progress rapidly.

A first beta detector has been constructed. The construction is straight forward but to test its performance is more difficult. The beta detector consists of a 12.5cm x 12.5cm NE104 plastic scintillator cylinder coupled to a 5 inch phototube. The beta detector scintillator is surrounded by a plastic scintillator anticoincidence shield with two 2 inch phototubes. The phototubes were glued to the plastic with Bicron BC600 glue. The complete beta counter, scintillators and phototubes, is mounted in a support. An initial test with gamma and beta sources was successful. More quantitative measurements and tests at higher β energy are still needed and will be completed shortly.

To achieve the highest possible count rate, with low background and low multiple scattering, the production and detection of the isotope decays will take place in two separate chambers. The radioactive isotope will be moved from one chamber to the other precisely and rapidly in a thin catcher foil by a 80cm "arm" attached to a stepping motor. An initial titanium arm has been constructed and a rotation in less then 0.3 seconds has been achieved. For comparision the isotopes of ^{8}Li and ^{8}B have a half life of approximately 1 second. The speed of the rotation should be improved if the mass of the arm is reduced, as it appears possible, and we learn more on tuning of the stepper motor feed back loop.

A couple of test runs to measure ^{8}Li production by α-α coincidence were undertaken. The

[1] Nuclear Physics Annual Report, University of Washington (1990) p. 31.

[2] A. Breskin *et al.*, Nucl. Instrum. Meth. **221**, 363 (1984).

measurements were very clean. The production of ^{8}Li with a 1 MeV deuterium on LiF was straight forward, and should not present an obstacle.

In the last year important milestones in the development of the apparatus have been passed and initial tests of the apparatus should occur in a year.

5.2 Experiment to Measure the PNC Spin Rotation of Cold Neutrons in a Liquid Helium Target

E.G. Adelberger, B.R. Heckel, S.K. Lamoreaux* and D.M. Markoff

Coherently scattered neutrons of positive and negative helicity states experience a different effective index of refraction in the medium, producing a rotation of the transverse spin polarization vector. This parity non-conserving (PNC) rotation can be expressed as a sum of weak interaction isovector and isoscalar meson exchange amplitudes. Discrepancy between experimental limits for the isovector pion exchange amplitude and theoretical calculations[1] motivates the study of n-α scattering in which this amplitude has a dominant contribution.[2,3]

We have completed the preliminary design for an apparatus to measure the PNC spin-rotation of transversely polarized neutrons through a liquid helium target. (See Figure 5.2-1.) The general technique for determining the spin rotation from counting neutrons emitted from a crossed polarization configuration with different settings of target position, neutron polarization (up or down), and π-coil spin precession has been previously described.[4]

The design is driven by the need to reduce systematic errors originating from axial magnetic fields that rotate the spin polarization vector. To separate out parity conserving (PC) spin rotation signals from the PNC signals, the experiment will be conducted with the target in two alternating positions located immediately in front of or behind the π-coil, which rotates the neutron spin about the vertical axis. Our four-chamber design allows both experimental configurations to be run at the same time, eliminating to first order, the time dependent effects from magnetic field drifts.

Off-axis scattering in the helium could produce target-position-dependent false signals resulting from changes in path length, and hence changes in time the neutron travels in the axial field. Previous experiments indicate that neutron scattering in the energy range of interest is nearly isotropic with a differential cross section of approximately 35mb/steradian.[5] To remove these scattered neutrons, the target chamber will be coated with nickel-copper that absorbs 4.5$\AA$ neutrons with incident angles greater than about 0.5 degrees. The guide tubes following the cryogenic target chamber will be coated with a beryllium layer which has similar absorptive properties. A rough estimate indicates that less than 1 in 10^5 of the incoherently scattered neutrons will reach the detector.

The total scattering cross section for neutrons with a wavelength of 4.5$\AA$ in liquid helium is 0.55barns[6] corresponding to a mean free path of 95cm. The constraints on target chamber size are thus limited by practical considerations and chosen to be 50cm each.

The maximum allowable axial magnetic field is determined by requiring the PC spin rotation to be less than our expected statistical error or roughly 10^{-8} radians. Taking into account the

*Department of Physics, University of Washington, Seattle, WA 98195.

[1]E.G. Adelberger and W.C. Haxton, Ann. Rev. Nucl. Part. Sci. **35**, 501 (1985).
[2]Y. Avishai Phys. Lett. **112B**, 311 (1982.)
[3]V.F. Dmitriev *et al.*, Phys. Lett. **125**, 1 (1983).
[4]B.R. Heckel *et al.*, J. Phys. (Paris) **45**, C3 (1984).
[5]P.A. Egelstaff and H. London, Proc. of Roy. Soc. **A242**, 374 (1957).
[6]H.S. Sommers Jr. *et al.*, Phys. Rev. **97** 4 855 (1955).

diamagnetism of the helium and the target position dependent scattering effects, we require the field to be less than 0.1mGauss. To achieve this, the magnetic shielding will consist of two mu-metal shielding layers outside the cryostat, and a coil of superconducting wire wrapped around the target chamber.

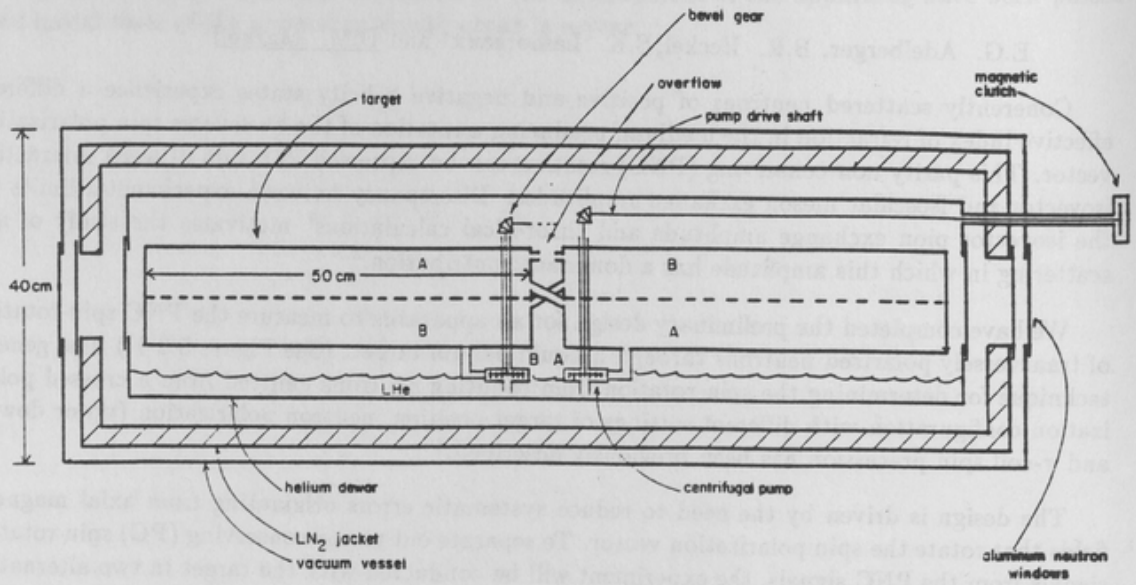

Figure 5.2-1. Preliminary design of target cryostat. The experiment is run with chambers A or B alternately filled with liquid helium.

5.3 Searching for New Macroscopic Interactions by Testing the Equivalence Principle in the Field of the Earth

E.G. Adelberger, B.R. Heckel and Y. Su

We are continuing to improve our rotating torsion balance test[1] of the weak equivalence principle in order to search for new macroscopic Yukawa interaction. Recent modifications include improvements to the autocollimator light source and cancellation of the Q_{22} gravity gradient. Our current 1-σ limits on the differential horizontal acceleration of Be/Cu and Be/Al test body pairs, are $(0.8\pm1.7)\text{x}10^{-11}\text{cm/s}^2$, and $(0.8\pm1.4)\text{x}10^{-11}\text{cm/s}^2$ respectively. In terms of the weak equivalence principle, these limits correspond to m_i/m_g(Cu)-m_i/m_g(Be)=(0.2 ± 1.0) x 10^{-11} and m_i/m_g(Al)-m_i/m_g(Be)=(0.1 ± 0.8) x 10^{-11}. Our data set new limits on composition-dependent interactions for ranges greater than 1m. For example, the limit on the 'fine structure constant' $g^2/4\pi\hbar c$ for an infinite ranged vector interaction coupled to B is $(2.0\pm2.8)\text{x}10^{-47}$. Data taking is continuing. We expect to improve these results further during the next few months.

5.4 Does Anti-matter Fall with the Same Acceleration as Ordinary Matter?

E.G. Adelberger, B.R. Heckel, C.W. Stubbs* and Y. Su

We have shown that equivalence principle experiments using electrically neutral test bodies composed of ordinary matter provide

1. cleaner (*i.e.*, null tests)
2. more general (*i.e.*, equivalent to free-fall experiments using antiprotons, antineutrons and positrons)
3. more sensitive (by many orders of magnitude)

tests of a proposed gravi-vector interaction[2] than do currently anticipated direct tests based on measuring the free-fall acceleration of antiparticles. Details of the argument have recently been published[3] in Physical Review Letters.

---

[1] E.G. Adelberger *et al.*, Phys. Rev. D **42**, 3267 (1990).

*Presently at Institute for Particle Astrophysics, Berkeley, CA.

[2] T. Goldman, R.J. Hughes, and M.M. Nieto, Phys. Lett. B**171** 217 (1986).

[3] E.G. Adelberger, B.R. Heckel, C.W. Stubbs, and Y. Su, Phys. Rev. Lett. **66** 850 (1991).

5.5 Development of a New Rotating-Source Torsion-Balance Instrument

E.G. Adelberger, J.H. Gundlach, M.G. Harris, B.R. Heckel, D.W. Sesko and H.E. Swanson

We are developing a new torsion pendulum apparatus to search for feeble macroscopic interactions via a violation of the weak equivalence principle. The instrument is designed to be sensitive to forces with Yukawa ranges down to 2cm corresponding to $m_{boson} < 10^{-5}$eV.

Contrary to previous experiments at this laboratory which searched for such a 'fifth force' using a rotating balance and a stationary source mass (the local hill, the entire earth or a 1.3 ton stationary Pb source), we will slowly and continuously rotate 3.2 tonnes of depleted Uranium around a stationary torsion pendulum. The source is approximately arranged in a semi-annulus with the closest distance to the center of the torsion pendulum being 10 cm. The source is configured to minimize unwanted gravitational gradients at the pendulum and it is counterbalanced with Pb on an $\approx$ 1m moment arm to reduce problems with 'floor tilt'. A hollow empty Al dummy mass is rotated on the opposite side to further reduce any systematic effect correlated with the position of the source.

Two different torsion pendula will be used. The first pendulum consists of a beryllium tray with initially Cu and Pb test masses arranged in a composition dipole. This configuration is maximized for its isospin content (N-Z). We expect this instrument will give a result at least 100 times more sensitive than that of our original Pb source experiment.[1] Other test body combinations probing for possible vector charges such as B-L will also be studied.

The second pendulum will carry a net electron spin polarization to search for monopole-dipole interactions proportional to $\vec{\sigma} \cdot \hat{r}$ that would macroscopically violate parity and time-reversal invariance as suggested by Moody and Wilczek.[2] This pendulum is made from Fe (100% electron spin magnetism) and SmCo (50% electron spin, 50% electron orbital angular momentum magnetism) magnets as flux return. We will employ extensive symmetry to minimize external magnetic stray fields. In addition, several layers of magnetic shielding will surround the pendulum and non-magnetic materials are used for the rotating parts of the experiment.

Noise from Brownian motion of the pendulum will be reduced by using high vacuum ($< 10^{-7}$torr) to achieve a Q of several thousand for the torsional motion. We will rotate the source mass in resonance with the torsion pendulum frequency to increase the effective observation time. We hope to reduce the effects of seismic noise with a 0.8 ton air suspension granite vibration-isolation table which will isolate the pendulum from the ground and the turntable. We are also developing a superspring mount for the fiber.

Currently, the Al vacuum chamber and inner structures, μ-metal shields, fiber mount system, W-torsion fiber, pendulum mass tray, large parts of the turntable and thermal shield, the optical readout, and the electronics have been built and are being tested. The vibration isolation is described separately in Sec. 5.6 of this report. A quartz torsion fiber is under development. The experiment will be located on the North side of the old cyclotron vault.

---

[1] C.W. Stubbs *et al.*, Phys. Rev. Lett. **62** 609 (1989).

[2] J.E. Moody and F. Wilczek, Phys. Rev. D **30**, 130 (1984).

5.6 Development of a Vibration Isolator for the Torsion Pendulum

E.G. Adelberger, J.H. Gundlach, M.G. Harris, B.R. Heckel, D.W. Sesko and H.E. Swanson

The sensitivity of the torsion pendulum described in Sec. 5.5 is currently limited by floor vibrations. This is readily seen in a day-night effect on the magnitude of the random noise observed in our data. We believe this difference to be due to the higher amount of traffic in and outside the building during the day, and are investigating methods of isolating the pendulum from vibrations which may pump its natural resonances.

The power spectrum of the earth's vibrations in the laboratory show several peaks starting at about 8 Hz whose amplitudes fall off steeply as $(1/f^2)$. Passive air suspensions used for optical tables have resonant frequencies around 1 Hz and have a transmission which falls off at $(1Hz/f)^2$. Thus, they are quite effective at isolating these higher frequencies. They do not however, provide very good stabilization of the position at lower frequencies.

While the air suspension is effective at isolation, it is subject to drift in its angular orientation. To keep this at the μ−radian level, we are using a system that actively servos the position of the table at frequencies well below the resonance.[1] The system has three TMC[2] air suspension legs supporting a large triangular granite table. The servo stabilizes the position of the table by changing the input/exhaust duty cycle of air to and from each leg. Preliminary results show a factor of 30 reduction in the peak-to-peak noise. Although this system reduces the overall seismic noise, it introduces a low frequency rocking motion of micron amplitude at the leg's resonance of 1.3 Hz, and a horizontal torsional resonance at 2 Hz. Currently, we are investigating ways of reducing the magnitude of this motion, and damping its effects on the pendulum.

A "superspring" vibration isolator is being developed as an alternative. Much smaller than the isolation table, it would suspend only the pendulum, rather than the entire apparatus. It consists of a vertical series of planar, slotted flexures, mounted to a rigid frame. The position of the lowest flexure relative to the frame is tracked capacitively, and used to magnetically servo the position of the uppermost flexure. Careful attention must be paid to the symmetry of the assembly, as well as its angular rigidity, in order to avoid any torsional motion. Prototypes are promising, and this method might work for our purposes.

[1] Jeff Greene (Personal Communication).
[2] Technical Manufacturing Corp.

6 ACCELERATOR MASS SPECTROMETRY (AMS)*

T.A. Brown, G.W. Farwell, P.M. Grootes and F.H. Schmidt†

6.1 AMS: Scientific Program

6.1.1 Studies of ^{14}C in atmospheric methane, an important greenhouse gas

This project, supported in part by a NASA grant under which P.D. Quay, School of Oceanography, is principal investigator, has reached the stage at which some interesting conclusions can be drawn, and the results to date are being published.[1] We found that the ^{14}C concentration in atmospheric methane (CH_4) collected from clean air at Cheeka Peak on the coast of the Olympic Peninsula, Washington, increased over the years 1987–89 by 1.5±0.4 pM/yr (pM expresses the sample ^{14}C concentration as a percentage of that of the modern standard). The mean value was 122 pM, in good agreement with earlier results.[1]

Mass balance calculations for methane and its isotopic forms $^{13}CH_4$ and $^{14}CH_4$ identified a source strength of 16±12% (90 Tg/yr) for fossil CH_4 and 11±14% (59 Tg/yr) for CH_4 derived from biomass burning (1 Tg equals 10^{12}g).

We plan to extend our collaboration with Dr. Quay. Continued monitoring of ^{14}C concentrations in atmospheric methane collected at clean air sites is planned to reduce the still large uncertainties in the calculated methane source strengths and to determine their latitudinal/hemispheric distribution. This will give a better understanding of the causes of the recent rapid increase in concentration of atmospheric methane.

6.1.2 Seasonal fluctuations in ^{14}C in corals

Our recently completed pilot study of ^{14}C in growth increments in annual bands in a *Pavona clavus* coral, collected in 1982 off Punta Pitt, San Cristóbal, Galápagos, shows significant seasonal variations in the ^{14}C concentrations of coral carbonate over the years 1970–1973 (Fig. 6.1-1). These seasonal ^{14}C changes seem to correlate with Galápagos sea surface temperature (SST).

In the eastern equatorial Pacific, where the Galápagos Islands are located, deeper ocean water that is cold and depleted in ^{14}C mixes with surface waters that are warm and richer in ^{14}C. During the El Niño phase of the Southern Oscillation this mixing of the deep water stops. This is reflected by the high ^{14}C and SST during the El Niño year 1972. The large seasonal changes in ^{14}C during the non-El Niño years of 1970 and 1973 indicate that significant changes in ocean mixing occur over each year under normal conditions. The ^{14}C in corals can thus be used as a tracer to study

*Our work was supported in part by NSF (Grant EAR-8115994, Environmental Geosciences Program) and by NASA (Grant NAGW-844).

†We regret the passing of our friend and colleague Professor Emeritus Fred H. Schmidt, who died on January 17, 1991.

[1] P.D. Quay, S.L. King, J. Stutsman, D.O. Wilbur, L.P. Steele, I. Fung, R.H. Gammon, T.A. Brown, G.W. Farwell, P.M. Grootes, and F.H. Schmidt, Global Biogeochemical Cycles (1991), in press.

local ocean mixing processes in the eastern equatorial Pacific and, by comparison with atmospheric El Niño/Southern Oscillation data, the air-ocean interaction that influences this mixing.

We plan to continue our collaboration with Dr. Minze Stuiver (Geological Sciences, Quaternary Isotope Laboratory) to extend the coral ^{14}C record and to determine the ocean mixing that it reflects.

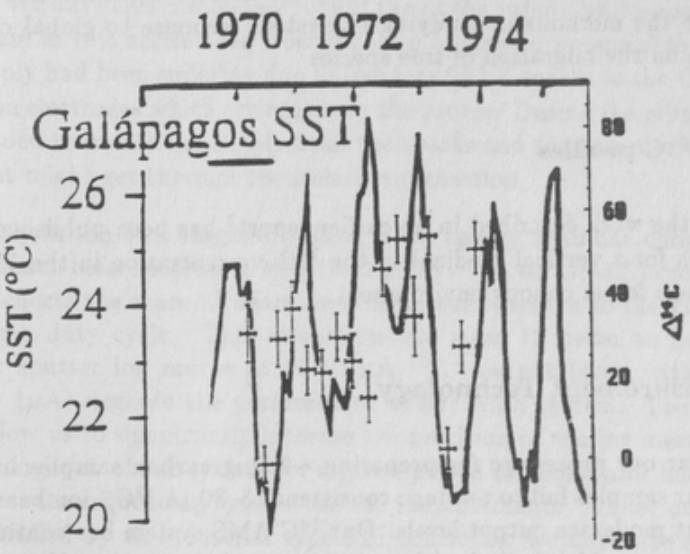

Fig. 6.1-1. ^{14}C concentration ($\Delta^{14}C$) in carbonate of a *Pavona clavus* coral collected off Punta Pitt, San Cristóbal, Galápagos (crosses). ($\Delta^{14}C$ expresses the departure of the ^{14}C concentration in $^{o}/_{oo}$ (per mil) from the standard for modern carbon.) Each sample represents one-fourth of an annual growth band. A clear seasonal cycle is seen which appears to be correlated with Galápagos sea surface temperatures (SST) (solid curve). The El Niño year 1972 exhibits high values of both $\Delta^{14}C$ and SST.

6.1.3 Pollen dating and paleoclimatology using ^{14}C AMS

The predominant source of information on continental paleoclimates is the study of pollen in lake sediment and peat cores. Until recently, the chronologies for the paleoclimatic records obtained from such studies were based on ^{14}C dating of bulk sediment or peat samples by low level decay counting. We have developed methods which allow the extraction of the pollen itself for ^{14}C dating by AMS. By extracting the pollen for dating we are able to avoid many of the potential sources of contaminating carbon that are unavoidable in bulk sediment dating. We believe that the dating of pollen extracts will significantly improve the reliability of the chronologies of the paleoclimatic studies and allow detailed study of the time-progressive nature of large-scale, relatively short-duration events such as the Younger Dryas cooling (at about 10,500 years before present (BP)) and the migration of tree species in response to global climate change.

We have completed a series of measurements of the ^{14}C contents of pollen concentrate samples from peat and lake sediment cores. While preliminary, the results indicate that consistent ^{14}C dates for a regional event (in our measurements, the Mazama Ash fall at about 6,600 BP) can be obtained from cores from different locations within the region. In preparing the samples for this series of measurements, methods were developed to remove coal dust and/or charcoal fragments from the pollen extracts; these contaminants had not been encountered in our previous measurements.

During the next several years we plan to complete the development of our pollen extraction methods and to use the methods in studying ecosystem response to global climate change, with particular emphasis on the migration of tree species.

6.1.4 Tree ring ^{14}C profiles

A second paper on the work described in an earlier report[2] has been published.[3] Our future plans still include a search for a vertical gradient in the ^{14}C concentration in the 1963 growth ring of a tree growing in a deep forest canopy environment.

6.2 AMS: Measurement Technology

During the past year our procedure for preparing $\sim 200\mu g$ carbon samples have become routine; fewer than 1% of our samples fail to produce consistent 15–30μA $^{12}C^-$ ion beams when our sputter source is operated at moderate output levels. Our ^{14}C AMS system has continued to operate with a precision and accuracy which is limited by counting statistics at the 1% level. More recent data obtained on coral samples from the Galápagos Islands (discussed above) and from a sample which has been measured previously by high-precision β counting (QL11658, M. Stuiver, pers. comm.) indicate that our ^{14}C AMS system can measure samples to an accuracy and precision of $\pm 0.5\%$. Figure 6.2-1 shows the series of AMS measurements made on sample QL11658 between June and November 1990; from these data we calculate a radiocarbon age of 6,150$\pm$30 years BP compared to the high-precision β counting date of 6,120$\pm$20 BP. The combined high precision and accuracy of our system and our ability to measure $\sim 200\mu g$ samples is comparable to the ^{14}C performance attained at the best dedicated AMS facilities in the world (*i.e.*, University of Arizona and ETH Zürich) and places our system at the forefront of those ^{14}C AMS facilities that share accelerators, as we do, with nuclear physics groups.

The nickel and gold-plated generating voltmeter (GVM) rotor mentioned in last year's Annual Report[4] has been installed; it is performing well and we believe that the Tandem terminal voltage is held to within $\pm$1KV at 7 MV. The stability of the Tandem under GVM regulation, which is critical to the performance of our AMS system. has been improved significantly over the last year due in part to the GVM modifications but also to the changes to the Tandem charging system discussed in Sec. 11.9. Unfortunately, a small 58 Hz ripple on the GVM signal remains. We believe

[2]Nuclear Physics Laboratory Annual Report, University of Washington (1989), p. 34.

[3]P.M. Grootes, G.W. Farwell, F.H. Schmidt, D.D. Leach, and M. Stuiver, Radiocarbon **31**, No. 3, 475 (1989).

[4]Nuclear Physics Laboratory Annual Report, University of Washington (1990), p. 87.

that this ripple is related to errors in the construction of the GVM stator plate and hope to replace this element with a more precisely-made component in the near future.

Our Universal Negative Ion Source has received considerable attention over the last year. With our 0.028 inch diameter carbon samples, the need for precise alignment of the source elements became critical to the performance of our AMS system. We have completed several small alterations to the electrodes and spacers of the source so that we can now consistently align the source elements to ± 0.003 inches. We have also completely rebuilt the power supply which allows us to steer the Cs^+ sputtering ion beam as it is accelerated from emission at ground potential to our sample surface at -25 kV. This supply had been suffering due to frequent 25 kV sparks to the Cs^+ steering electrodes from the extraction electrodes which are nearby in the source. During the rebuild considerable spark protection was added to isolate the supply from the sparks and to protect critical components from voltage spikes that might get through the isolation protection.

We are currently in the final stages of testing a low energy beamline chopper which attenuates the mass 13 ion beam before injection into the tandem Van de Graaff accelerator. The chopper electrostatically deflects the mass 13 beam away from the entrance to the tandem for a selectable fraction of its 10ms duty cycle. This attenuates the mass 13 beam to levels which will allow us to operate our sputter ion source at 50–70 μA $^{12}C^-$ output levels without having the large mass 13 beam ($\sim 1\mu$A) degrade the performance of our AMS system. The low energy beamline chopper should allow us to significantly increase the precision of routine measurements and/or the overall sample throughput of our system for a given period of accelerator beam time. We are also developing an alternate sequencing system for our measurements. Under our current system the sequencing is controlled by an industrial type 5TI controller; we alternate each 30s between two samples which are adjacent in the ion source sample wheel, as well as between ^{14}C and ^{13}C settings of the injection and analyzing magnets. The new sequencing system, which will run off the DEC VAX station 3200 used for data aquisition, will allow us to alternate between ^{14}C and ^{13}C settings of the magnets while remaining on one sample; this will increase the fraction of measurement time available for detecting ^{14}C from our unknown and standard samples.

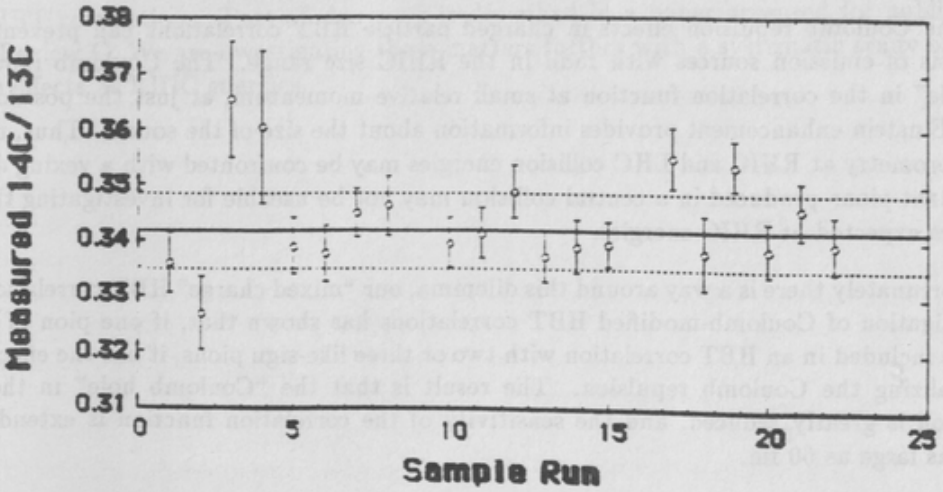

Fig. 6.2-1. Measured $^{14}C/^{13}C$ values (in arbitrary units) for sample QL11658 during the period from June to November, 1990. Solid line shows the weighted average and the dotted lines show $\pm 1\sigma$ (standard deviation) for the data.

7 ULTRA-RELATIVISTIC HEAVY IONS

7.1 Investigation of Coulomb Effects in Pion HBT Correlations at RHIC Energies

J.G. Cramer

The Hanbury-Brown Twiss (HBT) effect is a quantum optics technique first developed by astronomers for measurement of the sizes of nearby stars. When light from a suitable star is detected simultaneously in two telescopes and the detector signals from the telescopes are combined by multiplication, the composite signal shows an interference pattern that is characteristic of the diameter of the star. The same HBT technique, by a fortunate accident of scaling, can also be used with the coincident π mesons produced in a relativistic heavy ion collision.

At RHIC energies, a central collision of two gold nuclei is expected to produce thousands of pions and hundreds of kaons of each charge. The emission of so many Bose-Einstein particles acts as a brilliant "flash bulb" to illuminate the collision. The size, shape, and duration of the emitting source can, in principle, be determined to high accuracy using HBT interferometry of groups of two or more pions. The opportunity, unprecedented in nuclear physics, for event-by-event probing of single isolated nuclear collisions and establishing their characteristics in detail offers great promise for gaining understanding of the physical processes in this new frontier of energy density.

Two-pion Hanbury-Brown Twiss interferometry has been used extensively to determine source sizes in relativistic heavy ion collisions at the Bevalac (LBL), AGS (BNL), and SPS (CERN). In a few cases, 3-pion correlations have also been studied. However, the transverse radii of the pion sources in these cases have been between 1 and 8 fm. In RHIC-energy central collisions, on the other hand, many models predict that the pion source may be very large, with a transverse radius as large as 20 to 40 fm. This size translates to HBT correlation peaks that are very narrow in transverse relative momentum.

The Coulomb repulsion effects in charged particle HBT correlations can prevent meaningful analysis of emission sources with radii in the RHIC size range. The Coulomb repulsion makes a "hole" in the correlation function at small relative momentum, at just the position where the Bose-Einstein enhancement provides information about the size of the source. Thus, users of HBT interferometry at RHIC and LHC collision energies may be confronted with a vexing dilemma: the abundant pions produced in a central collision may not be useable for investigating the very large sources expected at RHIC energies.

Fortunately there is a way around this dilemma, our "mixed charge" HBT correlation technique. Investigation of Coulomb-modified HBT correlations has shown that, if one pion of the opposite sign is included in an HBT correlation with two or three like-sign pions, it has the effect of partially neutralizing the Coulomb repulsion. The result is that the "Coulomb hole" in the correlation function is greatly reduced, and the sensitivity of the correlation function is extended to source radii as large as 60 fm.

A paper describing the Coulomb approximations for multiparticle HBT correlations has been accepted for publication in Physical Review C. A second paper describing the mixed-charge corre-

lation technique is being submitted to Physical Review Letters. An invited paper on this work will be presented at the Spring Meeting of the American Physical Society in April, 1991.

7.2 Investigation of Coherence Effects in Pion HBT Correlations at RHIC Energies

W.J. Braithwaite,* J.G. Cramer and G.I. Opat*

It was mentioned in the previous article that a fortunate accident of scaling makes it possible to apply the HBT effect to pions as well as to optical photons. In ultra-relativistic collisions there may also may be a second lucky overlap with quantum optics, the possibility of *stimulated emission* of pions in ultra-relativistic heavy ion collisions.

Preliminary calculations indicate that in a RHIC-energy collision, the occupation number of phase space cells may be significantly larger than unity, and that the other criteria for stimulated emission are also met. This raises the possibility that well known quantum optic phenomena such as stimulated emission or super-radiance may be present. We are continuing this investigation.

A related issue is whether there are significant coherence effects in the HBT correlations of emitted pions. The conventional wisdom is that at RHIC energies the emission of pions will be completely incoherent because of the large source size as compared to the deBroglie wavelengths of the emitted particles. However, if the occupation number of phase space cells in the source is greater than unity, the emission process may contain a significant coherent emission component. It is somewhat counter-intuitive that the HBT correlation peak for emitted pions is *reduced* by source coherence, but this is the case. There is also a broadening of the HBT correlation peak produced by mixing of the coherent and incoherent components of the emission process.

We have used quantum optics techniques to derive the effects of source coherence in multi-particle HBT correlations. Part of this work is described in a paper accepted for publication in Physical Review C. We are investigating these matters further with a systematic study of possible coherence effects at RHIC energies.

*Permanent address: Department of Physics and Astronomy, University of Arkansas at Little Rock, AR.
†Present address: Department of Physics, University of Melbourne, Australia.

7.3 A Silicon Vertex Tracking Detector for the STAR Detector System at RHIC

W.J. Braithwaite,* J.G. Cramer, D.J. Prindle and T.A. Trainor

We have formed a University of Washington ultra-relativistic ion group which has joined the STAR collaboration, a consortium of 13 institutions that is proposing to construct a major mid-rapidity solenoidal detector for the RHIC relativistic heavy ion collider now being constructed at Brookhaven National Laboratory. The member institutions of the STAR collaboration are IRB/Zagreb, UC Davis, UCLA, Frankfurt/Main Univ., Johns Hopkins Univ., Kent State Univ., LBL/Berkeley, Purdue Univ., Texas A&M Univ., and the Univ. of Washington. The estimated cost of the detector is about $36.4 million. A letter of intent describing the preliminary design of the detector and the physics which it addresses was submitted in October, 1990, to the RHIC Program Advisory Committee and received strong favorable comments. The full proposal will be submitted in the Fall of 1991.

In the preliminary design phase of the STAR detector, our group is assuming responsibility, along with a similar group at LBL, for development of the multi-layer silicon vertex tracker (SVT) that will be placed near the collision vertex region. The role of the SVT is to provide precise information on the trajectories of pions in the spatial region near the collision vertex, and also to permit the identification of short lived particles that undergo decay in the vicinity of the primary vertex.

Our present working design for the SVT involves three cylinders of silicon, each cylinder consisting of two planes of short strips with a small stereo angle between them. At the time of this writing we are running FRITIOF/GEANT simulations of the response of the SVT to RHIC central and peripheral collisions. Preliminary results of these simulations is that both subsystems represent challenging but tractable problems in detector design. Figure 7.3-1 shows the hit pattern on the three cylinders, as generated by GEANT for a central Au + Au collision at 100 GeV/nucleon in each beam.

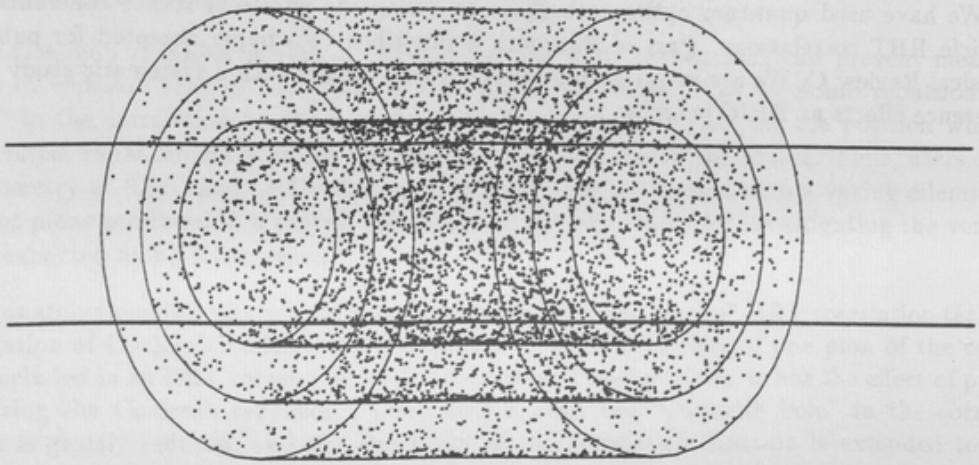

Figure 7.3-1. Hit pattern on 3-layer silicon vertex tracker.

*Permanent address: Department of Physics and Astronomy, University of Arkansas at Little Rock, AR.

7.4 Gas Multiplicity Detector for the STAR Detector System at RHIC

J.G. Cramer, D.J. Prindle and T.A. Trainor

Particle production in ultra relativistic collisions of heavy ions at RHIC is expected to be very large. Estimates in the case of symmetric gold-on-gold collisions at 100 GeV/u in each beam range as high as 10,000 charged particles generated in a central collision. For such large particle fluxes it is useful to rethink the detector strategies and technologies to be used. In particular it seems probable that large area planar avalanche detectors may play an important role.

The major features of a general purpose detector for the relativistic heavy ion collider (RHIC) include a tracking detector at midrapidity to do particle ID and examine various soft-physics issues such as multi-particle HBT correlations, and a calorimeter assembly to assess jet production and other hard QCD processes. The tracking detector would consist of a large volume TPC to reduce track densities to a value within the resolving capabilities of current TPC capability and a silicon vertex tracker (SVT) to improve tracking precision and search for secondary vertices arising from strangeness and charm production. Data rates after on-line data compression are estimated to be 1–10 Mbytes/sec. Because of the high particle numbers/event and consequent high data rate it is essential to have a fast, adaptable trigger so that only events of interest are processed. This provides one of the motivating factors for inclusion of planar avalanche detectors in a general purpose RHIC detector.

Planar avalanche detectors have come into wide use in the last ten years in low energy, heavy ion nuclear physics. The large stopping power of these heavy ions has required and made possible the use of thin gas detectors. Planar avalanche detectors are very adaptable to large areas and excellent position sensitivity. Run at low pressure in the Breshkin mode they provide excellent timing resolution. They are also comparatively inexpensive and radiation damage resistant. It is an attractive possibility, therefore, to adapt this technology to the RHIC environment. Unfortunately, almost all particles emanating from a RHIC central collision are minimum ionizing particles (mips). Therefore, the primary ionization available to form a detector signal is reduced by one thousand fold or more. However, strategies are available which will nevertheless insure the usefulness of these detectors.

If very fast timing is not essential one can increase the primary ionization/particle by increasing the detector operating pressure and the thickness of the region in which the primary ionization is formed (the conversion region). The detector time properties then scale with the electron drift time across this region ($\sim 1\mu s$). In addition, one may improve on the statistics of the collected charge and take advantage of the high particle flux, as well as reduce the cost of electronics, by segmenting the planar detector so that the mean occupancy/segment is significantly greater than one. In this case the detector can be viewed as a multiplicity counter or flux sampler. The segment size is a trade-off between electronics costs and charge statistics on the one hand and spatial distribution of significant flux variations on the other.

If fast timing is important one must return to the basic planar avalanche geometry, a thin gap with very high E/P ratio. Under these conditions it is seemingly hopeless to time on a particle-by-particle basis, because only a few primary charges are produced in the active region of the detector. But, for the purpose of timing the collision event one can again take advantage of the high flux of charged particles traveling out from the heavy ion collision in a spherical wave within

a few picoseconds of each other. As this wave passes over a planar avalanche counter the result can be seen to be equivalent to the action of a single highly ionizing heavy ion, except that the primary ionization is distributed over a substantial area. Even this can be advantageous in that segmentation and use of multiple electronics channels can reduce electronic contributions to time fluctuations by averaging.

In an envisioned specific application for the STAR (Solenoidal Tracker at RHIC) detector design two annular multiplicity counters would be placed just inside the solenoid pole pieces including the pseudorapidity $1< |\eta| <4$. Segmentation would be 10 in azimuth and 10 in η (pseudorapidity). With ~1000 particles expected through such a detector the η segmentation is adjusted so that the mean occupancy/segment is 10. These detectors would provide a fast trigger ($< 1\mu s$) on centrality and would characterize the general charged particle multiplicity distribution vs. η for large η. In addition some information on the scattering plane orientation may be obtainable.

Timing information about the collision event would be obtained by two annular fast avalanche counters placed just beyond the multiplicity counters. Timing resolution at the 100 ps level seems possible with the strategy described above. Relative timing between symmetrically placed detectors at this level would permit location of the primary collision vertex to within 1 cm by TOF and would constitute both an input into the fast trigger and a starting point for TPC and SVT track-finding routines.

We plan to conduct an R&D program on these detector concepts over the next year, with prototype tests to be conducted at the NA 35 detector system at CERN in Spring, 1992.

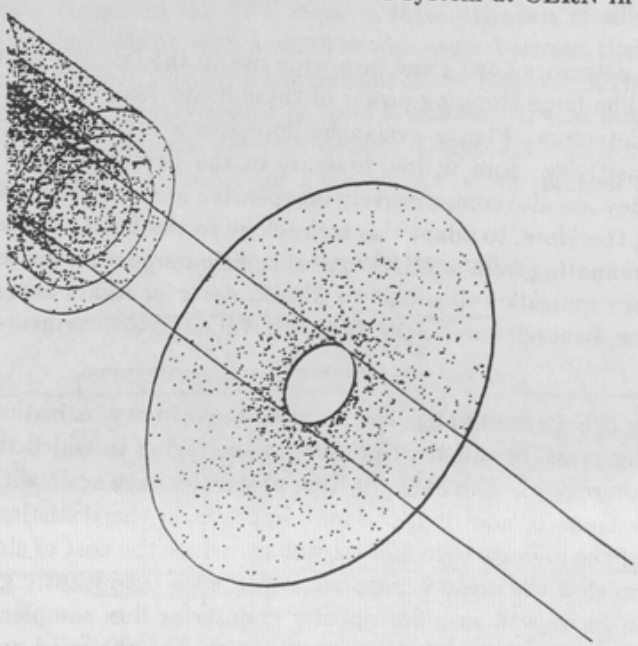

Figure 7.4-1. GEANT calculation showing ~1000 charged particle hits in an annular multiplicity detector. Also shown are the beam pipe and the three-layered silicon Vertex Tracker (SVT) proposed for STAR.

8 MEDIUM ENERGY

8.1 Analyzing Power Measurements in π-d Elastic Scattering at 50 MeV

P. Amaudruz,* J.T. Brack,† P.P.J. Delheij,* A. Feltham,† C.A. Gossett, N. Grion,‡ M. Hanna,† D. C. Healey,* B.K. Jennings,* R. R. Johnson,*,† M. Kohler,§ E.L. Mathie,¶ D.F. Ottewell,* R.A. Ristinen,§ F.M. Rozon,† R. Rui,‡ R.B. Schubank,†,‖ G. Sheffer,* Y.M. Shin,‖ G.R. Smith,* V. Sossi,† N.R. Stevenson,*,‖ R. Tacik,¶ D. Vetterli,† G.J. Wagner,** G.D. Wait,* P. Weber† and M. Yeomans¶

$\pi - d$ elastic scattering is one of the most extensively studied processes in intermediate energy physics. Measurements of cross-sections, analyzing powers, and polarizations[1,2] have been made up to T_π=300 MeV. Nevertheless, several outstanding problems yet remain to be resolved, such as the contribution of the relatively small P_{11} πN intermediate amplitude which plays an important role in the complementary absorption process.

To this end the vector analyzing power in π^+-d elastic scattering was measured at 50 MeV, much below the Δ resonance region, where the sensitivity to P_{11} may be enhanced. The analyzing power, iT_{11} was measured at five angles in the range 60–130° using the M13 channel at TRIUMF, the TRIUMF dynamically polarized target, and the QQD spectrometer. The target material was deuterated (D-) butanol and correction for target materials other than deuterium was made by subtraction of spectra measured with H-butanol.

The results of the measurements have recently been published[3] and are shown in Fig 8.1-1. The data are in good agreement with full NN-πNN model calculations and disagree with calculations with small or zero πN P_{11} amplitude. At higher energies the situation is opposite, that is, better agreement between theory and experiment when P_{11} is neglected. The apparent disparity between high and low energy measurements may indicate that effects which compensate or complement the P_{11} amplitude have been treated incorrectly in the NN-πNN models.

*TRIUMF, 4004 Wesbrook Mall, Vancouver, British Columbia, Canada V6T 2A3.
†Dept. of Physics, University of British Columbia, Vancouver, British Columbia, Canada V6T 1W5.
‡Instituto Nazionale di Fisica Nucleare and Dipartimento di Fisica, Università di Trieste, Trieste, Italy, 34127.
§Dept. of Physics, University of Colorado, Boulder, Colorado 80309.
¶Dept. of Physics, University of Regina, Regina, Saskatchewan, Canada S4S 0A2.
‖Dept. of Physics, University of Saskatchewan, Saskatoon, Saskatchewan, Canada S7N 0W0.
**Physikalisches Institut der Universitaet Tuebingen, Morgenstelle, D-7400 Tuebingen, Federal Republic of Germany.

[1] N.R. Stevenson and Y.M. Shin, Phys. Rev. C36, 1221 (1987), and references cited therein.
[2] N.R. Stevenson *et al.*, Phys. Rev. C39, 1488 (1989), and references cited therein.
[3] N.R. Stevenson *et al.*, Phys. Rev. Lett. 65, 1987 (1990).

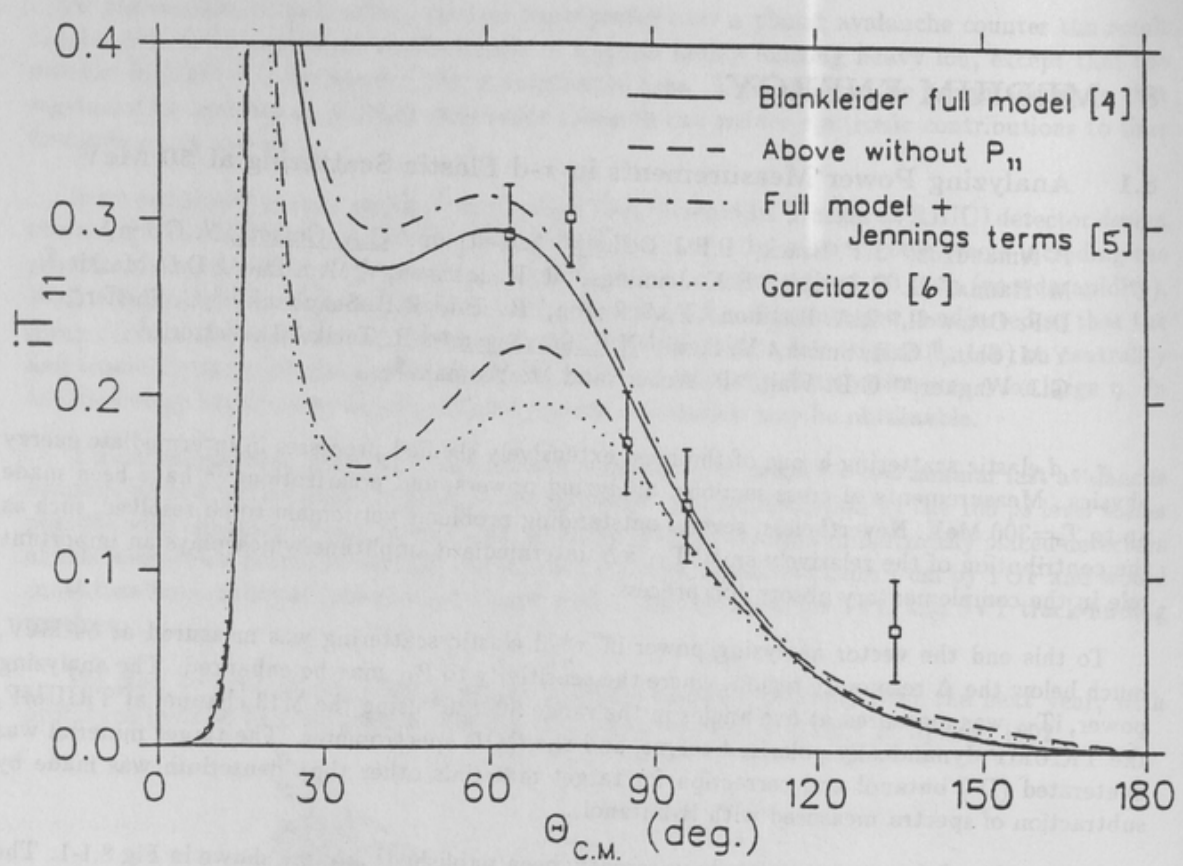

Figure 8.1-1. Measurements of iT_{11} in π^+-d elastic scattering at 50 MeV. The solid curve is the full NN-πNN model of Ref. 4; the dashed curve is the same model without P_{11}. The dot-dashed curve includes terms suggested by Jennings and Rinat [5] for diagrams previously neglected and the dotted curve is the calculation of Ref. 6.

[4] B. Blankleider and I.R. Afnan, Phys. Rev. C **31**, 1380 (1985).
[5] B.J. Jennings and A.S. Rinat, Nucl. Phys. **A485**, 421 (1988).
[6] H. Garcilazo, Phys. Rev. C **35**, 1804 (1987).

8.2 The A-dependence of Inclusive Pion Scattering Cross-sections in the Δ Resonance Region

I. Halpern, D.P. Rosenzweig and D.W. Storm

As we have pointed out before, pion inclusive scattering in the Δ resonance region is a particularly good way to explore the effects of the nuclear surroundings on projectile-nucleon scattering when the nucleon is inside a nucleus. Among the special features which the pion brings to such studies are the suppression of the multiple scattering background by true pion absorption and the fact that one can compare cross-sections for three charges ($\pi^{\pm}$ and π^0) in the exit channel and for two charges (π^+ and π^-) in the entrance channel.

In particular we have been carrying out classical transport calculations to study the dependence of inclusive pion cross-sections for the six combinations of T_Z in-and-out, on the mass number A of the target. We have found that since nuclei are quite black to pions near the resonance energy, these cross-sections can be written as the product of πR^2, the projected area of the nucleus, times several simple factors each of whose A dependence can be expressed in the form $A^{\Delta n}$. Among these factors are: (1) The modification, due to Coulomb refraction, of the probability that the pion reaches the nucleus, (2) The chance that the pion interacts with a nucleon whose isospin can lead to the reaction in question, instead of with the nucleon of opposite isospin. (For example, for $\pi^+ \rightarrow \pi^{+'}$ this chance is very nearly $Z\sigma_{++}/(Z\sigma_{++} + N\sigma_{+})$ where σ_{++} is the π^+p cross-section and σ_{+} is the π^+n cross-section. The latter leads mostly to charge exchange.) (3) The chance that the π-nucleon complex survives against true pion absorption. This factor is also isospin dependent. (4) Finally, the chance that the pion released in the decay of the complex manages to escape from the nucleus. The escape is easier from small nuclei than for large ones.

The 100 MeV pions for each of the 4 cited factors and the different possible reactions. The paired entries for double charge exchange reflect the assumption that this reaction involves the formation of two sequential π-nucleon complexes. The entries in the table are consistent with one another and are found to give a fairly good account of our own data[1] (on the relative A dependences of π^+ and π^- inclusive scattering and on the actual A dependence of either of these) as well as of charge exchange cross-sections measured by others.[2,3]

We are currently in the process of applying these considerations plus the effects of the nucleon motion in target nuclei to account for the observed spectra and angular distributions in these scattering reactions.

Table: A-Dependence Exponents Δn for Various Effects

In	π^+			π^-		
Out	$\pi^{+'}$	π^o	π^-	π^+	π^o	$\pi^{-'}$
(1) Coulomb Refraction	−0.05	−0.05	−0.05	+0.05	+0.05	+0.05
(2) Right Partner	−0.09	+0.17	+0.17 +0.12	−0.20 -0.14	−0.20	+0.06
(3) Avoiding absorption	−0.06	+0.07	+0.07 +0.07	−0.06 −0.06	−0.06	+0.06
(4) Succeeding to Escape	−0.08					−0.07

[1] To be published.

[2] T.J. Bowles *et al.*, Phys. Rev. C **23**, 439 (1981).

[3] P.A.M. Gram *et al.*, Phys. Rev. Lett. **62**, 1837 (1989).

8.3 Inclusive Photoproduction of Pions on a Variety of Nuclei

M. Doss,* K. Fissum,* M. Frodyma, I. Halpern, D.P. Rosenzweig, D. W. Storm and J. Vogt*

Two years ago[1] we described how we could complement our studies of pion inclusive scattering by measuring photoproduction of pions from nuclei. Last year[2] we presented results of some tests of the plastic counter telescope that was built for detecting positive pions. During the past year the tagger at Saskatoon Accelerator Laboratory (SAL) was commissioned, and our experiment was one of the first to run on it.

The combination of maximum electron energy and tagger setting provided a tagged photon energy range of 180 to 216 MeV. We used our counter and three similar counters built at SAL by the University of Melbourne group. A 6 mm thick counter was placed in front of each large counter. These telescopes were placed 30 cm from the target at angles of 50, 80, 110, and 140°. Each telescope solid angle was 0.13 steradian, determined by a lead aperture. The π^+ were identified both by their relative energy signals in the two counters and by detecting the delayed pulse from the π to μ decay. The 4 MeV kinetic energy of the muon was identified either as an excess signal in an ADC triggered with a delayed gate or by a discriminator trigger delayed with respect to the initial trigger. Since negative pions are captured before decaying, the muon signal serves to identify π^+.

The targets were natural C, Ca, Sn, and Pb. We also measured photoproduction on ^{1}H and ^{2}H, in polyethylene. The first was for calibrating the detector efficiencies, while the second was primarily used to provide monoenergetic protons from photoabsorption by ^{2}H. The target thicknesses and the total photon flux incident on each target are shown in the table. An upper limit for the number of pions that might be detected is obtained using the differential cross sections for photoproduction of π^+ on the proton times the number of protons in the target nuclei. We assume an efficiency of 50% for pion detection, based on the 20 ns dead time before we can possibly detect the muon signal. This limit is taken into account in the table.

There is Pauli blocking of some of the pion production events in the nucleus, and, once produced, the pion flux will be attenuated by interactions in the nuclear material. Studying these two physical processes is the goal of this experiment. These processes will reduce the number of pions produced from the upper limit given in the table; our goal is to see how these processes depend on the pion energy and on the A and Z of the nucleus. Preliminary analysis of the data indicates that the separation of pions from other particles is possible for all cases except perhaps for the most forward angle with the two high-Z targets. The data analysis should be completed during 1991.

*University of Saskatchewan, Saskatoon, S7N 0W0, Canada.

[1] M. D ss *et al.*, Nuclear Physics Laboratory Annual Report, University of Washington, p. 28 (1989).

[2] M. Doss *et al.*, Nuclear Physics Laboratory Annual Report, University of Washington, p. 47 (1990).

Table 8.3-1. Targets, thickness, photon flux, and estimated upper limit on number of pions produced.

Target	Thickness (gm/cm^2)	Photons ($\times 10^{10}$)	Pions (upper limit) ($\times 10^3$)
Carbon	0.51	11.	94
Calcium	1.00	5.9	99
Tin	0.29	7.6	42
Lead	0.54	9.1	64

8.4 Scattering and Absorption of 100 MeV π^+ on the Hydrogen and Helium Isotopes

I. Halpern and D. W. Storm

We have completed an analysis of the experiment which was performed at TRIUMF on inclusive π^+ and π^- scattering from the lightest isotopes.[1]

We had found with heavier nuclei that we could understand the measured ratios of the integrated inelastic scattering to absorption cross sections in terms of a simple model for the assumed quasi-elastic scattering process.[2] It is of interest to extend that analysis, the results of which depend on target Z/N ratios and presumably on nucleon densities, to lighter nuclei where these variables change much more rapidly from target to target than they do for heavy nuclei.

A summary of our results is shown in Table 8.4-2. The quantity B^{++} is the branching ratio for a π^+ – p complex formed in the nucleus to lead to meson absorption before it decays. The values of B^{++} were obtained from pion absorption cross sections and confirmed by our own scattering data. The analysis also provides values for the corresponding ratio B^+ for the π^+ – n complexes. From each of these branching ratios one can deduce the relative widths γ_a/γ_d for absorption to decay (second row in the table) for a π^+ – nucleon complex. This ratio is expected to depend both on the number of $T = 0$ nucleon pairs in the nucleus that are available to absorb pions (third row) and on the mean density of nucleons in the given nucleus. One would expect that when these two factors are unfolded from the measured γ_a/γ_d values, that the reduced γ_a/γ_d values would be the same in all the nuclei. This reduction is performed in the last row and it is seen that the values for ^{2}H, ^{3}H, and ^{3}He are reasonably equal, but that the ratio of pion absorption to emission in ^{4}He seems to be anomalously high. This anomaly must in part reflect the effect of the absence of available states in ^{4}He below 20 MeV of excitation. This increases the relative chance for absorption in this nucleus.

	^{2}H	^{3}H	^{3}He	^{4}He
B^{++}	0.130±.003	0.25±.08	0.15±.03	0.53±.08
$\gamma_a^{++}/\gamma_d^{++}$	0.149±.004	0.33±.14	0.19±.04	1.1 ±.3
P ($T = 0$ pairs per proton)	1.00	1.50	0.75	1.50
R_{rms} (Fermi)	1.92	1.68	1.68	1.41
$(\gamma_a^{++}/\gamma_d^{++})/(P/R_{rms}^3)$	1.06 ±.03	1.04±.45	1.20±.20	2.1 ±.6

Table 8.4-1. Deduced branching ratios and ratios of widths for true pion absorption and decay from π^+- p complexes. The results for π^+ on ^{3}H are obtained from π^- on ^{3}He measurements.

We are able to use the values of B^{++} to predict the scattering cross sections which we have actually measured in our experiments. To do so, we use a modified plane wave impulse approximation (PWIA) calculation[3] to predict how much of the quasi-free scattering will be inelastic rather than elastic scattering. The PWIA predictions for energy-integrated differential cross sections are compared with the data for the four measured cases in Fig. 8.4-1. It is seen that their shapes

[1] M.A. Khandaker, Ph.D. Thesis, University of Washington, 1986.

[2] K. Ar ol *et al.*, Phys. Rev C **33**, 208 (1986).

[3] T. K. Fowler and K. M. Watson, Nucl. Phys. **13**, 549 (1959).

are reproduced, and that the decrease in cross section at forward angles can be attributed to flux removal by the elastic channel. However, when both shadowing and absorption are included, but when multiple scattering is not included, the modified PWIA predicts a cross section reduced below the measured one.

We conclude that the inelastic scattering and absorption of 96.5 MeV pions by these very light nuclei are well described by a model in which a single pion – nucleon interaction takes place with the same cross section as in free scattering. Then absorption may occur with a width that depends on the density of nucleons which can form a $T = 0$ pair with the nucleon initially interacting with the pion. Otherwise scattering, which may be elastic, will take place with a width which is uniform for the nuclei with mass 2 or 3, but which appears to be reduced for ^{4}He, possibly due to the high threshold for pion emission. Our analyses also include accounts of the observed spectra and angular distributions and are explained in detail in a paper which has been prepared for publication.

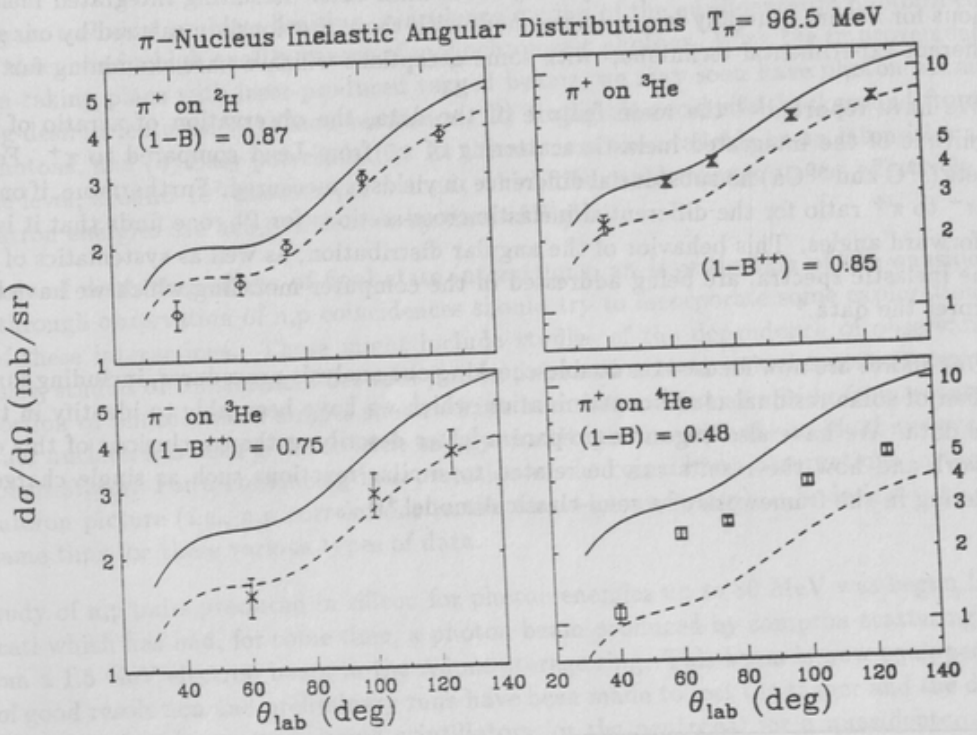

Figure 8.4-1. Differential cross sections for inclusive inelastic scattering from the hydrogen and helium isotopes, compared with the PWIA (solid) and modified PWIA (dashed) predictions discussed in the text.

8.5 Inclusive Scattering Spectra for $\pi^{\pm}$ at 100 MeV from a Variety of Nuclei

J.F. Amann,* R.L. Boudrie,* K.G.R. Doss,† D. Drake,* I. Halpern, M. Khandaker,‡ J. Nelson,§ D.P. Rosenzweig, D.W. Storm, D.R. Tieger§ and S.A. Wood§

Our group is finishing the analysis of LAMPF experiment 967. The data, obtained using the Clamshell spectrometer and Low Energy Pion Channel, provide us with spectra for both π^+ and π^- scattering at 100 MeV from targets spanning the mass range from Carbon to Lead. Spectra were measured at angles from 50 to 140°. The spectra extend to very high inelasticity, allowing us to study systematics of the scattering mechanism.[1] The analysis project has involved a lengthy process of tuning and retuning the event filtering routine. We have now achieved levels of muon contamination which don't seriously affect the experimental results. Additionally, improvements have been made in the determination of the spectrometer focal plane efficiency, as well as in the consistency of the run-to-run normalization. The uncertainties introduced to the spectra by each of these factors are typically 3% each. We have in the past reported persistent discrepancies between yields obtained in reflection and transmission target geometries: this problem has been reduced to the 5% level, by invoking better trajectory trace-back cuts. Resulting integrated inelastic cross-sections for π^+ are generally in good agreement with those previously measured by our group using a different experimental technique,[2] with some exceptions which we are examining further.

We have reported[1,3] the main feature of the data, the observation of a ratio of two in the magnitude of the integrated inelastic scattering of π^- from Lead compared to π^+. For the light targets (^{12}C and ^{40}Ca) no substantial difference in yields is measured. Furthermore, if one examines the π^- to π^+ ratio for the differential inelastic cross-sections for Pb, one finds that it is greater at the forward angles. This behavior of the angular distribution, as well as systematics of the shapes of the inelastic spectra, are being addressed in the computer modeling which we have be using to interpret the data.[4]

Our efforts are now focused on double-checking our analysis procedures, including further investigation of some residual muon contamination which we have been able to identify in the forward angle data. We have also begun to prepare a letter describing the conclusions of this experimental work and how the results can be related to similar reactions such as single charge exchange scattering in the framework of a semi-classical model.[4,5]

*Los Alamos National Laboratory (LAMPF), Los Alamos, NM 87545.
†University of Saskatchewan, Saskatoon, S7N OWO Canada.
‡University of Maryland, College Park, MD 20742.
§Massachusetts Institute of Technology, Cambridge, MA 02139.

[1] Nuclear Physics Laboratory Annual Report, University of Washington (1990) p. 49.
[2] K. Aniol *et al.*, Phys. Rev. C **33**, 208 (1986).
[3] D. Rosenzweig *et al.*, Bull. Am. Phys. Soc., **34**, 1204 (1989).
[4] Nuclear Physics Laboratory Annual Report, University of Washington (1990) p. 50.
[5] Nuclear Physics Laboratory Annual Report, University of Washington (1991) Sec. 8.2.

8.6 Photoabsorption by Quasideuterons at Photon Energies to 80 MeV

I. Halpern* and Ladon Group (Frascati)

Although the integrated photoabsorption cross section from about 30 to 140 MeV amounts to about one classical sum-rule's worth, and although the dominant absorption mechanism in this region, it is generally agreed, occurs on correlated neutron-proton pairs, rather little has been learned about this correlation from experiments.[1,2] The reasons for this are both technical and intrinsic. The intrinsic reasons are the distortions of the observations by final state interactions, either interactions of the escaping photonucleons with individual nucleons in the nucleus or their refraction by the full nuclear field. Both these interactions become increasingly severe as one goes to lower incident photon energy. The smearing of the n-p opening angle by refraction at the nuclear edge is as much as 40° at energies below photomeson threshold. At higher energies, where these effects are smaller, the dominant photoabsorption mechanism becomes photomeson production. Unfortunately this absorption can lead to confusing n-p pairs when a photomeson is reabsorbed.

The main technical problem limiting coincidence studies of the quasideuteron photoprocess has been the absence of a high quality source of monochromatic photons. With the improvements that have been taking place with laser-produced tagged beams, we may soon have photon beams with some long-desired features: (1) Good resolution, (2) Negligible accidental background from lower energy photons, and (3) Easy polarizability. At the moment the available beam intensities are still below the level, around 10^7 photons per second, which one could manage to use effectively where photoneutron energies are being measured by time of flight.

Because of distorting effects of final state interactions, an investigation of the quasideuteron process through observation of n,p coincidences should try to incorporate some exploration of the effects of these interactions. These might include studies of the dependence of observations on nuclear size, studies of coincidences between proton pairs and extensive singles measurements. The upper portion of photonucleon singles spectra have been interpreted as arising from events where the partner nucleon has been given so little energy that it remains with the residual nucleus, in one of its bound states. For a convincing interpretation of the coincidence observations in terms of a quasideuteron picture (*i.e.*, n,p correlations in the target ground state), it is desirable to account at the same time for these various types of data.

A study of n,p pairs produced in silicon for photon energies up to 80 MeV was begun last year at Frascati which has had, for some time, a photon beam produced by compton scattering of laser light from a 1.5 GeV electron beam in the Adone storage ring. This beam is now equipped with a tagger of good resolution and preliminary runs have been made to test the tagger and the detectors (silicon counters for the protons, liquid scintillators for the neutrons) for a quasideuteron study. The experiment is continuing this year with the intention of accumulating enough data to make a useful contribution to the long-standing problem of photoabsorption by quasideuterons.

*On sabbatical at Ladon, Frascati, Italy (1989–1990).

[1] A. Wattenberg *et al.*, Phys. Rev. **104**, 1710 (1956).
[2] S.N. Dancer *et al.*, Phys. Rev. Lett. **61**, 1170 (1988).

8.7 Photon Absorption Beyond the Giant Resonance Region

I. Halpern and D.W. Storm

Some years ago we made some studies of the (n,γ)[1] and (γ,n)[2] reactions on Pb, Cd and Ca at energies extending to twice that of the giant dipole resonance. We observed strong forward asymmetries of the n and γ emitted to low lying levels and we interpreted them in terms of the interference of the expected giant E2 isovector resonance with an underlying E1 background. It was, however, not possible to account adequately for the extracted widths and strengths of the presumed resonance in different nuclei in terms of the standard direct/semi-direct theory.[2]

Recently we have extended our earlier work to higher energies and as a result of the new data[3] and of related work of others[4] we now feel that there is even only slightly above the dipole resonance, a substantial contamination of the single-particle absorption process of the direct/semi-direct model by absorption by correlation n-p pairs of nucleons, i.e., by so-called quasi-deuterons.

The evidences for this contamination include

1. The observation that γ,n and γ,p cross-sections to low lying levels at somewhat higher photon energy are comparable and that both cross-sections can be plausibly interpreted in terms of absorption by quasi-deuterons.[4]

2. The fact that the curves giving forward/back (γ,n) asymmetries have much the same shape for all nuclei. In particular, in order to account for the universal absence of negative asymmetries (backward peaking), one must assume unexpectedly uniform contributions from E2 isoscalar absorption in different nuclei.

3. The dependence of the ratio of the $90°(\gamma,n)$ yield to the average yields at 55° and 125°. As the photon energy increases beyond the E2 resonance this ratio falls off noticeably, although one would expect it to rise; and finally,

4. The recognition that the observed shift of the asymmetry curve to lower energies in heavier nuclei cannot be taken as definite evidence for the collective character of the photoabsorption since such a shift would also occur for quasi-deuteron absorption.

It seems fair to say that the photon absorption mechanism (or mechanisms) beyond the giant dipole region and below meson threshold are still not very well understood. The technology of photon beams has, however, been steadily improving and soon one should have monochromatic beams of $\sim 10^7$ photon/sec which are produced by compton scattering of GeV electrons from laser light making photons in the required energy range. Such beams have the advantage, over even tagged bremsstrahlung beams, that they have very little accidental background from lower energy photons and can be very easily polarized.

[1] D.M. Drake *et al.*, Phys. Rev. Lett. **47**, 1581 (1981).

[2] T. Murakami *et al.*, Phys. Rev. C **35**, 479 (1987).

[3] A. Freytag, Ph.D. Thesis, University of Illinois, 1988; D.W. Storm *et al.*, Can J. Phys,. **65**, 677 (1987); T. Murakami *et al.*, J. Phys. G: Nucl. Phys. **14**, Suppl. S275 (1988).

[4] S.N. I ancer *et al.*, Phys. Rev. Lett. **61**, 1170 (1988); A. Håkanssen *et al.*, Nucl. Phys. **A512**, 399 (1990).

The main non-technical problems in studying photoabsorption have been and will continue to be the final state interactions and it remains necessary in any experimental study, to learn as much about these interactions as one can.

One of us(I.H.) was on sabbatical leave last year working with the LADON group at Frascati on a laser-beam study of n/p coincidences from a Si target observed with a tagged laser beam. This experiment is still running at Frascati. Our group here plans to develop a proposal to study n/p and p/p coincidences from lighter targets, most likely using the tagged photon facility[5] at Brookhaven National Laboratory.

[5]C.E. Thorn *et al.*, Nucl. Instrum. Meth. **A285**, 447 (1989).

8.8 Electron Scattering from the Proton and the Deuteron

J. Alster,* R.G. Arnold,† P.E. Bosted,† C.C. Chang,‡ F.S. Dietrich,§ R.A. Gearhart,¶ K.A. Giffioen,‖ R. Hicks,** C.E. Hyde-Wright, S.E. Kuhn,†† J. Lichtenstadt,* R. Miskimen,** G. Peterson,** G.G. Petratos,‡‡ S.E. Rock,† S.H. Rokni,§ Z. Szalata,† and K. van Bibber§

Data analysis is underway for an extensive set of high Q^2 elastic and inelastic H(e,e') and quasi-elastic and quasi-Δ D(e,e') data.[1] The data also include inclusive D(e,π) spectra. The data have been reduced to differential spectra and are now being parameterized in order to unfold the radiative tails and to separate the longitudinal and transverse cross sections.

The inclusive D(e,e') process depends upon the deuteron wave function, the reaction mechanism (including the neutron form factor and meson exchange currents), and the final state, including both *pn* and $NN\pi$ final states. In this simplest of all nuclei, it may be possible to compare the data with *ab initio* calculations. However, the deuteron provides an excellent test case for the quasi free model used in finite nuclei. From our inelastic H(e,e') data, the D$(e,e')NN\pi$ channel can be estimated by smearing over the deuteron wave function. This permits a model-dependent extraction of the D$(e,e')np$ cross section in the quasi-elastic and dip region (in between the quasi-elastic and quasi-Δ peaks). This "elastic" (no pion-production) cross section is particularly elegant, since it involves a purely two body system.

A recent analysis of old H(e,e') elastic and inelastic data indicates that the $H(e,e')\Delta$ form factor approaches the pQCD scaling law $G(Q^2) \propto Q^{-4}$, much more slowly than the elastic form factor.[2] Our new separated data on the elastic proton form factor and the delta production form factors on H and D will help clarify the approach to scaling for both the electric and magnetic form factors.

*Tel Aviv University, Ramat Aviv 69978 Israel.
†The American University, Washington DC 20016.
‡University of Maryland, College Park MD 20742.
§Lawrence Livermore National Laboratory, Livermore, CA 94550.
¶Stanford Linear Accelerator Center, Stanford, CA 94305.
‖University of Pennsylvania, Philadelphia, PA 19104.
**University of Massaschusetts, Amherst MA 01003.
††Stanford University, Stanford CA 94305.
‡‡University of Rochester, Rochester, NY 14627.

[1] Unive sity of Washington Nuclear Physics Laboratory Annual Report 1990, p. 55.

[2] P. Stoler, *Hadronic Physics with Electrons beyond 10 GeV*, Proceedings to be published in Nucl Phys.

8.9 Exclusive Virtual Compton Scattering

M. Frodyma and C.E. Hyde-Wright

We have studied the $p(e,e'\gamma)p$ reaction for the Pegasys proposal.[1] We are interested in deep inelastic electron scattering kinematics. This reaction is a second order electromagnetic probe of the proton structure. We use perturbative QCD (pQCD) calculations[2] as a guide to count rate estimates.

The unpolarized $p(e,e'\gamma)p$ cross section has the form

$$\frac{d\sigma(e,e'\gamma)}{dQ^2 d\nu d\phi_e dt d\phi_{kq}} = \frac{1}{2\pi}\frac{d\Gamma}{dQ^2 d\nu}\left[v_L\frac{d\sigma_L(\gamma,\gamma')}{dt} + v_T\frac{d\sigma_T(\gamma,\gamma')}{dt} + v_{LT}\frac{d\sigma_{LT}(\gamma,\gamma')}{dt}\cos\phi_{kq} + v_{TT}\frac{d\sigma_{TT}(\gamma,\gamma')}{dt}\cos(2\phi_{kq})\right].$$

$d\sigma_\Lambda(\gamma,\gamma')$ are the cross sections for elastic photon-proton scattering with a virtual photon in the initial state. The virtual photon polarization tensor is defined by Λ = L,T, LT, or TT corresponding to longitudinal or transverse polarized virtual photons, or the two interference terms. $d\Gamma v_\Lambda$ is the virtual photon differential flux. Q^2 is the virtual photon invariant mass, ν is the (lab frame) energy transfer, ϕ_e is the (trivial) electron azimuth, t is the net invariant momentum transfer squared to the proton, and ϕ_{kq} is the azimuth of the photon around the virtual photon direction.

The pQCD scaling laws[3] predict that $S^6 d\sigma_\Lambda/dt$ is a function only of Q^2/S and t/S (or θ^{CM}, the photon-proton CM scattering angle) and not a function independently of S (the photon + proton invariant mass squared). We exploit this scaling law to rewrite the cross section as follows:

$$\frac{d\sigma(e,e'\gamma)}{d(Q^2/S)dS\,d\cos\theta^{CM}\,d\phi_{kq}} = \left|\frac{\partial t}{\partial\cos\theta^{CM}}\right|\frac{1}{S^6}\frac{d\Gamma}{d(Q^2/S)dS}\left\{v_L\left[S^6\frac{d\sigma_L(\gamma,\gamma')}{dt}\right] + v_T\left[S^6\frac{d\sigma_T(\gamma,\gamma')}{dt}\right] + v_{LT}\left[S^6\frac{d\sigma_L T(\gamma,\gamma')}{dt}\right]\cos\phi_{kq} + v_{TT}\left[S^6\frac{d\sigma_T T(\gamma,\gamma')}{dt}\right]\cos(2\phi_{kq})\right\},$$

where the terms in square brackets are independent of S in the pQCD calculations. The top figure on the following page displays the cross section after integrating the flux factors over $S > 5.0$ GeV^2 and over the two azimuthal angles, for $Q^2/S = 0.25, 0.5, 0.75, 1.0$. In the bottom panel, we show the $Q^2/S = 0.25$ result for the ratio of the LT interference term to the noninterference cross section. The LT term is obtained by weighting the cross section by $\frac{1}{\pi}\cos\phi$.

These curves do not include the radiative tail of elastic electron-proton scattering, which interferes coherently with the compton amplitude. We have calculated this amplitude and it is a small contribution to the integrated cross section for most of the kinematics.

Independent of whether or not pQCD is valid in the range of momentum transfers reached with a 14 GeV electron beam, the calculations illustrate some of the physics issues of virtual

[1] SLAC Report 377 Nov. 1990.

[2] G.R. Farrar and H. Zhang, Phys. Rev. D **41** 3348 (1990), and D **42** 2413(E) (1990).

[3] S.J. Brodsky and G.R. Farrar, Phys Rev Lett, **31** 1153 (1973).

compton scattering. The magnitude and oscillations of the LT term indicate that the amplitude for longitudinal photons is large and complicated. This indicates that virtual compton scattering is not a trivial extrapolation real photon compton scattering.

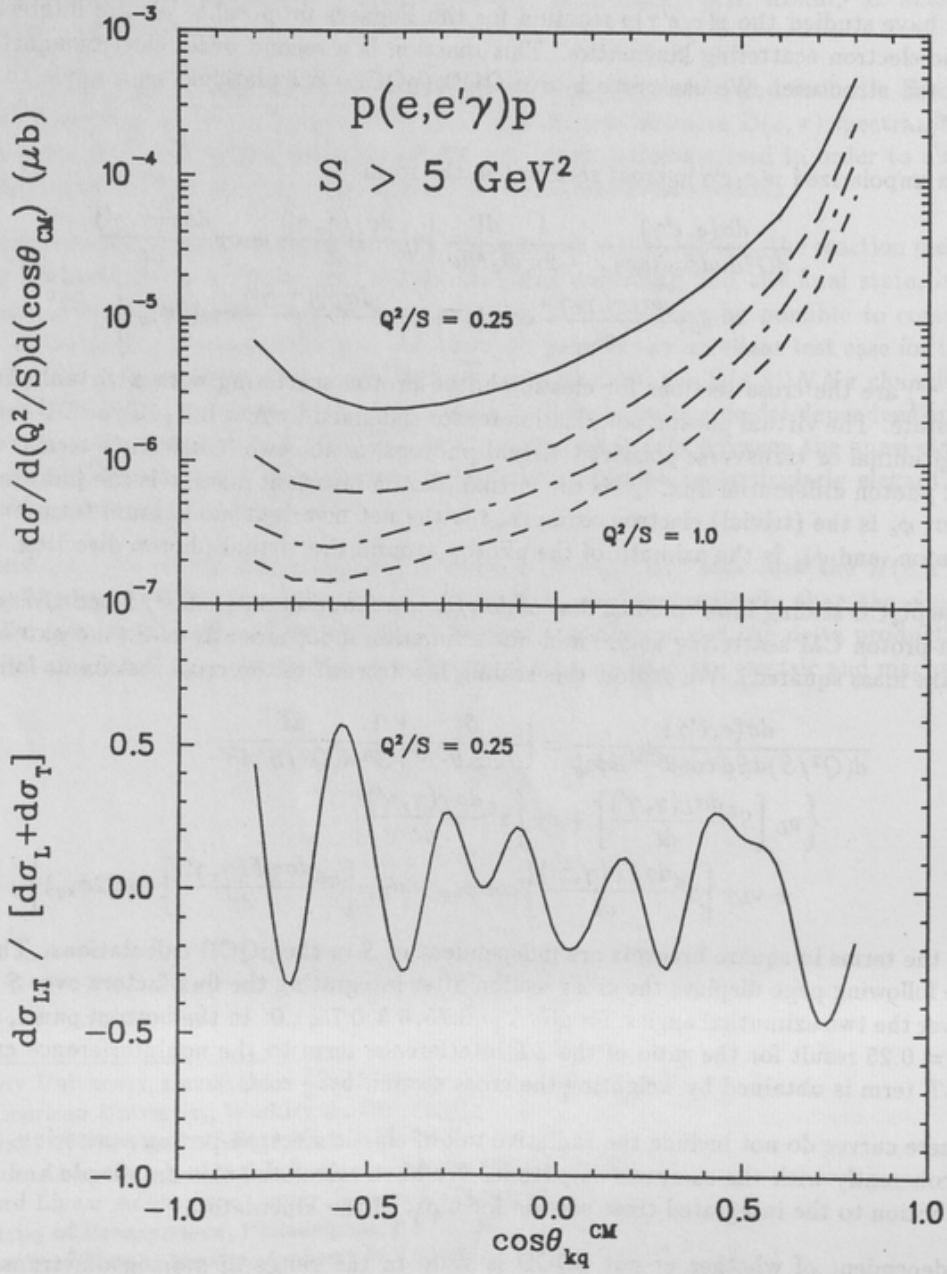

Figure 8)-1. Integrated compton cross-sections (top) and longitudinal-transverse interference asymmetry (bottom.)

9 EXTERNAL USERS

9.1 Cosmic Ray Effects in Microelectronics

B. Hughlock* and A. Johnston*

Space electronics are exposed to cosmic radiation, which includes energetic heavy ions. The passage of a heavy ion through a microelectronic integrated circuit (IC), produces a track of electron-hole pairs. If this occurs in a sensitive area of the circuit it could produce a logic upset (SEU) or transform the circuit to an anomalous state that no longer responds to input signals (SEL).

The Van de Graaff accelerator was used to provide heavy ion beams, which were used to study the basic mechanisms responsible for producing SEU[1] and SEL.[2]

Once these mechanisms are understood it is hoped that IC process techniques or circuit design techniques can be developed that are hardened to these effects. This work is important in the development of future reliable space electronic systems.

*High Technology Center, Boeing Space and Defense Group, Seattle, WA 98124.

[1]B.W. Hughlock, G.S. LaRue and A.H. Johnston, IEEE Trans. Nuc. Sci., **37** 1894 (1990).

[2]A.H. Johnston and B.W. Hughlock, IEEE Trans. Nuc. Sci., **37** 1886 (1990).

9.2 Determination of Cross Sections and Neutron Yields from ^{3}He Reactions on Oxygen, Carbon, and Boron

K.A. Krohn,* J.M. Link,* W.G. Weitkamp and D.I. Will

A collaboration between the Department of Radiology and the Science Applications International Corporation is developing a radiofrequency quadrupole (RFQ) accelerator and targetry for the production of radionuclides for positron emission tomography (PET) medical imaging. This RFQ accelerator has been designed to accelerate ^{3}He ions to 8.0 MeV. The collaborative responsibility of the researchers at the University of Washington is to confirm that the system as designed is capable of producing ^{11}C, ^{13}N, ^{18}F, and ^{15}O in sufficient amounts to be useful for PET imaging and to develop the targets and target chemistry for the RFQ.

Our first effort has been to measure the nuclear reaction cross sections, thick target radionuclide yields and neutron yields with ^{3}He on targets of B, C and O. The design energy of the RFQ (8 MeV) was selected using literature values[1] for nuclear reaction cross sections for each of these targets to estimate yields which would provide sufficient quantities of radioisotope to meet the needs of a clinical PET program; but these cross sections require verification. It is expected that ^{3}He induced reactions will produce few neutrons, a major advantage of the ^{3}He RFQ for medical use. Carbon targets will only yield neutrons from the ^{12}C(^{3}He,n)^{14}O and ^{12}C(^{3}He,pn)^{13}N reactions. Neutron yields should also be measured.

The ^{3}He beam from the tandem Van de Graaff accelerator is ideal for these experiments. We have had four runs over the past 14 months to measure cross sections and yields from both thin and thick B, C and O targets with up to 1 μA of ^{3}He and for energies from 4 to 14 MeV.

The thick target yields for CNOF radionuclides are the most practical outcome from these measurements, but we also measured thin target yields for estimating nuclear reaction cross sections. The latter are more sensitive in selecting the correct energy for the PET-RFQ and can be compared with the cross sections reported in the literature, which used stacked targets and have $\sim$1 MeV uncertainties in ^{3}He energy. They are also important because they show possible structure in the cross sections from direct interactions. The thick target yields for production of ^{11}C and ^{13}N from elemental carbon agree well with those calculated from the literature. The yields we measured from boron are less for ^{11}C and more for ^{13}N than those in the literature. The thick target saturation yields measured for production of ^{15}O and ^{18}F from ^{16}O are greater than those calculated from literature cross sections by $\sim$20%.

Cross sections for the production of ^{15}O and ^{18}F from ^{16}O were in reasonable agreement with those reported in the literature. We have some indication that the cross section in the literature for ^{15}O production should be shifted upward in energy; the energies for our data points are accurate to two percent. Such a precise knowledge of energy for the ^{15}O cross section is critical for design of the RFQ.

Neutrons yields were measured at the same time, using Bonner spheres and liquid scintillators. The results generally confirmed the feasibility of the PET-RFQ design. Neutron yields were mea-

*Department of Radiology, University of Washington, Seattle, WA.

[1]R.L. Hahn and E. Ricci, Phys. Rev. **146**, 650 (1966) and Nucl. Phys. A **101**, 353 (1967).

sured from the following targets: elemental C, Kapton, B_2O_3, SnO_2, CuO, WO_3, Ta_2O_5, SiO_2, Al and Ta. The latter two materials would be useful in construction of targets. Results of these measurements given in Fig. 9.2-1 below.

This research is supported by SDIO-84-89-C-0046, subcontract 13-900224-49.

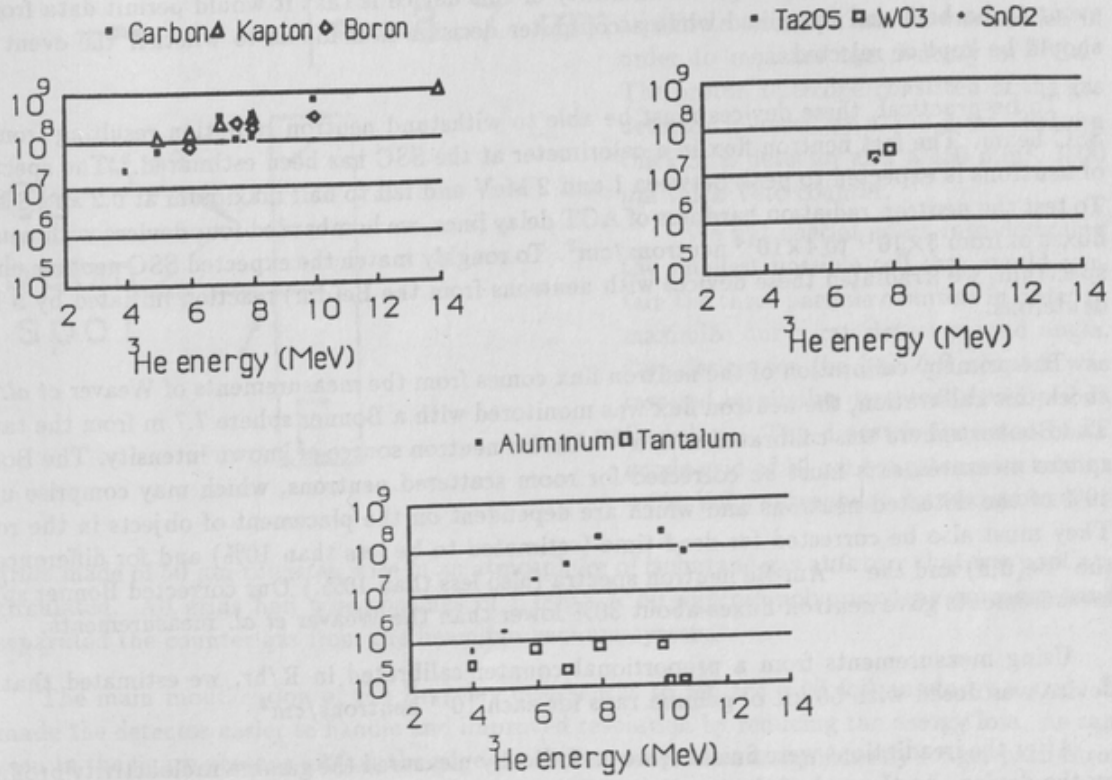

Figure 9.2-1. Thick target neutron yields from targets indicated per μC of incident $^3He^{2+}$ beam.

9.3 Neutron Irradiation of Acoustical Charge Transport Delay Lines

R.J. Davisson,* W.M. Dougherty,* M.S. Kaplan, H. Lubatti,* W.G. Weitkamp and J. Wilkes*

Acoustical charge transport (ACT) delay lines are being evaluated for possible use in future SSC based experiments.[1] These devices[2] can store analog signals for several μsec; the length of the delay is externally variable. The signals stored in the device can be non-destructively read out at an intermediate time. The potential utility of this device is that it would permit data from an event to be held and examined while a computer decision is made as to whether the event data should be kept or rejected.

To be practical, these devices must be able to withstand neutron radiation resulting from the SSC beam. The fast neutron flux in a calorimeter at the SSC has been estimated.[3] The spectrum of neutrons is expected to peak between 1 and 2 MeV and fall to half maximum at 0.2 and 8 MeV. To test the neutron radiation hardness of ACT delay lines, we bombarded four devices with neutron fluxes of from 5×10^{11} to 4×10^{14} neutrons/cm^2. To roughly match the expected SSC neutron energy spectrum, we irradiated these devices with neutrons from the Be(d,n) reaction initiated by 9 MeV deuterons.

The primary calibration of the neutron flux comes from the measurements of Weaver *et al.*[4] To check this calibration, the neutron flux was monitored with a Bonner sphere 7.7 m from the target. The Bonner sphere was calibrated with a ^{241}Am-Be neutron source of known intensity. The Bonner sphere measurements must be corrected for room scattered neutrons, which may comprise up to 40% of the detected neutrons and which are dependent on the placement of objects in the room. They must also be corrected for dead time (estimated to be less than 10%) and for differences in the ^{9}Be(d,n) and the ^{241}Am-Be neutron spectra (also less than 10%.) Our corrected Bonner sphere measurements gave neutron fluxes about 30% lower than the Weaver *et al.* measurements.

Using measurements from a proportional counter calibrated in R/hr, we estimated that the device was dosed with 50 kR of gamma rays for each 10^{14} neutrons/cm^2.

After the irradiations were finished, we periodically measured the gamma radioactivity produced by the device. At the end of the irradiation, about 85% of the radioactivity was from ^{76}As, with a 26.5 hour half life; the rest was primarily from 15 hour ^{72}Ga.

An ACT delay line given a dose of 1×10^{14} neutrons/cm^2 has been tested for electronic performance.[5] The result is that although the device shows signs of radiation damage, the key operational parameters are barely affected by the neutron dose. Consequently the device shows sufficient neutron hardness for SSC application.

---

*Department of Physics, University of Washington, Seattle, WA 98195.

[1] R.J. Davisson, W.M. Dougherty, H.J. Lubatti, R.J. Wilkes, D. Fleish, R. Kansy and G. Pieters, Nucl. Instrum. and Meth. **A295**, 344 (1990).

[2] M.J. Hoskins and B.J. Hunsinger, 1986 IEEE Ultrasonics Symposium Proceedings, p. 439.

[3] "Radiation Levels in SSC Calorimetry" SSC Central Design Group Report SSC-229, 1989.

[4] K.S. Weaver, J.D. Anderson, H.H. Barschall and J.C. Davis, Nucl. Sci. and Eng. **52**, 35 (1973).

[5] Communication from Electronic Decisions Inc., 1776 E. Washington St., Urbana IL 61801.

10 INSTRUMENTATION

10.1 Ultra-thin Gas Counter for High-efficiency and High-resolution Measurements of β-delayed Protons

E.G.Adelberger, A.García, P.V. Magnus, D.M. Moltz* and D Wells

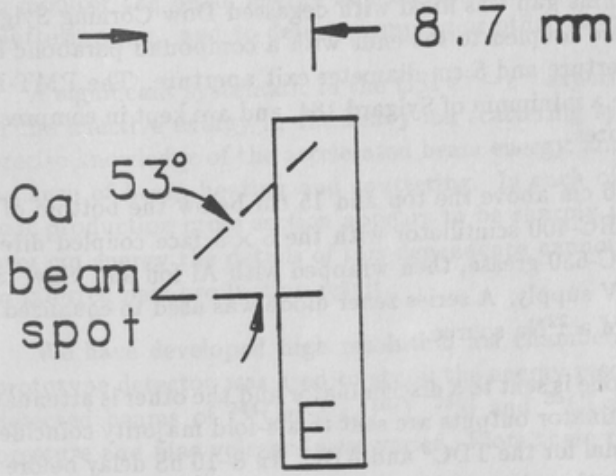

We have developed an ultra-thin gas counter to be used as the ΔE element of a particle telescope which was needed in order to measure the β-decay of ^{37}Ca.[1] The proton telescope consisted of the gas detector followed by a 150 mm^2, 300 μm thick Si E detector and a 450 mm^2, 1000 μm thick Veto counter.

We put special effort into designing the smallest possible cell that would contain the three particle counters in order to maximize our γ-ray detector solid angle. Our design for the gas ΔE counter was inspired by similar detectors developed at Berkeley[3]. The detector consisted of an anode grid of 10 μm tungsten wire held at +600 Volts surrounded by two grounded grids made of 50 μm tungsten wire in an atmosphere of isobutane gas at 9 torr that was continually circulated. All grids had wire spacings of 1 mm. A 50 μg/cm^2 polypropylene entrance window separated the counter gas from the beamline vacuum system.

The main modification of the Berkeley design was to replace a Ni foil anode by a grid. This made the detector easier to handle and improved resolution by reducing the energy loss. As can be seen in the figure protons hitting the edge of the E counter have a significantly longer path through the gas and anode than those hitting the center. This was an important concern in our experiment since we wanted to attain the best possible resolution for protons with energies from 0.5 to 6.0 MeV. However, in order to obtain a reasonable signal from the small energies deposited in the ΔE detector, we needed higher anode voltages which requires additional care in the cell design to avoid sparking.

In section 4.1 of this report it is shown that we were able to attain a resolution of $\approx$ 16 keV for $\approx$ 1 MeV protons, which means that the energy spread due to energy loss in the ΔE detector was negligible and that the resolution was dominated by noise in the E counter. The total efficiency of our telescope was $\approx$ 11%.

*Lawrence Berkeley Laboratory, Berkeley, CA 91125.

[1]See this Report, Section 4.1.

[2]D.M. Moltz, to be published Nucl. Inst. and Meth.

10.2 The Scintillator TOF Prototype for PEGASYS

J.F. Amsbaugh and C.E. Hyde-Wright

Two pieces of SCSN-38[1] scintillator (5.3 × 10 × 100 cm and 5.3 × 10 × 230 cm) have been used in a prototype study with cosmic ray muons. Each scintillator was wrapped loosely with 6 mil polyethylene sheeting then wrapped with an overlapping layer of 2 inch wide 1 mil vinyl tape. The two pieces are clamped, 10 cm face up, to a supports six inches from the ends of each piece with a millimeter gap between the scintillators. This gap was filled with degassed Dow Corning Sylgard-184. Hamamatsu R329-05 5 cm PMTs were coupled to the ends with a compound parabolic light guide with 5 × 8 cm rectangular input aperture and 5 cm diameter exit aperture. The PMT-light guide and light guide-scintillator joints use a minimum of Sylgard 184, and are kept in compression by rings and tie rods to the clamping fixtures.

Two trigger detectors are positioned 16 cm above the top and 15 cm below the bottom of the long bar. Each trigger is a 5 × 5 × 1 cm BC-400 scintillator with the 5 × 5 face coupled directly to Hamamatsu H1949 5 cm PMTs with BC-630 grease, then wrapped with Al foil and vinyl tape. Each pair of PMTs was powered by one HV supply. A series zener diode was used to equalized the gains, as calibrated by the compton edge of a ^{22}Na source.

Each PMT provides two anode signals; one is sent to a discriminator and the other is attenuated, delayed and sent to the ADC.[2] The discriminator outputs are sent to a 4-fold majority coincidence unit to define the event signal and start signal for the TDC[3] and ADC. An 8–10 nS delay before the discriminator of the top anode signal assures that the top always defines the start in the coincidence. The 2249SG ADC requires inhibiting the discriminator during digitization and clearing after any non-coincident gate.

Data has been taken with the trigger at five positions along the long bar with a leading edge discriminator (LED), LRS 623B, and at four positions with a constant fraction discriminator (CFD), Ortec 935. Amplitude time walk corrections are made by least-squares fit to

$$TDC_i = A_i + \frac{\kappa_i}{\sqrt{ADC_i}} + \frac{\kappa_t}{\sqrt{ADC_{top}}}$$

where A_i is a constant delay and i labels bottom, left, and right PMTs. The correction is applied to the LED data and the corrected mean timing $(ctdc_l + ctdc_r)/2$ of the two ends is calculated which removes the width contribution from the trigger spatial extent.

A gaussian fit to the mean timing yields the time resolution, σ_{mt}, which includes the top trigger resolution. Preliminary results for the center trigger position are:
LED data: σ_{mt} = 260 pS, σ_b = 320 pS before corrections,
LED data: σ_{mt} = 199 pS, σ_b = 180 pS after corrections,
CFD data: σ_{mt} = 205 pS, σ_b = 193 pS before corrections.

[1] Kyowa Gas Chemical Co. donation arranged by Mitsui Plastics.
[2] LeCroy model 2249SG 0.25 pC/count.
[3] LeCroy model 2228A, 50 pS/count.

10.3 Precision Ion Chambers for 1.4 GeV Uranium

B. Thompson, T.A. Trainor and S.P. Van Verst

As part of the APEX monitoring system (see Sec. 2.7) two ion chambers will be placed at $\pm 11°$ with respect to the beam in the vertical plane. These chambers will detect elastically scattered beam particles with good energy resolution. The primary purpose is to provide normalization and to monitor the beam energy and target condition, including changes in average thickness due to sputtering, e.g., and to detect clumping or other changes in uniformity due to beam heating.

A significant systematic in the GSI $e^+ - e^-$ experiments has been the lack of precise knowledge of the effective energy in the heavy ion scattering system. This is due to changes in and lack of precise knowledge of the accelerated beam energy, and due to development of target nonuniformity because of beam heating and sputtering. In each of the heavy ion systems studied the $e^+ - e^-$ pair production cross section appears to be sharply peaked near 6 MeV/u. Without good control over cm energy the details of this dependence cannot be obtained, and non-statistical fluctuations in inferred pair production result.

We have developed high resolution ion chambers to be used for beam-target monitoring. A prototype detector was used to study the energy resolution systematics for this detector type. We detected beams of ^{244}Cm α's, ^{16}O, ^{28}Si and ^{35}Cl at various energies. In addition the detector pressure and bias voltages were varied. From these results we made the following observations.

The entrance window of the detector bows outward. Therefore, care must be taken to collect the charge deposited in this region to avoid a 1–2% systematic. In our case the aluminized mylar window is placed at the cathode potential. If an ion chamber is segmented for dE/dx measurements so that a uniform field is required, then bowing must be minimized by a dielectric support grid. We also tilt the window $\sim 10°$ from normal to the particle trajectory to make sure that all charge falls to the anode.

The Frisch grid is fabricated with only transverse wires (50μ wire on 2.5 mm centers) so that the amount of charge intercepted is independent of track position.

We observed that the resolution of the prototype was pressure dependent, with resolution improving with gas pressure by very significant amounts (20–100%). We traced this to the delta ray component of track ionization. At typical chamber pressures (50–150 Torr) δ electrons have ranges of 10 mm or more. A significant fraction of these (several percent of the total track charge) can then be intercepted by electrodes and the secondary ionization not collected. If the entrance aperture size is a significant fraction of the electrode spacing, and especially if there is asymmetry in the electrode placement, a very significant pressure-dependent resolution component results. As the pressure increases the δ-electron range decreases and the resolution improves. We have responded by using a narrow (1.6 mm) slit aperture normal to the E-field, centered on a large electrode spacing (50 mm). At the operating pressure of 150–200 Torr this geometry eliminates the 8 electron resolution contribution.

We used a 220 μg/cm^2 aluminized mylar window for these studies. We find that the thickness variation over the entrance opening is 10–15%. Similar or worse variations occur in thinner (80–100μg/cm^2) stretched polypropylene windows. However, with a sufficiently small window area one

can use interference fringes to select a more uniform section of polypropylene for the window. The window nonuniformity problem depends on the range of the incident particle. For instance, for APEX we detect uranium-like particles with a range of ~12mg/cm^2 in carbon. They lose about 2% of their energy in the window. This means the window resolution contribution for these particles is 0.2–0.3%. This is expected to be the dominant resolution component. A 0.3% resolution is quite satisfactory for APEX.

We observe signal reduction due to recombination at higher gas pressures but no increase in the resolution width for the beams studied. However, the very highly ionizing uranium-like particles to be detected with APEX may produce plasmas of sufficient density that recombination is a problem. We have designed the production ion chambers to operate at 10kV across the cathode-Frisch grid gap. This results in a fairly high E/P of 10–15 volts/Torr-cm. The voltage is essentially limited by general breakdown between major electrodes in isobutane at these pressures. One can exceed 100 Volts/Torr-cm in a PPAC at significant count rates, but only with very smooth planar electrodes. Significant recombination studies await installation on the APEX system and operation with ATLAS beams.

Performance with the prototype detector system is shown in Fig. 10.3-1. This is with a 42 MeV ^{16}O beam at 30° in the lab. The resolution is dominated by kinematic broadening and window nonuniformity. The energy resolution is 0.67%.

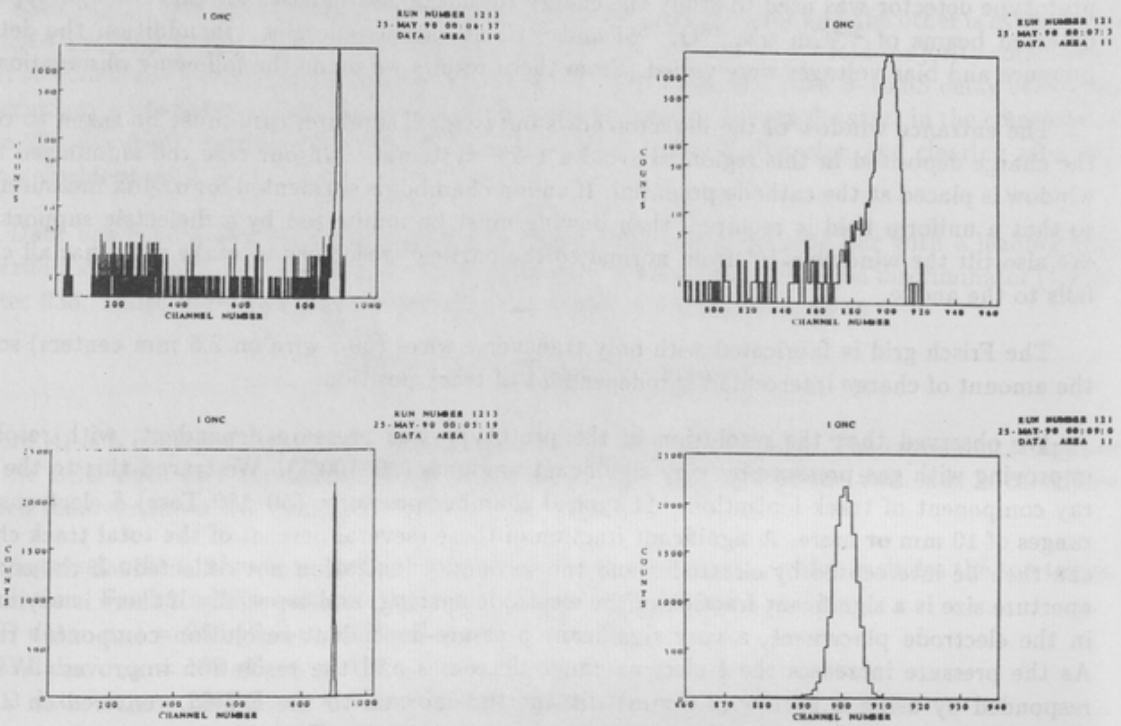

Fig. 10.3-1. Prototype ion chamber spectrum for 42 MeV ^{16}O scattered from 150 μg/cm^2 Au. Top: Log plot. Bottom: Linear plot. Energy resolution is 0.67%.

10.4 APEX Silicon Array Gas Cooling System

T.A. Trainor

The gas cooling system for the APEX silicon arrays (see Sec. 2.7) consists of a thin, cylindrical kapton shroud around each array, and cold gas generators which deliver up to 1 atm-ℓ/sec of N2 gas at about 100K through the detector array. The shroud manufacture is essentially as previously described[1] except that the diameter has increased to 5 cm to accommodate changes in the array design.

The cold gas system consists of a pressure stabilized LN2 boiler, double-wall gas transfer lines, insulated valve box, and throttled mechanical pump. The LN2 boiler is a double-wall, 15 liter stainless steel dewar. Dewar pressure is maintained at 2–3 psig by means of a 400 watt immersion heater driven by an Omega CN-1201 digital PID controller and an Omega PX 126 differential pressure transducer.

Cold gas from this dewar or warm N2 from a standard gas bottle can be switch selected to pass through a cryogenic throttle valve for reduction to the shroud operating pressure of 100–150 Torr. The throttle valve and ASCO cryogenic solenoid valves are contained in an evacuated valve box. Gas is then delivered to the array via a double wall evacuated transfer line about 2 m long.

"Warm" gas from the array exits the shroud region and passes over an Omega CIR 300 watt rod heater centered in the transfer line. This heater is driven by an Omega 6103 temperature controller and iron-constantin thermocouple to return the gas to near ambient temperature.

The gas finally flows through an MKS 253A electric throttle valve driven by an MKS 252-C valve controller and MKS 122AA Baratron pressure transducer. This system maintains the shroud pressure at 100–150 Torr for a broad range of gas flow rates. The throttle valve is backed by a Leybold D25B 20CFM mechanical pump.

[1] Nuclear Physics Laboratory Annual Report (1990), Univ. of Washington, p. 74.

10.5 High Resolution Mass Analysis with the Injector Deck Beam Transport System

T.A. Trainor, R. Vandenbosch and D.I. Will

The injector deck beam transport system[1] was designed to achieve a mass resolution $m/\Delta m$ ~100 to match the mass acceptance range of our linear accelerator. This design figure was based in part on typical emittance figures for sputter-type heavy ion sources at the time of the design. With the installation of the modified Model 860 sputter source[2] we observed, however, mass resolutions as high as 600 without object slits, that is, based only on the object defined by the cesium beam on the sputter target.

This high mass resolution has recently become important in connection with studies of molecular-fusion (see Sec. 2.3) in which we are interested in producing beams of deuterated organic molecules in the mass region 100–250. Figure 10.5-1 shows some examples of mass spectra obtained while producing organic molecular beams from the Model 860 sputter source.

The bottom spectrum shows a scan with a stearic acid sample. What one observes is that under some source operating conditions high carbon polymers essentially stripped of hydrogen are produced. By repeated scanning one can find source operating conditions under which the molecular beam of interest is enhanced relative to this polymer production.

Of special interest is the complex near mass 108 which is expanded immediately above. This consists of the two isotopes of silver, and between them a broad peak due to the Al_4 polymer. This peak is broad, with a deep dip in the center, because the object is an annular region of the aluminum sample holder surface around the stearic acid plus silver powder sample (3 mm diameter). The peaks for aluminum polymers Al_5 and Al_6 in the bottom scan can also be seen to be hollow. Returning to the upper left trace one can also see a small peak in the center of the Al_4 peak which is the C_9 polymer. This same complex is shown in a wire scanner trace at upper right with greater clarity. The scanner is placed just upstream of the image slits.

The center scan shows excellent mass resolution above mass 200. This mass scan segment was obtained with a chrysene/silver sample and shows the isotopic distribution for the Ag_2 dimer.

[1]Nuclear Physics Laboratory Annual Report, University of Washington (1986), p. 71.
[2]Nuclear Physics Laboratory Annual Report, University of Washington (1986), p. 52.

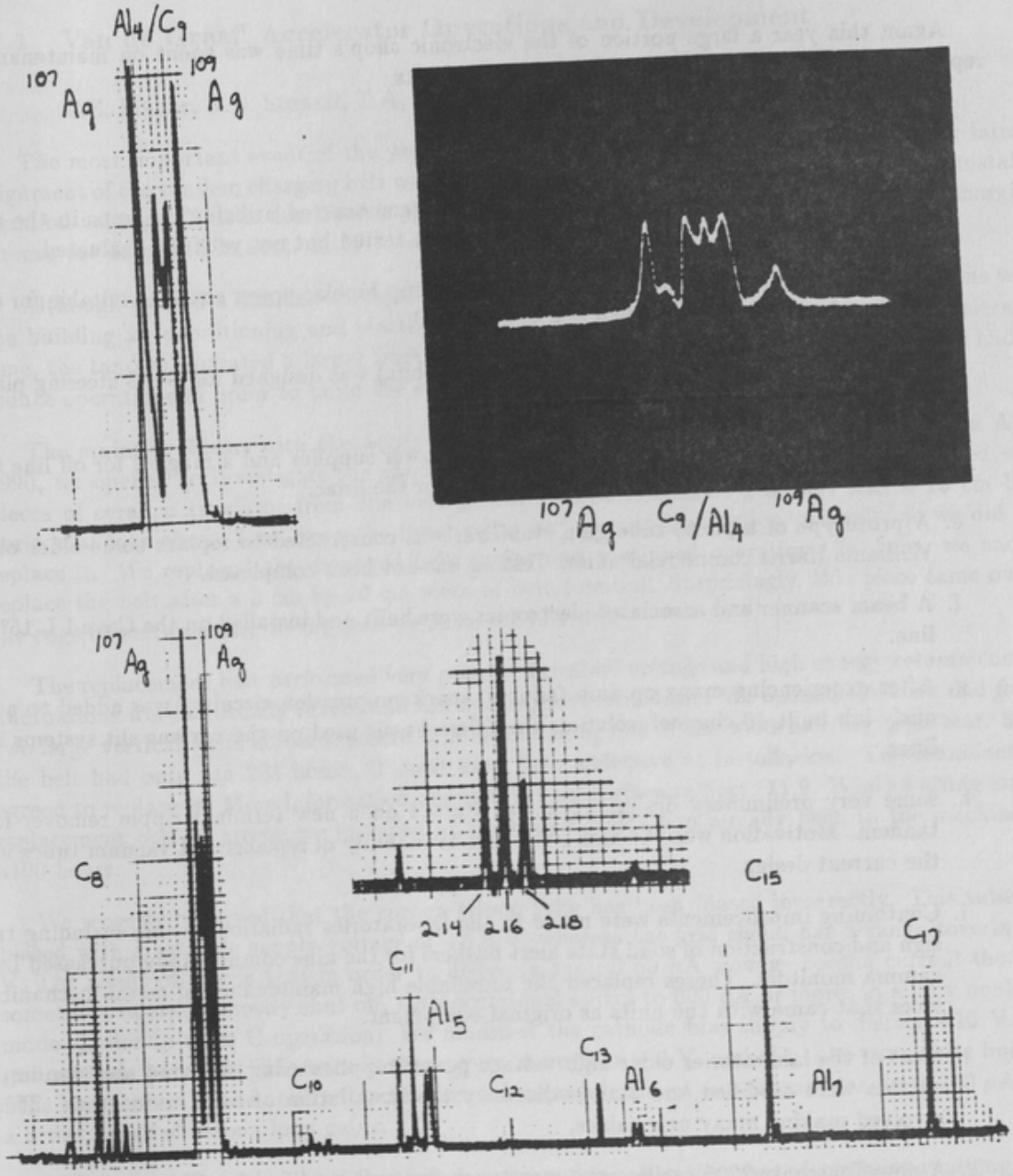

Figure 10.5-1. Representative magnetic field scans and scanner trace with organic molecular samples.

10.6 Electronic Equipment

R.E. Stowell and T.D. Van Wechel

Again this year a large portion of the electronic shop's time was spent on maintenance and repair rather than on design and construction projects.

Some projects that were undertaken included:

a. A prototype of an active photo-tube base was constructed utilizing op amps in the dynode string as the active element. The unit has been tested but not yet fully evaluated.

b. Two portable constant current adjustable ±5 amp bipolar power supplies suitable for driving various magnets were designed and constructed.

c. A high voltage bipolar op amp circuit (±150 volts) was designed for DEIS steering plates on the injector deck.

d. A test bench was set up with the necessary power supplies and a magnet for off line testing of the commercial Bruker NMR's purchased for the linac.

e. A prototype of a photo-tube gain stabilizer was constructed to replace some older obsolete Williams Harris commercial units. Testing has not been completed.

f. A beam scanner and associated electronics were built and installed on the Cave 1 L 15° beam line.

g. After experiencing many op amp failures, spark suppression circuitry was added to a previously lab built 16 channel isolation amplifier chassis used on the various slit systems on the linac.

h. some very preliminary design work was started on a new terminal ripple remover for the tandem. Motivation was the high price and availability of replacement vacuum tubes used in the current design.

i. Continuing improvements were made to the laboratories radiation system including the design and construction of solid state alert flashers for the nine commercially purchased Ludlam gamma monitors. Theses replaced the unreliable high maintenance bi-metal mechanical devices that came with the units as original equipment.

j. Most of the laboratories older high voltage power supplies using outdated non standard connectors were modified and standardized by the installation of SHV connectors. This also involved making many new cables.

k. A new Tektronix 2205 oscilloscope was purchased and modified for Caves 1 and 2 beam line scanner observation. It replaces an obsolete scope on the tandem console.

l. A chassis containing eight 12 bit DAC's and associated logic was built for the off deck optics stack to allow computer control of the various electrostatic and magnetic deflectors.

11 ACCELERATORS AND ION SOURCES

11.1 Van de Graaff Accelerator Operations and Development

C.E. Linder, R.E. Stowell, T.A. Trainor, T.D. Van Wechel and W.G. Weitkamp

The most important event of the year for the tandem was the discovery that improper lateral alignment of the tandem charging belt was causing excess high energy column currents and unstable terminal voltages. This is described in detail in Section 11.11. Experiences with tandem charging screens are described in Sect. 11.10.

Although we had a number of major accelerator tank openings and a number of problems with the building air conditioning and electric power systems, all of which resulted in lost accelerator time, the tandem operated a larger fraction of the time than any year since 1984, when we had to reduce operations in order to build the superconducting booster.

The major problems with the accelerator tank have been related to charging belts. In April 1990, we opened to investigate the cause of excessive sparking and found the floor littered with pieces of ceramic insulator from the belt guides outside the belt. The belt had a 15 cm long horizontal tear about 7 cm from the lower edge, but seemed to function properly, so we did not replace it. We replaced the damaged belt guides and continued operation. In June, we had to replace the belt after a 3 cm by 20 cm piece of belt tore out. Surprisingly, this piece came out of the edge of belt opposite to the tear we observed in April.

The replacement belt performed very poorly. Terminal voltage and high energy column current fluctuations were unusually severe and did not improve with time. We opened the tank and found two large vertical welts across the belt. The fabric along one of the welts had begun to tear. Since the belt had only run 234 hours, it must have been defective at installation. The manufacturer agreed to replace it. More information about this belt is given in Sect. 11.9. While waiting for the replacement belt to arrive, we installed an older belt which had already been in the machine for 3100 hours.

We recently observed that the corona triode tube has been biased incorrectly. This tube was biased with a cathode supply voltage of +6.5 V, whereas the grid signal has a range covering ±8 V. The result of this is that in order to deliver a typical 50 μA average corona current the tube sometimes operates mostly shut off, with occasional spikes to 500 μA or more, in a very nonlinear mode similar to class C operation. We modified the cathode bias supply to deliver +10 V. The grid-cathode potential difference is then never more than −2 V, and the tube runs quite linearly. This has resulted in the ability to achieve excellent regulation at any corona bias up to 150 μA over a broad range of corona loop gains.

In January 1991, we entered the tank to refoil and investigate causes of excessive sparking. The belt had many small vertical tears so we replaced it. It had run a total of 6580 hours, which is typical of our experience with belt lifetimes. We also observed damage to the glass in beam tube section 2, just upstream from the terminal. Since we fortuitously had a spare for this beam tube section, we replaced it. The section had been in the machine for about 42,500 operating hours.

We have finished our tests of new resistor assemblies for the column and have decided to install

an assembly consisting of 4 Kobra[1] resistors in a PVC tube. Each resistor has a value of 100 MΩ, a tolerance of 1% and a maximum operating voltage of 32 kV. We are assembling enough elements to replace 20% of our aging (16 year old) resistors.

We have arranged for local firms to rewind and remetalize the bearings on two old drive motors. The windings of the motors were also carefully cleaned, which is important for minimizing overheating. We have also stepped up the voltage to the drive motors by 10%, to a value of 222V, in hopes of further reducing the likelihood the motor will overheat.

During the year from March 1, 1990 to February 28, 1991 the tandem operated 4922 hours. Additional statistics of accelerator operations are given in Table 11.1-1.

Table 11.1-1
Tandem Accelerator Operations
March 1, 1990 to February 28, 1991

Activity	*Days Scheduled*	*Percent*
A. Nuclear Physics Research, Tandem Alone		
Light Ions	54	15
Polarized Ions	37	10
Heavy Ions	43	12
Accelerator Mass Spectrometry	18	5
Subtotal	152	42
B. Nuclear Physics Research, Booster and Tandem Coupled		
Light Ions	9	2
Polarized Ions	5	1
Heavy Ions	49	13
Subtotal	63	16
B. Outside Users		
Boeing Corporation	6	2
University of Washington Department of Physics	6	2
University of Washington Department of Radiology	3	1
Subtotal	15	5
C. Other Operations		
Tandem Development	34	9
Tandem Maintenance	76	21
Unscheduled Time	25	7
Subtotal	135	37
Total	365	100

[1]K&M Electronics, West Springfield MA 01089.

11.2 The Crossed-Beams Polarized Ion Source

D.T. Corcoran, J.K. Eisenberg, C.A. Gossett, G.C. Harper and J.A.Rogers

The use of the polarized ion source for nuclear physics experiments has been rapidly increasing and the range of energies of the accelerated beams has varied from 1 to 33 MeV. In the past year we have had seven data taking runs ranging in time from four days to over two weeks.

During the past year we have continued to concentrate on the reliability of the polarized ion source. In the past, the voltage on the ten element voltage gradient, which provides an axial "push" toward the extraction region of the ionization solenoid, has been provided by a resistor string external to the vacuum system. The ten associated electrical connections have been tedious to make and somewhat unreliable. In addition we have experienced frequent high voltage breakdowns in the area of the connections for these 10 wires. We have gone to a system in which we have a resistor string internal to the vacuum system which has greatly improved the ease of maintenance of the system and eliminated a source of sparking. We have not observed any vacuum degradation due to the resistors.

We also invested some time in rearranging the feedthrough ports in the ionization region of the source. The H^- extraction region of the source is housed in a cylindrical chamber with eight ports around its circumference. In the original design several high voltage leads criss-crossed one another. We have observed some high voltage breakdowns which appeared to be between high voltage leads to the einzel and ion extraction lenses. (The lenses are physically quite separated so direct sparking between them is unlikely.) We also experienced some high voltage breakdowns which seemed to be either beam related or beam induced, perhaps cesium metal condensation or deposition of sputtered material which contributed to sparking, in particular from the einzel lens. We have modified the design of our einzel lens and have rearranged the high voltage and vacuum feedthroughs to reduce the interaction of the leads. Changes to simpler and more reliable connections internal to the vacuum system have improved the ease of maintenance of the source. In our last two experimental runs we have not had any interruption of the source operation due to sparking.

We are currently testing a new radio frequency oscillator supply for the weak field hyperfine transition. The original unit was difficult to tune, relied on vacuum tube components which were expensive and difficult to replace, and for lack of a circuit diagram was very inconvenient to repair. The new unit is a fairly standard transceiver which we are operating at 14.5 MHz. We have added a keying function which allows for rapid switching for fast polarization reversal. We are currently testing the new unit and plan to add a feedback circuit to control the power level in the cavity.

Recently we have constructed a small chamber and port which will allow us to measure the intensity of momentum analyzed beams directly out of the source. Currently the beam must pass some distance through several transport elements before we can test the beam intensity. We hope to use this new chamber to test to what extent we may be losing beam intensity in the low energy beam transport and in particular through a pair of 90° cylindrical electrostatic deflectors which translate the beam from the polarized source axis to the tandem axis. The new port will also facilitate work at improving the beam intensity allowing us to test the effects of changes to the H^- extraction geometry independent of several downstream beam transport elements.

11.3 Booster Operations

D.T. Corcoran, G.C. Harper, M.A. Howe, D.W. Storm, D.I. Will and J.A. Wootress

During the calendar year 1990, the booster was operated for 67 days, as compared to 52 days in the previous year. Beams ranged in mass from protons to ^{58}Ni, with the majority of beams of mass between 16 and 32. The maximum available fields obtained from the resonators was the same as during the previous two years, namely 2.4 MV/m from the high-β resonators and 2.8 from the low-β ones. These fields are the average of all resonators during actual long term operation. However, we expect to be able to improve these figures during the next year, since we have been able to achieve consistent success in test platings of several resonators. Now we have begun replacing some of the poorly operating resonators with newly plated ones.

By the end of 1990 we had three resonators that were inoperable. Two had stuck couplers and one had an open circuit in the power rf cable. We have removed these cryostats and corrected the problems, and are preparing the resonators and cryostats for regular linac operation.

For the first time we had to cancel a linac run. One of the three RS compressors for the helium refrigeration system failed. The motor windings shorted, which is the common failure mode for these compressors. We have determined that we can start the motors by applying line voltage to both the windings simultaneously, rather than waiting 1/2 second between application of line power to the first and second winding. The original setup was supposed to protect the line from transients, but at a cost of heavily loading the first motor winding for 1/2 second. The present scheme does not cause noticeable line transients, and presumably saves the motor windings from excess heating upon starting. The two remaining compressors now have run for about 38k hours. As a replacement compressor costs about $40k, extending the compressor life is important.

11.4 Injector Deck and 860i Sputter Source

G.C. Harper and D.I. Will

Several of the offdeck optics parameters have been connected to interfaces in the injector deck satellite computer enabling them to be controlled or sensed remotely. The most useful of these are the 2 sets of X-Y magnetic steerers in the drift space between the deck and the tandem. Since there was no hard-wired control panel for these steerers in the tandem control room, operation was only possible in the tunnel. In addition to the steerers, connections were made to the grid lens in the deck accelerator tube, the offdeck einzel lens, 2 electrostatic quadrupole triplets, the offdeck faraday cup control and current sense, and the injector deck voltage readback. A menu was written to include these parameters in the portable knob boxes available for use in the tunnel and control room. In each case, the knobs have been scaled to increase the resolution of the tuned parameter. Future connections are being planned for 2 sets of electrostatic X-Y steerers and the 5 inch pre-tandem einzel lens.

The main acceleration gap insulator on the deck-mounted 860i sputter source[1] failed in 1990. During the summer the insulator interior surface repeatedly developed high resistance leakage paths to ground requiring more frequent source cleaning than had been usual historically. By September, the base vacuum was elevated and somewhat erratic. Several leaks were located around the circumference of the adhesive joints using a helium leak detector. On cleaning the insulator, the two adhesive joints between the epoxy insulator and its two end flanges exhibited a gummy fluid oozing out of the joints into the vacuum space. Several unsuccessful attempts were made to reseal the joints. Because the adhesive joint was still physically strong, separating the epoxy insulator from its flanges was not attempted. Instead the assembly was patched temporarily with Torr Seal,[2] and a new high-alumina glazed ceramic insulator was ordered. Flanges for the new insulator were made in the lab machine shop and attached with Torr Seal. This opportunity was taken to lengthen the main insulator from one and one-half inches to four inches. The ground electrode was also extended to maintain lens and acceleration gap geometry. This new insulator has worked well to 50 kV bias although the 860i is regularly operated at 30 kV bias. (The electrode actually sees approximately 40 kV to 20 kV, respectively.) The source will need additional anticorona shielding if it is operated above 40 kV bias regularly.

[1]This is a General Ionex Corporation Model 860 Negative Ion Sputter Source modified as described in Nuclear Physics Laboratory Annual Report, University of Washington (1988) p. 52.

[2]Trademark of Varian Associates, Inc.

11.5 Cryogenic Operations

M.A. Howe, D.I. Will and J.A. Wootress

The booster linac is cooled by liquid helium which is thermally shielded by liquid nitrogen. In 1990 liquid nitrogen consumption increased 17% to 246,000 gallons.[1] The helium is purchased as high purity bulk gas and liquified by our helium refrigerator. Usage of 153,000 SCF in 1990 was essentially unchanged from that in 1989 despite four power outages of from 8 to 24 hours. All four were associated with replacement of a PCB filled transformer by a dry transformer.

In 1990 we suffered our first compressor failure. Our RS compressor skids from Koch Process Systems utilize a close-coupled motor and compressor hermetically sealed in a welded, certified pressure vessel, This pressure vessel and its contents are called the compressor core. In March ('90) the motor windings of our # 3 screw compressor shorted to ground. We replaced the shorted compressor core with a new core (called # 3a and bought from Koch) and are operating the new core successfully. The total elapsed hours and status of each of our compressor cores (as of 1991 March 11) is indicated in the following table which also summarizes our maintenance for 1990 January 1 to 1991 January 1:

Item	Use	Major Services	Times Performed
Refrigerator			
Cold Box	99%	warm/pump/purge	2
Main Dewar	99%	warm/pump/purge	1
Top Expander	~5750 Hrs	warm/pump/purge	13
	~100 RPM	main seals	3
		wristpin, crank, and cam follower brngs	2
		flywheel bearings	1
Middle Expander	~7400 Hrs	warm/pump/purge	8
	~130 RPM	main seals	3
		wristpin, crank, and cam follower brngs	1
Wet Expander	~4000 Hrs	warm/pump/purge	7
	~40 RPM	main seals	2
		wristpin, crank, and cam follower brngs	1
Screw Compressors			
RS-1	40,643 Hrs	total/running	
	7751 Hrs	1990/replaced charcoal/oil	1
RS-2	37,409 Hrs	total/running	
	6919 Hrs	1990/replaced charcoal/oil[2]	2
RS-3	22,752 Hrs	total/shorted to ground	
	908 Hrs	1990/core removed	
RS-3a	6,995 Hrs	total/running	
	5438 Hrs	1990/installed as new core	
Distribution System	99%	warm/pump/purge lines	9

[1] Nuclear Physics Laboratory Annual Report, University of Washington (1990) p. 79.

[2] One load of charcoal was shipped from Massachusetts to Washington by truck freight and it appeared excessivel· dusty on receipt. On installation it plugged a felt outlet filter and the main screen filter on the inlet of our helium refrigerator. To avoid further blockage, we changed charcoal a second time.

11.6 Resonator Plating Development

D.T. Corcoran, M.A. Howe and D.W. Storm

During 1990 we plated and tested two different resonators 5 times. As we had been unable to obtain good performance in the tests we had been doing during the previous year, we replaced the plating solution with one made from new chemicals, and we only tested resonators which appeared to have a very high quality plating. After we found that we could reproduce our previous resonator performance with our standard thick plate (10 micron) and polish technique, we tested resonators that were plated with about 2 microns of lead and not polished. The thin plating technique has been successful elsewhere, and it is easier to do than the thick plating.

We found that thin plated resonators can have very high low field Q factors, but these Q factors decrease with increasing field in the resonators. The rate of decrease with increasing field is gradual enough that the resonators have satisfactory Q factors at the desired operating field of 3 MV/m. Some examples are shown in the figure. Either of these resonators will exceed 3 MV/m fields using rf power below 6 Watts. We will install these two resonators in the linac, replacing two that perform poorly.

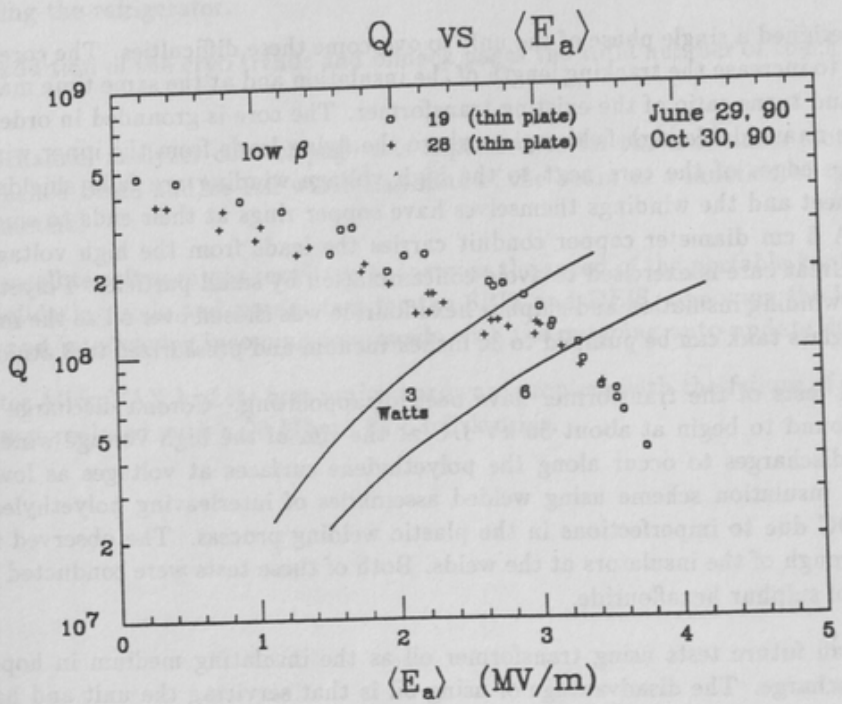

Figure 11.6-1. Q plotted versus electric field for two thin plated resonators.

11.7 Injector Deck Isolation Transformer

G.C. Harper

The injector deck AC power is provided by a 3 phase, 30 kVA transformer designed for 300 kV DC isolation. The primary is delta connected 450 VAC at 20 A, the secondary is wye connected 208 VAC at 83 A, and both windings are electrostatically shielded. The core is biased at the mid-potential of the isolation voltage. The commercially manufactured unit was first put into operation in 1986 and has always been plagued with problems at high isolation voltages. Similar units at other laboratories have suffered from the same engineering difficulties. Two different commercial designs have been tested at this lab. The first used a single core and tank for the 3 phase power. The present design uses 3 cores and tanks, one for each phase.

Inspection of the commercial units revealed fundamental design flaws, particularly in the electrostatic layout. Sharp core edges were left unshielded even when in close proximity to the small diameter flying leads from the windings. Mylar was used for the inter-winding insulation which, although it has a very high dielectric strength, is more prone to tracking than lower density materials such as polyethylene. Metal filings, presumably from the sheared core segments, were observed floating in the insulating oil and resting on the core and winding surfaces. The fiberglass tanks could not be pumped to remove gases from the oil without collapsing from external atmospheric pressure.

We designed a single phase of the unit to overcome these difficulties. The core and windings are designed to increase the tracking length of the insulation and at the same time match the excitation current and turns ratio of the existing transformer. The core is grounded in order to eliminate the otherwise unavoidable high field region where the flying leads from the inner winding pass by the core. The edges of the core next to the high voltage winding are fully shielded with grounded copper sheet and the windings themselves have copper rings at their ends to smoothly radius this region. A 6 cm diameter copper conduit carries the leads from the high voltage winding to the header. Great care is exercised to avoid contamination by small particles. Polyethylene is used for the inter-winding insulation and sulphur hexaflouride was chosen over oil as the insulating medium. The fiberglass tank can be pumped to 30 inches vacuum and pressurized to 3 atmospheres absolute.

Initial tests of the transformer have been disappointing. Corona discharge in the insulating gas was found to begin at about 50 kV DC at the rim of the high voltage winding. This caused tracking discharges to occur along the polyethylene surfaces at voltages as low as 150 kV DC. A second insulation scheme using welded assemblies of interleaving polyethylene cups failed at 210 kV DC due to imperfections in the plastic welding process. The observed failure mode was punch through of the insulators at the welds. Both of these tests were conducted in 2 atmospheres absolute of sulphur hexaflouride.

We plan future tests using transformer oil as the insulating medium in hopes of eliminating corona discharge. The disadvantage of using oil is that servicing the unit and handling the parts after they have been submerged is inconvenient. However, if it eases the tracking problem on the surface of the polyethylene sheet the inconvenience will never arise.

11.8 Booster Main Control Status

G. Harper, M.A. Howe, D.J. Seymour and D. Will

The domain of the Booster main control program (CSX) was extended closer to the Tandem this year with the addition of remote control for some of the offdeck optic elements. In addition to the injector deck and polarized ion source, the deck satellite now has interface electronics and software to control the grid lens, einzel, two magnetic X-Y steerers, faraday cup, and two electrostatic quadrupoles. The deck elevation voltage is also read back. The two electrostatic X-Y steerers and the 5 inch einzel will be added in the near future. A touch screen page was developed for this section of beamline. The console knobs and the two portable knob boxes have full access to the offdeck parameters.

The cryogenic monitoring capabilities of CSX were extended to the liquid helium refrigerator. The expansion engine speed, on/off status, and overspeed status are reported. In addition, all critical temperatures and the supply and return pressures are also monitored. Many more refrigerator parameters will be added to the system in the near future.

A 24 hour log is now kept for all cryogenic levels, refrigerator temperatures, and expansion engine speeds. Hardcopy plots of these trends can be made on the laserwriter and have been helpful in tuning the refrigerator.

With the addition of the cryo trends and offdeck pages the total number of touch screen pages is fifty-three.

The multichannel analyzer control page was expanded to let the user make plots of the percentage of bunched beam and/or full width half max of the beam as a function of the low energy buncher parameters.

The deck satellite software was rewritten to increase the speed of the portable knob boxes. This involved consolidating code and parameters for the SPIS and DEIS, removing the local terminal control code, and interleaving incoming commands with the outgoing auto-update data.

The booster MicroVAX had its first major hardware problem with the failure of the 30 Mbyte user disk. It was replaced with a 70 Mbyte RD53 disk drive.

11.9 Diagnosis of a Cracked Belt

C.E. Linder, T.A. Trainor and W.G. Weitkamp

Following a belt replacement in June the tandem regulated very poorly even in the absence of HECC excess. Terminal voltage noise contained spikes at 2.42 Hz which saturated our stripper regulator and disrupted the regulation loops. A screen malfunction was ruled out by inspection. Figure 11.9-1 shows the HECC under these conditions.

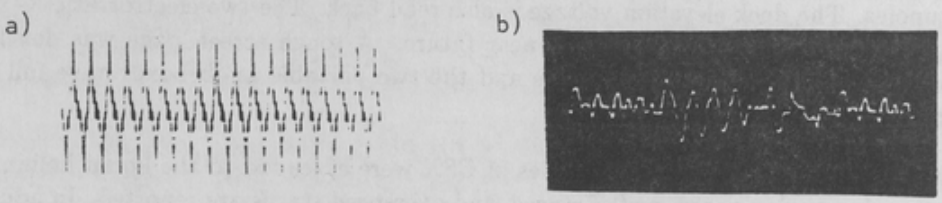

Figure 11.9-1. HECC. a) Chart recorder output, peaks separated by 420 ms. b) CRT trace, 500 ms span.

These signals suggested that some anomalous surface feature of the belt was hitting the screens and dislodging them from the belt surface for about 200 ms (1/2 belt length). The CRT trace especially indicated that an impulse to the screen system caused the thick section to rise above its normal position, thus unloading the fast thin section and reducing its ability to track the cure stripes. This situation is modelled in Figure 11.9-2.

Careful inspection of the new belt surface revealed a transverse crack with surrounding raised belt surface ~10 mils high and ~1/4 inch wide across most of the belt width. We received credit for this belt as obviously defective in manufacture.

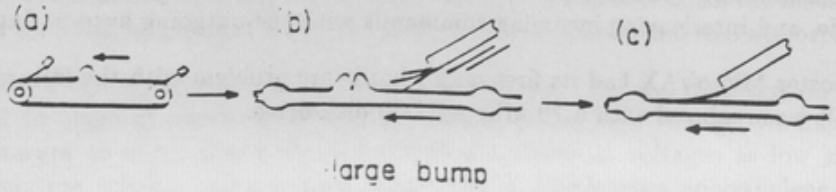

Figure 11.9-2. a) Belt with upcharge and collector screens, showing bump. b) Bump passes under screen forcing thick section well above its equilibrium position. Thin section is unloaded and does not track cure stripes properly. c) Screen restored to equilibrium position; tracking occurs properly.

11.10 Tandem Charging Screens

C.E. Linder, T.A. Trainor and W.G. Weitkamp

For the past year we have used and optimized "compound" (two-component) charging screens.[1] These were preceeded by a succession of finger strips, Be-Cu shim and single leaf stainless-steel shim screens in attempts to minimize voltage noise contributions from belt edge flutter and cure stripes after it was realized that much or all of the fluctuations in delivered belt charge arise from loss of contact between screen and belt surface.[2,3,4]

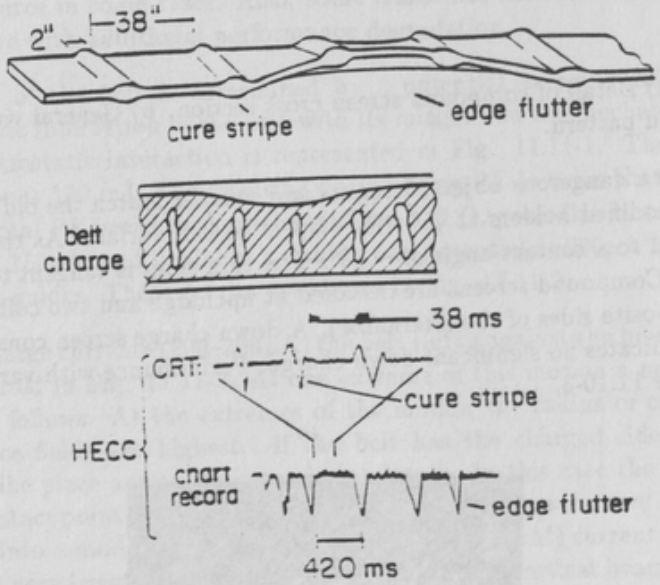

Figure 11.10-1. Relationship between physical belt properties (top), belt surface charge distribution (middle), and HECC signal features (bottom).

Figure 11.10-1 summarizes this situation. The compound screens have been optimized to match the dynamics required to best track the moving belt surface and maintain contact with it. The present configuration is shown in Figure 11.10-2. The two shim thicknesses are fixed. The width of protruding thin shim w is now closer to 1/16 inch and the overall width (presently 1-1/2 inch) will be reduced to 1-1/4 inch or 1 inch soon. The smaller these numbers are the larger the bandwidth for tracking surface bumps but the smaller the dynamic range. We will gradually reduce these dimensions until we feel an optimum has been reached (probably 1/16 inch, 1 inch). The corners of each screen have a radius of ($\sim$1/2 inch) as shown. The spot weld pattern is random with mean spacing $\sim$1/2 inch. Do not accumulate wrinkles or bends when spotwelding. All edges are carefully

[1] Nuclear Physics Laboratory Annual Report, University of Washington (1990) p. 84.

[2] *Symposium of North Eastern Accelerator Personnel:* Yale University, 24–27 Oct. 1988 (World Scientific, J.W. McKay, H.R. McK. Hyder, eds., 1989) p. 51.

[3] *Symposium of North Eastern Accelerator Personnel*; Oak Ridge National Laboratory, 23–26 Oct. 1989 (World Scientific, N.F. Ziegler, G.D. Mills, M.J. Meigs, R.C. Juras, N.L. Jones, C.M. Jones, D.L. Haynes, E.D. Berners, eds., 1990) p. 157.

[4] T.A. Trainor, Nucl. Instr. and Meth. **A287** 103 (1990).

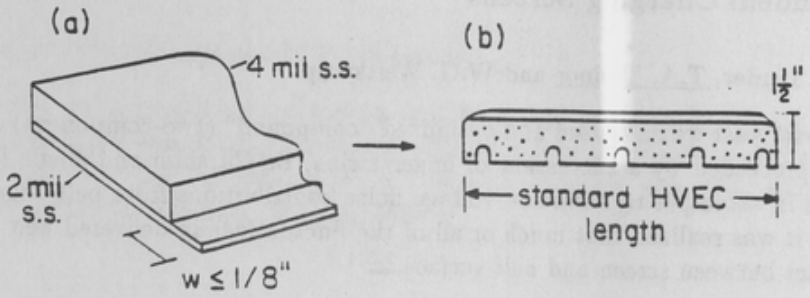

Figure 11.10-2. a) Detail of compound screen cross section. b) General view of compound screen showing spot weld pattern.

deburred. This is a dangerous object! Lengths and notches match the old HVEC screens. Screens are clamped in modified holders at 45° with respect to belt surface. As they approach the belt they curve around to a contact angle of $\sim 10°$. The thin shim is tangent to the belt surface over $\sim 1/2$ its length. Compound screens are installed at upcharge and two collector screen positions (the latter on opposite sides of the alternator). A down charge screen consisting of a single s.s. shim presently indicates no significant down charge. Performance with various screen geometries is shown in Figure 11.10-3.

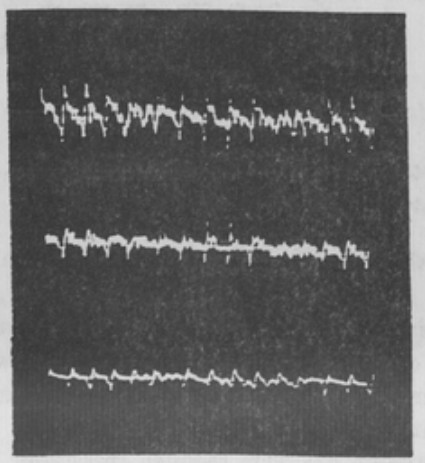

Figure 11.10-3. HECC signals for various charging screen geometries.

All are 100 mV/cm and 500 ms span. The top trace is with a simple 3 mil thick s.s. shim 1-3/4 inch long. The middle trace is with a 2 mil x 4 mil compound screen 1-1/2 inch long with $w = 1/4$ inch. The bottom trace is the same as the middle, except $w = 1/8$ inch. The three traces are with the same belt and the traces have been shifted in phase to line up specific belt surface features.

11.11 Transverse Charging Belt Motion

C.E. Linder, T.A. Trainor, and W.G. Weitkamp

Proper description of the transverse motion of the Van de Graaff charging belt is essential for a complete understanding of sources of terminal voltage noise sources and their reduction. The FN charging belt carries up to 100 μCoulombs of charge at 9 MV. Transverse belt motion induces axial image currents which constitute a nontrivial fraction of the total noise current and may even be the dominant noise source in some cases. Also, some transverse motion may result in charge loss to the column structure with additional performance degradation.

Transverse motion of the belt is determined by a potential energy resulting from the belt tension, the electrostatic interaction of the belt with its images and the mechanical presence of the belt guides. The electrostatic interaction is represented in Fig. 11.11-1. The total electrostatic energy at 200μA is about 100 mJ. The resulting destabilizing PE is twice that of the belt tension at this current. The total PE varies with upcharge from a H.O. potential at no charge to a nearly flat potential at about 150μA, and finally to a double well potential at 300μA which forces the belt against one set of belt guides. These results are shown in Fig. 11.11-2.

At the higher upcharge currents (200–300μA) the belt riding against the belt guides can undergo axial sway as represented in Fig. 11.11-3. At one extreme of this motion a new point of stability can be established as follows. At the extremes of the motion the radius of curvature of the belt is smallest and surface fields are highest. If the belt has the charged side against the guides charge transfer can take place across the ceramic insulators. In this case the reduced belt charge downstream of the contact point makes this asymmetric configuration the new stable configuration. The system is locked into a mode in which substantial (up to 100μA!) current is transferred to the column. The result is very irregular terminal voltage and severe vertical beam jitter with inclined field tubes. If the charge is lowered temporarily, or there is a tank spark, the belt will leave this mode. But axial sway fluctuations will eventually restore it. The remedy for this problem is to move the belt pulleys sideways 2–3 mm so that the charged belt section is closer to the inside belt guides. The charged belt then always falls to the inside and the charged side of the belt is not in contact with the ceramics.

In the interval from 100–200μA upcharge the transverse PE progresses from a flat bottom to a shallow double well. Such a system is well known to be susceptible to chaotic motion. This motion is represented in Fig. 11.11-4. As mentioned above transverse belt motion results in axial image currents. This means that over a range of belt currents a chaotic component is to be expected in the terminal voltage noise. This is found to be true as shown in Fig. 11.11-5. The terminal voltage is found to be noisiest near 4MV with a dominant chaotic component. At low and high voltages the chaotic component is minimal. The dominant noise is periodic, at harmonics of the 2.4 Hz belt fundamental. The chaotic component is lessened by the pulley shift recommended above because the PE well is deepened at the equilibrium belt position.

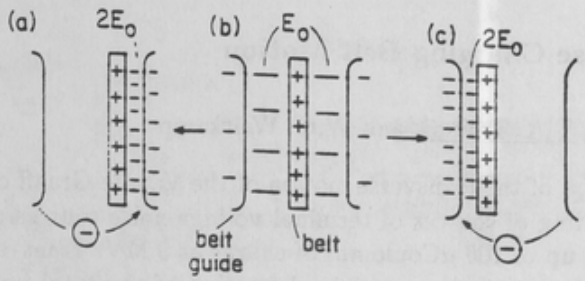

Figure 11.11-1. Cross section of charged belt between belt guides.

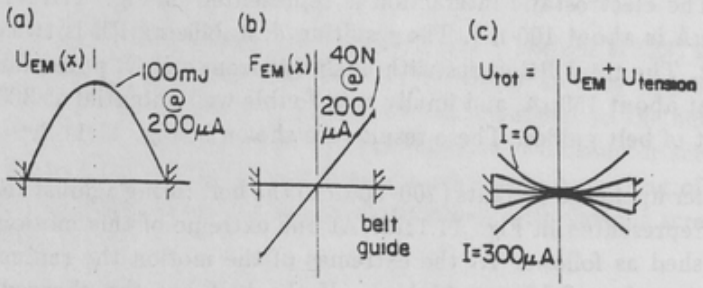

Figure 11.11-2. Force and energy diagrams for transverse belt motion.

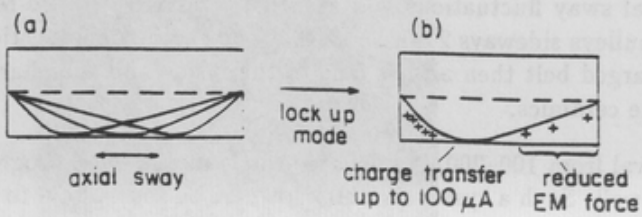

Figure 11.11-3. Pictorial representation of axial sway belt motion and development of charge transfer. The transverse dimension has been exaggerated.

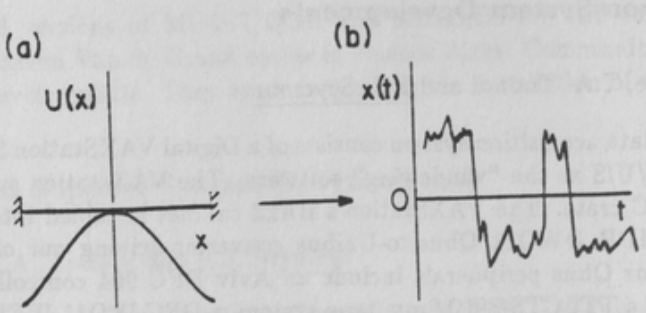

Figure 11.11-4. a) Double well potential for transverse motion of charging belt with upcharge $\geq 150\mu$A. b) Motion resulting from periodic driving of system in double well potential.

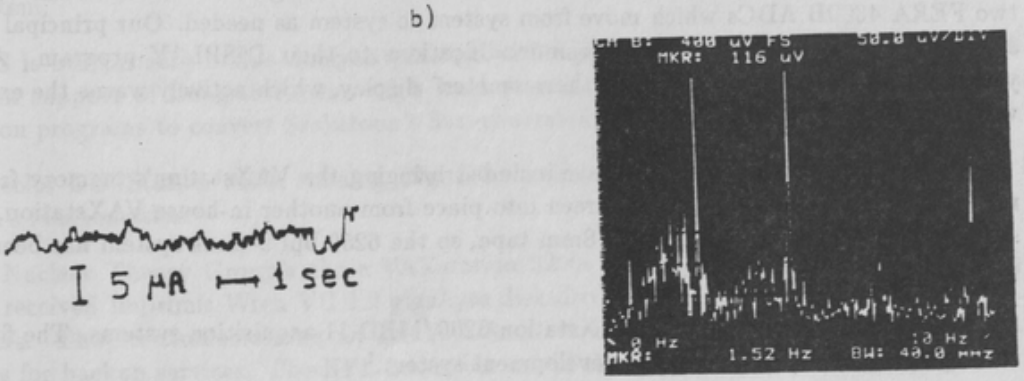

Figure 11.11-5. a) Corona current showing predominantly chaotic signal. b) Power spectrum of corona current showing lines at harmonics of the belt fundamental (2.42Hz) and a broad distribution of power corresponding to the chaotic current component.

12 COMPUTER SYSTEMS

12.1 Acquisition System Developments

M.A. Howe, T.A. Trainor and R.J. Seymour

Our principal data acquisition system consists of a Digital VAXStation 3200 running VMS v4.7a. We still use VWS/UIS as the "windowing" software. The VAXstation supports a BiRa MBD-11 controlled CAMAC crate. The VAXStation's BA23 cabinet is cabled into a BA23-CC expansion cabinet, with a MDB DWQ11 Qbus-to-Unibus converter driving our old PDP 11/60's Unibus expansion bay. Our Qbus peripherals include an Aviv DFC 904 controller with a 760 megabyte Maxtor disk drive, a TTI CTS-8000 8mm tape system, a DEC IEQ11 IEEE-488 bus controller, and a DEC DRV11-J. The Unibus bay contains the MBD-11, a DR11-C and our Printronix's lineprinter controller. This main CAMAC system contains interface modules for our dozen Tracor Northern TN-1213 ADCs.

Additional CAMAC space is available for our LeCroy 2249's, 2228's and 2551's. We are still beset by the LeCroys' problem with lockup if gates arrive during their Clear interval. We now have two FERA 4300B ADCs which move from system to system as needed. Our principal acquisition software is TUNL's XSYS, with major modifications to their DISPLAY program. Among this year's changes are a live diskspace "thermometer" display, which actively warns the experimentor when the disk gets above 95% full.

This year's hardware changes have included bringing the VAXstation's memory from 8 to 16 megabytes, and swapping a color screen into place from another in-house VAXstation. All acquisition taping is now down with the 8mm tape, so the 6250-bpi 9-track system has been moved to one of our offline analysis stations.

We now have two additional VAXstation 3200/MBD-11 acquisition systems. The first of these was described last year as a TPC development system.[1]

We also created an XSYS system in collaboration with LBL for the Calcium-37 Beta decay run at CERN (see section 3.2). An MBD-11, Able Qniverter and an XSYS software tape were taken to LBL, installed in a VAXstation II, and shipped to CERN. After that run we purchased a VAXstation 3100/38. That went into analysis service in place of a VAXstation 3200. The 3200 became our third acquisition computer, using the MBD-11 and Able Qniverter to create a "minimal" system. This machine is running as a diskless VAXcluster member, sharing the TPC system's disk drives and controller.

Cluster operations survive the acquisition load well, unless one of the MBD-11's goes into a race condition. This is usually caused by a CAMAC program which fails to clear a LAM, thereby moving erroneous data into the VAXstation at a speed only limited by the MBD-11, Qbus and VAXstation memory system. Since the same condition also "freezes" a standalone system, such behavior is not cluster-related.

We shall always be upgrading the local version of XSYS documentation. What had started out

[1] Nuclear Physics Laboratory Annual Report, University of Washington (1990) p. 88.

as a six-page "Cookbook" has grown past 60 pages with a chapter structure and full indexing.

Our PDP-11-based versions of MULTI/QDA and SINGLES are still running at TANDAR, Argentina's vertical tandem Van de Graaff center in Buenos Aires. Communication and visits keep us informed of their developments. They are investigating the installation of our version of XSYS.

12.2 Analysis and Support System Developments

M.A. Howe, T.A. Trainor and R.J. Seymour

Our principal interactive system is still an 8 megabyte VAX 11/780 running VMS version 4.7, with connections to thirty-odd local terminals. It is connected via ethernet to eight VAXStation 3200's, one VAXStation 2000, two VAXStation 3100's and a color DECStation 3100 in our building, and via fiber optic ethernet to the rest of the campus. Two of the acquisition VAXstations run as a VAXcluster. TGV's Multinet provides us with TCP/IP access to Internet. Our principal Internet address is npl.npl.washington.edu. Bitnet access is via the campus central site's VAXes and IBM 3090 system.

XSYS is our primary offline analysis package, although we also run LAMPF's Q on a VAX-Station in support of Douglas Rosenzweig's work (see section 8.5). We have also written small translation programs to convert Saskatoon's Sun-generated Q data tapes.

Our color DECStation 3100, running Digital's version of Unix (Ultrix), is primarily used for Wolfram's Mathematica.

The Nuclear Theory Group's three VAXstation 3200s saw growth in two areas. First, two of them received Imprimis Wren VII 1.2 gigabyte disk drives on CMD CQD-220-TM Qbus/SCSI controllers. That controller allows an Exabyte 8mm tape drive to be moved between the two machines for backup services. The NPL has made use of the space available as a staging area for our own backups to 8mm tape.

The second area of growth was in usage due to the creation of the Institute for Nuclear Theory. Their visitors are provided with accounts on one of the VAXstations. Their offices are located 2 miles away, so a 16-port Xyplex 1800 terminal server was installed at the remote site, along with two Apple LaserWriters and two Macintosh computers. The VAXstation provides local compute and printing services for the visitors and office staff, and the TCP/IP-compatible terminal server provides direct connection to the visitors' home systems.

LINAC-related computer items are covered in Section 11.7.

13 APPENDIX

13.1 Nuclear Physics Laboratory Personnel

Faculty

Eric G. Adelberger, Professor
John G. Cramer, Professor
George W. Farwell, Professor Emeritus
Cynthia A. Gossett, Research Assistant Professor
Pieter M. Grootes, Joint Senior Research Associate, Geological Sciences and Physics
Isaac Halpern, Professor
Blayne R. Heckel, Associate Professor
Charles E. Hyde-Wright, Assistant Professor
Geoffrey I. Opat, Visiting Professor[1]
Fred H. Schmidt, Professor Emeritus[2]
Kurt A. Snover, Research Professor
Derek W. Storm, Research Professor; Director, Nuclear Physics Laboratory
Thomas A. Trainor, Research Associate Professor
Robert Vandenbosch, Professor
William G. Weitkamp, Research Professor; Technical Director, Nuclear Physics Laboratory

Research Staff

Ludwig de Braeckeleer, Research Associate
Marc Frodyma, Research Associate
Jens H. Gundlach, Research Associate
Mitchell Kaplan, Research Associate
Paul Magnus, Research Associate
David Sesko, Research Associate
Scott P. Van Verst, Research Associate[3]
Douglas Wells, Research Associate

---

[1]Permanent address: School of Physics, University of Melbourne, Parkville Vic Australia 3052.
[2]Deceased.
[3]Now at: Department of Physics, University of Virginia, Charlottesville, VA 22901.
[4]Now at: Department of Physics, University of Washington, Seattle, WA 98195.
[5]Now at: University of Minnesota, Department of Chemical Engineering and Materials Science, Minneapolis, MN 554455.

Predoctoral Research Associates

John A. Behr
Jeff Bierman
Thomas A. Brown
Aaron Charlop
Ziad M. Drebi
Jon Eisenberg[4]
Alejandro García
Michael Harris
Weidong Jiang
Yihan Liu[5]
S. John Luke
Diane Markoff
Brian McLain
Douglas P. Rosenzweig
Gregory Smith
Yue Su
Kenneth Swartz
Bruce Thompson
John Winchester[4]

Professional Staff

John F. Amsbaugh, Research Engineer
Gregory C. Harper, Research Engineer
Mark A. Howe, Research Engineer
Duncan Prindle, Research Scientist
Richard J. Seymour, Computer Systems Manager
Rod E. Stowell, Electronics Engineer/Electronics Shop Supervisor
H. Erik Swanson, Research Physicist
Timothy D. Van Wechel, Electronics Engineer
Douglas I. Will, Research Engineer

Technical Staff

Robert L. Cooper, Instrument Maker
Dean T. Corcoran, Engineering Technician
Louis L. Geissel, Instrument Maker, Student Shop Leadman
Carl E. Linder, Engineering Technician
Hendrik Simons, Instrument Maker, Shop Supervisor
John A. Wootress, Accelerator Technician

Administrative Staff

María G. Ramírez, Administrative Assistant
Ida M. Tess, Program Assistant

Part Time Staff

Kevin Arnal
Michael Carius
Christopher Cochran
Erik Dybwad
Philip Fisher
Wendy Kameoka
Nancy Mar
Kevin McMurry
Laurence Norton
John A. Rogers
Manish Rohila
Junji Urayama
Eric Vandervort
David Wright

13.2 Degrees Granted, Academic Year 1990–1991

Ph. D. Degrees:

"The Search for Parity Non-Conservation in Hydrogen ," Peter W. Wong, Ph. D. Thesis, University of Washington (1990).

13.3 List of Publications

Published Papers:

"Spin distribution of the compound nucleus formed by $^{16}O + ^{154}Sm$," S. Gil, R. Vandenbosch, A. Charlop, A. García, D.D. Leach, S.J. Luke and S. Kailas, Phys. Rev. C **43**, 701 (1991).

"Observation of mean-spin barrier bump in sub-barrier fusion of ^{28}Si with ^{154}Sm," S. Gil, D. Abriola, D.E. DiGregorio, M. Di Tada, M. Elgue, A. Etchegoyen, M.C. Etchegoyen, J. Fernández Niello, A.M.J. Ferrero, A.O. Macchiavelli, A.J. Pacheco, J.E. Testoni, P. Silveira Gomes, V.R. Vanin, A. Charlop, A. García, S. Kailas, S.J. Luke, E. Renshaw and R. Vandenbosch, Phys. Rev. Lett. **65**, 3100 (1990).

"Effective interactions and nuclear structure using 180 MeV protons, I: $^{16}O(p,p')$", J.J. Kelly, J.M. Finn, W. Bertozzi, T.N. Buti, F.W. Hersman, C. Hyde-Wright, M.V. Hynes, M.A. Kovash, B. Murdock, P. Ulmer, A.D. Bacher, G.T. Emery, C.C. Foster, W.P. Jones, D.W. Miller, B.L. Berman, Phys. Rev. C **41** 2504 (1990).

"Elastic magnetic electron scattering from ^{41}Ca," H. Baghaei, A. Cichocki, J.B. Flanz, M. Frodyma, B. Frois, Y. Han, R.S. Hicks, J. Martino, R.A. Miskimen, C.N. Papanicolas, G.A. Peterson, S. Platchkov, S. Raman, S.H. Rokni and T. Suzuki, Phys. Rev. C **42**, 2358 (1990).

"Importance of biospheric CO_2 in a subcanopy atmosphere deduced from ^{14}C AMS measurements," P.M. Grootes, G.W. Farwell, F.H. Schmidt, D.D. Leach and M. Stuiver, Radiocarbon **30**, No. 3, 475 (1989).

"The University of Washington AMS system: a 6-year technical update," F.H. Schmidt, T.A. Brown, G.W. Farwell and P.M. Grootes, Nucl. Instr. Meth. **B52**, 229 (1990).

"^{14}C AMS at the University of Washington: measurements in a shared facility at the 1% level on 0.4 mg samples," T.A. Brown, G.W. Farwell, P.M. Grootes, P.D. Quay and F.H. Schmidt, Nucl. Instr. Meth. **B52**, 351 (1990).

"The University of Washington polarized ion source," C.A. Gossett, D.R. Balsley, G.C. Harper, C.M. Bitz, J.K. Eisenberg and J.A. Rogers, Rev. Sci. Instrum. **61**, 445 (1990).

"Role of the π-N P_{11} interaction in π-d elastic scattering," N.R. Stevenson, R.B. Schubank, Y.M. Shin, P. Amaudruz, P.P.J. Delheij, D.C. Healey, B.K. Jennings, D.F. Ottewell, G. Sheffer, G.R. Smith, G.D. Wait, J.T. Brack, A. Feltham, M. Hanna, R.R. Johnson, F.M. Rozon, V Sossi, D. Vetterli, P. Weber, N. Grion, R. Rui, M. Kohler, R.A. Ristinen, E.L. Mathie, R. Tacik, M. Yeomans, C.A. Gossett and G.J. Wagner, Phys. Rev. Lett. **65**, 1987 (1990).

"Oblate deformed shapes of hot, rotating nuclei deduced from giant dipole resonance decay studies," J.H. Gundlach, K.A. Snover, J.A. Behr, C.A. Gossett, M. Kicinska-Habior and K.T. Lesko, Phys. Rev. Lett. **65**, 2523 (1990).

"High energy gamma emission in heavy ion collisions at E/A = 9–14 MeV/nucleon," C.A. Gossett, J.A. Behr, S.J. Luke, B.T. McLain, D.P. Rosenzweig, K.A. Snover and W.T. Hering, Rapid Communications, Phys. Rev. C **42**, R1800 (1990).

"Fusion cross section for the system ^{6}Li + ^{28}Si at $E \sim 36$ MeV," S. Kailas, R. Vandenbosch, A.W. Charlop, A. García, S. Gil, S.J. Luke, B.T. McLain and D.J. Prindle, Pramana-J. Phys. **35**, 5 (1990).

"Testing the equivalence principle in the field of the Earth: particle physics at masses below 1 μeV?," E.G. Adelberger, C.W. Stubbs, B.R. Heckel, Y. Su, H.E. Swanson, G. Smith, J.H. Gundlach and W.F. Rogers, Phys. Rev. D **42**, 10 (1990).

"Does antimatter fall with the same acceleration as ordinary matter?," E.G. Adelberger, B.R. Heckel, C.W. Stubbs and Y. Su, Phys. Rev. Lett. **66**, 850 (1991)

"Fission angular distributions for the systems ^{9}Be + ^{232}Th, ^{235}U," S. Kailas, R. Vandenbosch, A.W. Charlop, S.J. Luke, D.J. Prindle, and S.P. Van Verst, Phys. Rev. C **42**, 5 (1990).

"Eötvös experiments, lunar ranging and the strong equivalence principle," E.G. Adelberger, B.R. Heckel, G. Smith, Y. Su and H.E. Swanson, Nature **347**, 6290 (1990).

"^{37}Ca β^{+} decay and the efficiency of the ^{37}Cl detector for high energy neutrinos," A. García, E.G. Adelberger, H.E. Swanson, T.F. Lang and D.M. Moltz, Phys. Rev. C **42**, 775 (1990).

"High spin states in ^{76}Br," D.F. Winchell, J.X. Saladin, M.S. Kaplan and H. Takai, Phys. Rev. C **41**, 1264 (1990).

"Spin dependence of the giant dipole resonance strength function in highly excited nuclei in the mass region A=39–45," M. Kicinska-Habior, K.A. Snover, J.A. Behr, G. Feldman, C.A. Gossett and J.H. Gundlach, Phys. Rev. C **41** 2075 (1990).

"Gyro results," E.G. Adelberger, Nature **345**, 6271 (1990).

"Status of and operating experience with the University of Washington superconducting booster linac," D.W. Storm, J.F. Amsbaugh, D.T. Corcoran, G.C. Harper, M.A. Howe, R.E. Stowell, T.D. Van Wechel, W.G. Weitkamp and D.I. Will, Nucl. Instr. and Meth. **A287**, 247 (1990).

"Coriolis and magnetic forces: the gryocompass and magnetic compass as analogues," G.I. Opat, Am J. Phys. **58**, 1173 (1990).

"Measurements of the deuteron and proton magnetic form factors at large momentum transfers," P.E. Bosted, A.T. Katramatou, R.G. Arnold, D. Benton, L. Clogher, G. DeChambrier, J. Lambert, A. Lung, G.G. Petratos, A. Rahbar, S.E. Rock, Z.M. Szalata, B. Debebe, M. Frodyma, R.S. Hicks, A. Hotta, G.A. Peterson, R.A. Gearhart, J. Alster, J. Lichtenstadt, F. Dietrich and K. van Bibber, Phys. Rev. C **42**, 38 (1990).

"Effective interaction for ^{16}O(p,p') at $E_p = 318$ MeV," J.J. Kelly, A.E. Feldman, B.S. Flanders, H. Seifert, D. Lopiano, B. Aas, A. Azizi, G. Igo, G. Weston, C. Whitten, A. Wong, M.V. Hynes, J. McClelland, W. Bertozzi, J.M. Finn, C.E. Hyde-Wright, R.W. Lourie, P.E. Ulmer B.E. Norum, B.L. Berman, Phys. Rev. C **43**, 1272 (1991).

"The 'missing' 3^{+} state of ^{18}Ne and explosive ^{17}F(p,γ) burning," A. García, E.G. Adelberger, P.V. Magnus, D.M. Markoff, K.B. Swartz, M.S. Smith, K.I. Hahn, N. Bateman, and P.D. Parker, Phys. R .v. C **43**, 2012 (1991).

Papers Submitted or to be Published:

"Empirical density dependent effective interaction for nucleon-nucleus scattering at 500 MeV," B.S. Flanders, J.J. Kelly, H. Seifert, D. Lopiano, B. Aas, A. Azizi, G. Igo, G. Weston, C. Whitten, A. Wong, M.V. Hynes, J. McClelland, W. Bertozzi, J.M. Finn, C.E. Hyde-Wright, R.W. Lourie, B.E. Norum, P. Ulmer, B.L. Berman, submitted to Phys Rev C, December 1990.

"Electroexcitation of negative-parity states in ^{18}O," D.M. Manley, B.L. Berman, W. Bertozzi, T.N. Buti, J.M. Finn, F.W. Hersman, C.E. Hyde-Wright, M.V. Hynes, J.J. Kelly, M.A. Kovash, S. Kowalski, R.W. Lourie, B. Murdock, B.E. Norum, B. Pugh and C. P. Sargent, submitted to Phys Rev C, October 1990.

"Electron scattering from ^{9}Be," J.P. Glickman, W. Bertozzi, T.N. Buti, S. Dixit, F.W. Hersman, C.E. Hyde-Wright, M.V. Hynes, R.W. Lourie, B.E. Norum, J.J. Kelly, B.L. Berman and D.J. Millener, submitted to Phys Rev C, October 1990.

"Spectrum of ^{9}Be from proton scattering," S. Dixit, W. Bertozzi, T.N. Buti, J.M. Finn, F.W. Hersman, C.E. Hyde-Wright, M.V. Hynes, M.A. Kovash, B.E. Norum, J.J. Kelly, A.D. Bacher, G.T. Emery, C.C. Foster W.P. Jones, D.W. Miller, B.L. Berman, submitted to Phys Rev C, October 1990.

"Carbon isotopic composition of atmospheric CH_4: fossil and biomass burning source strengths," P.D. Quay, S.L. King, J. Stutsman, D.O. Wilbur, L.P. Steele, I. Fung, R.H. Gammon, T.A. Brown, G.W. Farwell, P.M. Grootes and F.H. Schmidt, Global Biogeochemical Cycles (1991), in press.

"Accelerator mass spectrometry dates on bones from Old Crow Basin, Northern Yukon Territory," R.E. Morlan, D.E. Nelson, T.A. Brown, J.S. Vogel and J.R. Southon, Canadian Journal of Archeology (1991), in press.

"T-violation experiments using Mössbauer transitions," A. Schäfer and E.G. Adelberger, Zeitschrift für Physik A, to be published.

"Searches for new macroscopic forces," E.G. Adelberger, C.W. Stubbs, B.R. Heckel and W.F. Rogers, submitted to Ann. Rev. Particle and Nuclear Science.

"High spin and shape coexistence in ^{73}Se," M.S. Kaplan, J.X. Saladin, D.F. Winchell, H. Takai, J. Dudek, submitted to Phys. Rev. C.

"Inclusive inelastic scattering of 96.5 MeV π^+ and π^- by the hydrogen and helium isotopes," M.A. Khandaker, M. Doss, I. Halpern, T. Murakami, D.W. Storm, D.R. Tieger and W.J. Burger, submitted to Phys. Rev. C.

"Search for high energy γ rays from the spontaneous fission of ^{252}Cf," S.J. Luke, C.A. Gossett and R. Vandenbosch, submitted to Phys. Rev. C.

"Analysis of multiparticle Bose-Einstein correlation in ultra-relativistic heavy ion collisions," J.G. Cramer, accepted by Phys. Rev. C (1991).

"Statistical analysis of neutron interferometer detection systems," G.I. Opat, submitted to Rev.

Sci. Instrum.

"Theory of an earth-bound clock comparison experiment as test of the principle of equivalence," G.I. Opat and W.G. Unruh, submitted to Phys. Rev. D.

"Stark effect for a rigid symmetric top molecule: exact solution," G.I. Opat and J.V. Hajnal accepted by J. Phys. B. Atomic, Molecular and Optical Physics.

"The fall of charged carticles under gravity," T. Darling, F. Rossi, G.I. Opat and G. Moorhead, submitted to Rev. Mod. Phys.

"The electrical potential outside conducting surfaces caused by patch potentials," G.I. Opat, G. Moorhead and F. Rossi, submitted to Phys. Rev. B15.

"Electric and magnetic mirrors and gratings for slowly moving neutral atoms and molecules," G.I. Opat, S. Wark, J.V. Hajnal and A. Cimmino, submitted to J. Opt. Soc. Am. B.

"The precession of a Foucault pendulum viewed as a beat phenomenon of a conical pendulum to a coriolis force," G.I. Opat, accepted by Am. J. Physics (1991).

" 'Mixed-Charge' HBT interferometry for large pion sources," J.G. Cramer, submitted to Phys. Rev. Letters.

"Quantum poker: a portrait of quantum behavior," J.G. Cramer (1990).

"The solution of a charging belt problem," W.G. Weitkamp, T.A. Trainor and C.E. Linder, in *Proceedings of the Symposium of Northeastern Accelerator Personnel*, Kansas State University, to be published.

Published Conference Proceedings and Invited Talks:

"Near-barrier heavy ion fusion (panel discussion)," R. Vandenbosch, Workshop on Heavy Ion Collisions at Energies Near the Coulomb Barrier, Inst. Phys. Conf. Ser. No. 110: Section 2, Daresbury Lab., England, July 5–7 1990.

"Status of and operating experience with the University of Washington superconducting booster linac," D.W. Storm, J.F. Amsbaugh, D.I Corcoran, G.C. Harper, M.A. Howe, R.E. Stowell, T.D. Van Wechel, W.G. Weitkamp and D.I. Will, Proceedings of SNEAP, 1989.

"Recent results on GDR decays in highly excited nuclei," K.A. Snover, International Symposium and Workshop on Future Directions in Nuclear Physics with 4π gamma Detection Systems of the New Generation, Strasbourg, France, March 4–16, 1991 (invited talk).

"The giant dipole resonance in hot nuclei," K.A. Snover, Hanna Symposium, Stanford University, Palo Alto, Ca, March 16, 1991 (invited paper).

"A low-energy frontier of particle physics," E.G. Adelberger, Proceedings of the 1990 PANIC Conference, Boston (in press).

"Testing the equivalence principle in the field of the earth: particle physics at masses below 1 μeV?" E.G. Adelberger, in *The Standard Model and Beyond*, Proceedings of the Fifth Lake Louise

Winter Institute, eds. A. Astbury *et al.*, World Scientific (Singapore), 1990, p. 284.

"Recent development of the University of Washington crossed-beams polarized ion source," C.A. Gossett, Proceedings of the International Workshop on Polarized Ion Sources and Gas Jets, KEK, Japan, Feb. 1990, KEK Report 90-15, p. 101 (invited talk).

"Experimental tests of the universality of free fall and of the inverse square law," E.G. Adelberger, in *General Relativity and Gravitation*, 1989, Proceedings of the 12^{th} International Conference on General Relativity and Gravitation, ed. by N. Ashby, D.F. Bartlett and W. Wyss, Cambridge University Press (NY), 1990, p. 273.

"Hard photon production in heavy ion collisions," C.A. Gossett American Physical Society Meeting, Apr. 1991, Bull. Am. Phys. Soc. **36**, 1259 (1991). (invited talk).

"Analyzing power measurements in π-d scattering at 50 MeV," N.R. Stevenson, R.B. Schubank, Y.M. Shin, P. Amaudruz, P.P.J. Delheij. D.C. Healey, B.K. Jennings, D.F. Ottewell, G. Sheffer, G.R. Smith, G.D. Wait, N. Grion, R. Rui, J.T. Brack, A. Feltham, M. Hanna, R.R. Johnson, F.M. Rozon, V. Sossi, D. Vetterli, P. Weber, M. Kohler, R.A. Ristinen, E.L. Mathie, R. Tacik, M. Yeomans, C.A. Gossett, G.J. Wagner and B.E. King, Proceedings of the 7^{th} International Conference on Polarization Phenomena in Nuclear Physics, p. C6-391, Paris, July, 1990.

Abstracts and other Conference Presentations:

"High energy γ rays from p + X, X=Cu, Ag, Au at 33.5 MeV," S.J. Luke, C.A. Gossett, M.S. Kaplan, B.T. McLain, D.P. Rosenzweig, R. Vandenbosch and D. Wells, Bull. Am. Phys. Soc. (1991).

"Polarized protons from the ^{59}Co(^{3}He,pX) reaction," W.G. Weitkamp, D.I. Will, M. Frodyma, J.L. Allen, A.R. Crews, S.K. Lamoreaux, S.L. Rosell, H. Willmes, S. Kailas and K. Sagara, 7th International Conference on Polarization Phenomena in Nuclear Physics, Paris 1990, Abstract 86B.

"Does antimatter fall with the same acceleration as ordinary matter?," E.G. Adelberger, B.R. Heckel, Y. Su and C.W. Stubbs, Bull. Am. Phys. Soc. (1991).

"Search for high energy γ rays from the spontaneous fission of ^{252}Cf," S.J. Luke, C.A. Gossett and R. Vandenbosch, Bull. Am. Phys. Soc. (1991).

"Searching for new interactions by testing the equivalence principle in the field of the Earth," Y. Su, E.G. Adelberger and B.R. Heckel, Bull. Am. Phys. Soc. (1991).

"β^+ decays of ^{37}Ca," A. García, E.G. Adelberger, P.V. Magnus and H.E. Swanson, Bull. Am. Phys. Soc. (1991).

"Nuclear rainbow scattering in ^{6}Li + ^{12}C at 14.5 MeV/nucleon," J.G. Cramer, S.J. Luke, B.T. McLain and D.J. Prindle, Bull. Am. Phys. Soc. **36**, 1272 (1991).

"Charged pion Hanbury-Brown Twiss interferometry with large ultrarelativistic sources," J.G. Cramer, Bull. Am. Phys. Soc. **36**, 1323 (1991).

"High energy gamma-ray emission following fusion of ^{58}Ni and ^{92}Zr," M.S. Kaplan, K.A. Snover, D.P. Wells and Z.M. Drebi, Bull. Am. Phys. Soc. (1991).

"Giant dipole radiation and isospin purity in highly excited compound nuclei," J.A. Behr, K.A. Snover, C.A. Gossett, J.H. Gundlach, Z.M. Drebi, M.S. Kaplan and D.P. Wells, Bull. Am. Phys. Soc. (1991).

"The University of Washington polarized ion source," C.A. Gossett, G.C. Harper, D.T. Corcoran and J.A. Rogers, Proceedings of the 7^{th} International Conference on Polarization Phenomena in Nuclear Physics, Paris, July, 1990.

"Analyzing power measurements in ^{2}H(d,γ)^{4}He at E_d = 1 MeV," C.A. Gossett, M.S. Kaplan, S.J. Luke, S.P. Van Verst and D. Wells, Proceedings of the 7^{th} International Conference on Polarization Phenomena in Nuclear Physics, Paris, July, 1990.

"Emilio Segré, Enrico Fermi, Pu-240, and the atomic bomb," G.W. Farwell, Symposium to Commenorate the 50^{th} Anniversary of the Discovery of Transuranium Elements; Book of Abstracts, 200th ACS National Meeting, Washington, D.C., August 26–31, 1990 (Abstract No. 85, NUCL/PROGRAM).

"Perturbative QCD calculations of exclusive virtual compton scattering," C.E. Hyde-Wright, G.R. Farrar and K. Van Bibber, Contributed paper, PANIC XII, International Conference on Particles and Nuclei, MIT June 1990.

"New measurements of the electric and magnetic elastic form factors of the proton and neutron at high momentum transfers," P.E. Bosted, L. Clogher, A. Lung, L. Stuart, J. Alster, R.G. Arnold, C.C. Chang, F. Dietrich, W.R. Dodge, R. Gearhart, J. Gomez, K. Griffioen, R. Hicks, C. Hyde-Wright, C. Keppel, S. Kuhn, J. Lichtenstadt, R. Miskimen, G.G. Petratos, G.A. Peterson, S.E. Rock, S.H. Rokni, W.K. Sakumoto, K. Swartz, Z.M. Szalata, and L.H. Tao, Contributed paper, PANIC XII, International Conference on Particles and Nuclei, MIT June

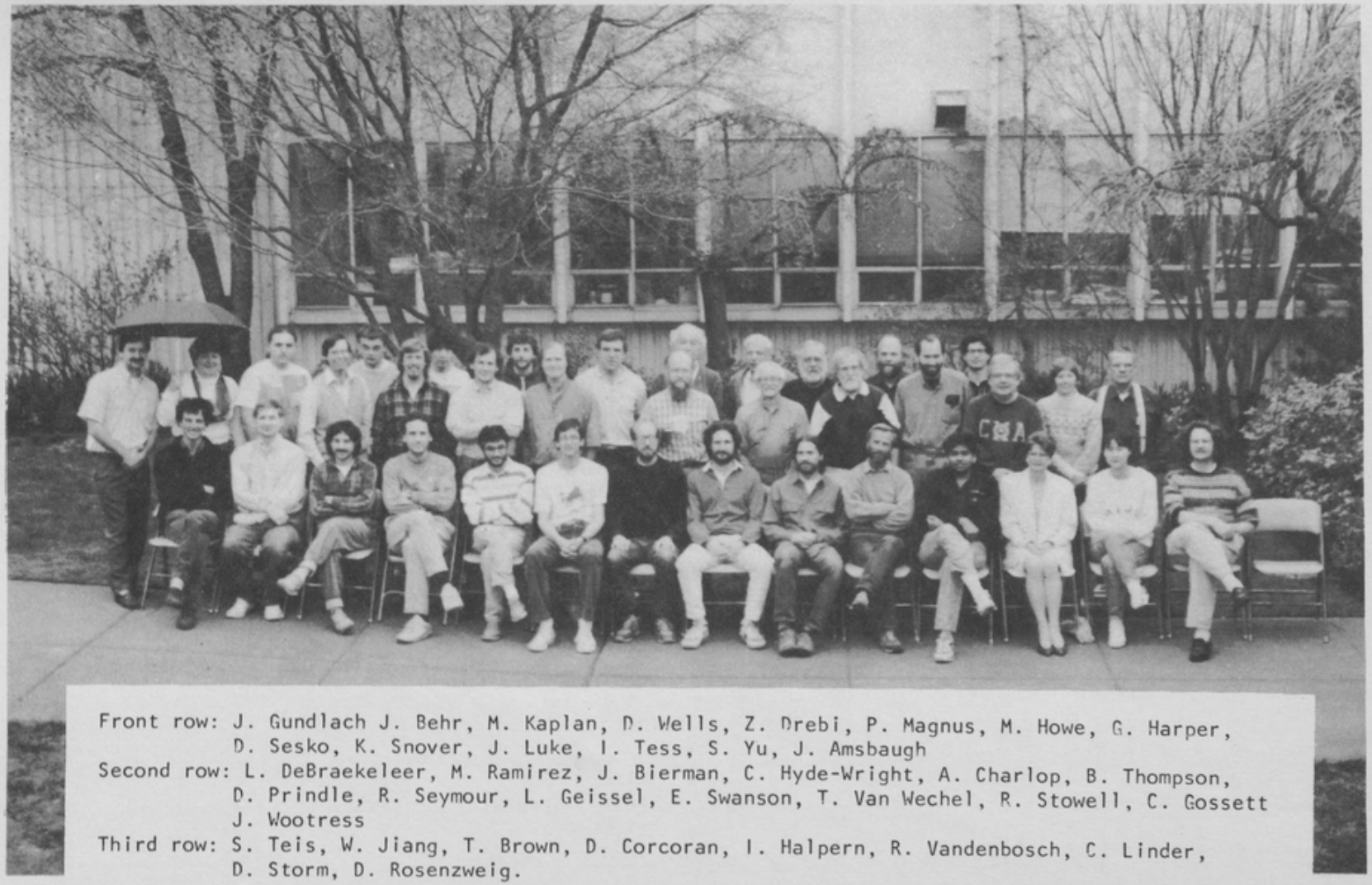

Front row: J. Gundlach J. Behr, M. Kaplan, D. Wells, Z. Drebi, P. Magnus, M. Howe, G. Harper, D. Sesko, K. Snover, J. Luke, I. Tess, S. Yu, J. Amsbaugh
Second row: L. DeBraekeleer, M. Ramirez, J. Bierman, C. Hyde-Wright, A. Charlop, B. Thompson, D. Prindle, R. Seymour, L. Geissel, E. Swanson, T. Van Wechel, R. Stowell, C. Gossett J. Wootress
Third row: S. Teis, W. Jiang, T. Brown, D. Corcoran, I. Halpern, R. Vandenbosch, C. Linder, D. Storm, D. Rosenzweig.